Aus dem Institut für Physiologie und Pathophysiologie
Geschäftsführender Direktor: Prof. Dr. Dominik Oliver

des Fachbereichs Medizin der Philipps-Universität Marburg

The serine/threonine protein kinase SGK3 stimulates endosomal recycling of the potassium channel Kir2.2.

Inaugural-Dissertation zur Erlangung des Doktorgrades der Naturwissenschaften (Dr. rer. nat.)

dem Fachbereich Medizin der Philipps-Universität Marburg vorgelegt von

Katrin Grothus aus Coesfeld

Marburg, 2015

Angenommen vom Fachbereich Medizin der Philipps-Universität Marburg am: 01.10.2015

Gedruckt mit Genehmigung des Fachbereichs.

Dekan: Prof. Dr. Helmut Schäfer
Referent: Prof. Dr. Dr. Jürgen Daut
1. Korreferent: Prof. Dr. Yalcin Cetin

Ever tried. Ever failed. No matter.

Try again. Fail again. Fail better.

Samuel Beckett (Worstward Ho 1983)

Table of contents

Abstract

Serum- and glucocorticoid-inducible kinase 3 (SGK3) increases the expression of various membrane proteins at the cell surface. In this study, the mechanism by which SGK3 increases the surface expression of the potassium channel Kir2.2 was investigated using two-electrode voltage clamp, luminometric surface expression measurements and fluorescence microscopy in a mammalian cell line (COS-7) and *Xenopus laevis* oocytes.

A number of different mechanisms by which SGK3 increases the membrane expression of various channel and transporter proteins has been proposed, including phosphorylation of the ubiquitin ligase Nedd4-2, phosphorylation of the transcription factor FOXO3a and phosphorylation of the phosphoinositide kinase PIKfyve. The results obtained in this study suggest that none of these mechanisms is responsible for the increased surface expression of Kir2.2 induced by SGK3. They furthermore indicate that SGK3 neither affects the amount of endocytosed Kir2.2 channels nor the number of newly synthesized channel molecules.

An antibody-based recycling assay showed that a substantial amount of Kir2.2 was internalized and recycled back to the plasma membrane during two 30 min time periods. It further indicated that coexpression of a constitutively active SGK3-mutant leads to an increased number of recycled channel proteins in comparison to coexpression of a dominant negative mutant.

Live-cell fluorescence imaging with two different colors revealed that Kir2.2 channels, SGK3 and the small G-protein Rab7 were extensively colocalized in a PI(3)P positive endosomal compartment. Furthermore, frequent interactions of Kir2.2-positive, SGK3-positive or Rab7-positive vesicles with the Rab11-positive recycling endosome were observed. I line with these results, a mutant of SGK3 that does not bind to PI(3)P had a much smaller effect on Kir2.2 surface expression than the wild-type kinase, suggesting that the intracellular localization of SGK3 to endosomal membranes plays a crucial role for its effect on Kir2.2.

Taken together, the results obtained in this study suggest that SGK3 promotes the recycling of Kir2.2 channels from a PI(3)P and Rab7-positive intracellular compartment that represents an intermediate stage of maturing early endosomes. The recycling of the channel back to the plasma membrane possibly occurs via Rab11 positive recycling endosomes.

Zusammenfassung

Die Serum- und Glucocorticoid-induzierbare Kinase 3 (SGK3) erhöht die Oberflächenexpression zahlreicher Membranproteine. In dieser Arbeit wurde der Mechanismus, durch den SGK3 die Oberflächenexpression des Kaliumkanals Kir2.2 erhöht, in *Xenopus laevis* Oozyten und einer Säugerzelllinie (COS-7) untersucht. Dazu wurden die Zwei-Elektroden-Spannungsklemme, luminometrische Oberflächen-Assays und Fluoreszenz-mikroskopie eingesetzt.

Eine Vielzahl unterschiedlicher Mechanismen, durch die SGK3 die Oberflächenexpression von verschiedenen Membranproteinen und Transportern erhöht, wurde bereits beschrieben. Darunter die Phosphorylierung der Ubiquitin-Ligase Nedd4-2, die Phosphorylierung des Transkriptionsfaktors FOXO3a und die Phosphorylierung der Phosphoinositid-Kinase PIKfyve.
Die Ergebnisse dieser Arbeit legen nahe, dass keiner dieser Mechanismen für die erhöhte Anzahl von Kir2.2-Kanälen in der Membran verantwortlich ist. Sie lassen weiterhin den Schluss zu, dass SGK3 weder einen Effekt auf die Anzahl der endozytierten Kir2.2-Kanäle, noch auf die Anzahl der neu synthetisierten Moleküle hat.

Mit einem auf Antikörpern basierenden Recycling-Assay konnte gezeigt werden, dass ein Großteil der Kanäle während zweier dreißigminütiger Inkubationszeiten internalisiert und anschließend zurück an die Zellmembran transportiert wurde. Weiterhin wurde beobachtet, dass die Ko-Expression einer konstitutiv aktiven SGK3-Mutante im Vergleich zu der Ko-Expression einer dominant-negativen Mutante zu einer erhöhten Anzahl von recycelten Kir2.2 Kanälen führte.

Fluoreszenzmikroskopie-Aufnahmen mit lebenden COS-7 Zellen und zwei verschiedenen Fluoreszenzfarbstoffen zeigten, dass der Kaliumkanal Kir2.2, die Kinase SGK3 und das kleine G-Protein Rab7 in hohem Maße in PI(3)P positiven, endosomalen Kompartimenten kolokalisiert waren. In Übereinstimmung mit diesen Ergebnissen konnte gezeigt werden, dass eine SGK3-Mutanten, die nicht mehr in der Lage ist an PI(3)P zu binden, einen

deutlich geringeren Effekt auf die Oberflächenexpression von Kir2.2 hat, als die Wildtyp-Kinase. Diese Beobachtungen legen die Vermutung nahe, dass die intrazelluläre Lokalisation von SGK3 an endosomalen Membranen eine wichtige Rolle für ihren Effekt auf Kir2.2 spielt.

Zusammengefasst lässt sich sagen, dass die in dieser Arbeit erzielten Ergebnisse darauf hinweisen, dass SGK3 das Recycling von Kir2.2-Kanälen aus einem PI(3)P und Rab7 positiven Kompartiment stimuliert. Bei diesem Kompartiment handelt es sich um ein Zwischenstadium im Reifungsprozess von frühen zu späten Endosomen. Während des Recyclings zurück an die Zellmembrane werden die Kanäle wahrscheinlich durch das Rab11-positive Recycling Endosom geschleust.

1. Introduction

1.1 Ion channels

The plasma membrane is a selectively permeable barrier that separates the intracellular from the extracellular space, allowing the cell to maintain a constant internal environment. It is impermeable to most water-soluble molecules as well as ions, so the transport of these molecules into and out of the cell requires the assistance of specialized membrane proteins. One type of transport protein that facilitates the movement of ions across the cell membrane down their electrochemical gradient is the ion channel. Ion channels are pore-forming transmembrane proteins that selectively or preferentially allow one ionic species to cross the lipid bilayer. Together with ATP powered ion pumps that transport ions against their electrochemical gradient, ion channels generate an electric potential across the plasma membrane by establishing different concentrations of the principal cellular ions K^+, Na^+, Ca^{2+} and Cl^- on both sides of the membrane. The membrane potential of non-excitable cells and the membrane potential of excitable cells in the absence of excitation are called resting membrane potential and range between -30 mV and -80 mV, depending on the cell type.

Besides maintaining the resting membrane potential, plasma membrane resident ion channels have a fundamental importance for the transmission of electrochemical nerve impulses and indirectly influence the contraction of cardiac, skeletal and smooth muscle cells. Ion channels can be modulated by different stimuli including changes in the membrane potential, temperature, pH, mechanical stimulation and the binding of ligands (Hille 2001).

1.1.1 Potassium channels

Potassium channels are transmembrane proteins that selectively conduct potassium ions across the cell membrane down their electrochemical gradient. Their molecular diversity is larger than that of any other group of ion channels. In humans there are 78 different genes encoding for potassium channels and they are expressed in virtually all cell types, where they regulate the electrical

excitability and contribute to the maintenance of the resting membrane potential. In a typical mammalian cell, the resting membrane potential is mainly determined by potassium ions. Due to potassium channels which are open at negative potentials and allow potassium ions to diffuse down their concentration gradient, the resting cell membrane is more permeable to K^+ than it is to other ions. The intracellular concentration of potassium ions $[K^+]_i$ (~150 mM) is considerably higher than the extracellular concentration $[K^+]_o$ (~4 mM), the chemical driving force for potassium ions is therefore directed out of the cell. However, as potassium ions are positively charged, they leave a negative charge behind when they leave the cell, creating an electrical driving force for cations that is directed into the cell. The potential across the membrane at which electrical and chemical forces counterbalance and prevent a net flow of ions is called reversal potential or equilibrium potential for K^+, E_K, and can be calculated using the Nernst equation:

$$E_K = \frac{RT}{zF} ln \frac{[K^+]_o}{[K^+]_i} = -96mV$$

As the resting membrane potential E_R (-30 mV to -80 mV) is more positive than the potassium equilibrium potential E_K, there is a net electrochemical driving force for potassium ions to diffuse out of the cell. Under physiological conditions, potassium channels therefore always conduct the flow of potassium ions out of the cell, leading to a shift of the membrane potential in the negative direction (towards the potassium equilibrium potential). In the long run, the maintenance of a stable resting potential depends on the presence of sodium-potassium pump. It simultaneously pumps two K^+ ions into and three Na^+ ions out of the cell against their concentration gradients and thus helps to maintain a chemical gradient for K^+ across the cell membrane.

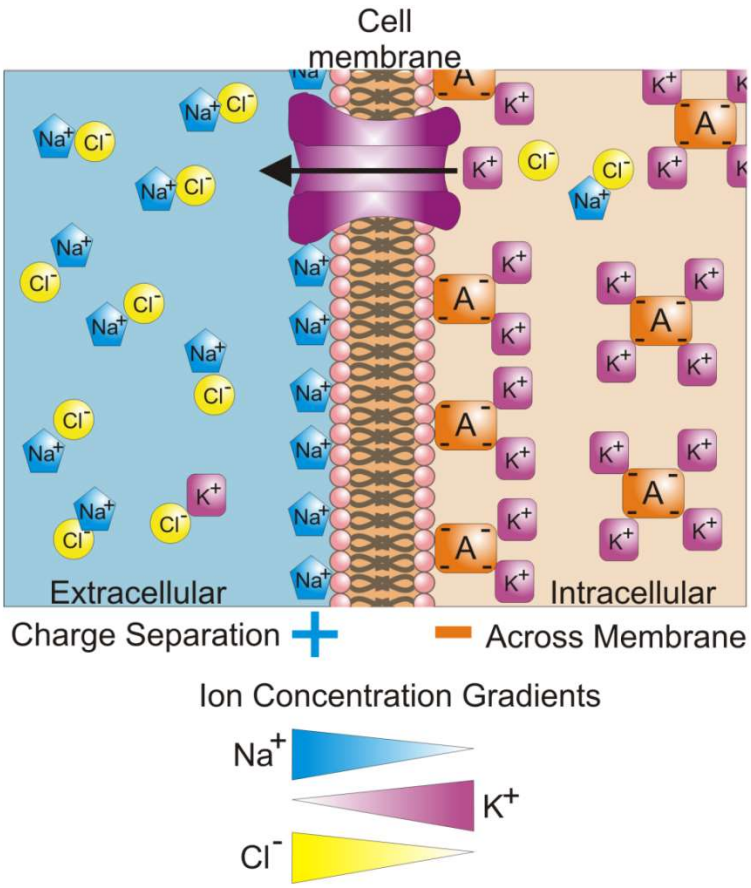

Figure 1.1: The resting membrane potential is caused by different concentrations of the principal cellular ions on both sides of the cell membrane. The concentration of K^+ ions is larger inside the cell, while the concentrations of Na^+ and Cl^- ions are larger outside the cell, leading to concentration gradients that are directed out of or into the cell, respectively. (Vojtěch Dostál, Wikipedia)

Potassium channels are multimers that consist of either two or four subunits. However, the basic pore structure always comprises a four-fold assembly of two transmembrane helices connected by a pore-loop. The pore-loop contains the highly conserved selectivity filter that is formed by five amino acids, TxGYG, and termed signature sequence. This sequence adopts a unique structure by aligning its electro-negative carbonyl oxygen atoms toward the centre of the pore and thus building four sequential K^+ binding sites, S1 to S4, each of which is formed by eight oxygen atoms.

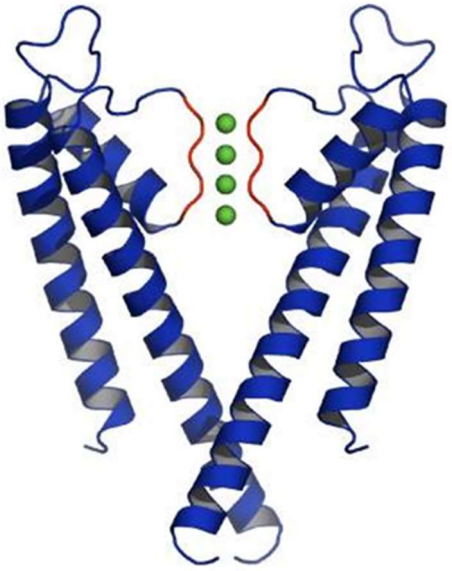

Figure 1.2: Two subunits of a tetrameric potassium channel. The selectivity filter region is colored red; K^+ ions that occupy the four possible binding sites are shown as green circles. (Valiyaveetil *et al.,* 2006)

As ions in solution strongly interact with water molecules that form a hydration shell around the atom, potassium ions are generally surrounded by eight water molecules. When K^+ ions enter the pore of the potassium channel, they are stripped of their hydration shell and the oxygen atoms of the first K^+ binding site act as surrogate H_2O molecules. This process allows K^+ ions to be passed through the narrow pore at a relatively low energy cost. It is the basis of the selectivity of potassium channels, which excludes the passage of other cellular cations, and of the high transport rate. Ca^{2+} ions are too large to fit through the pore and Na^+ ions are too small to bind to all eight carbonyl oxygens that line the selectivity filter, resulting in a much higher activation energy for the passage through the pore (Doyle *et al.,* 1998; Morais-Cabral *et al.,* 2001; Zhou *et al.,* 2001). High-resolution structural studies and electron density maps indicate that, in the conducting state, there are two alternating states by which K^+ ions move through the channel (Figure 1.3).

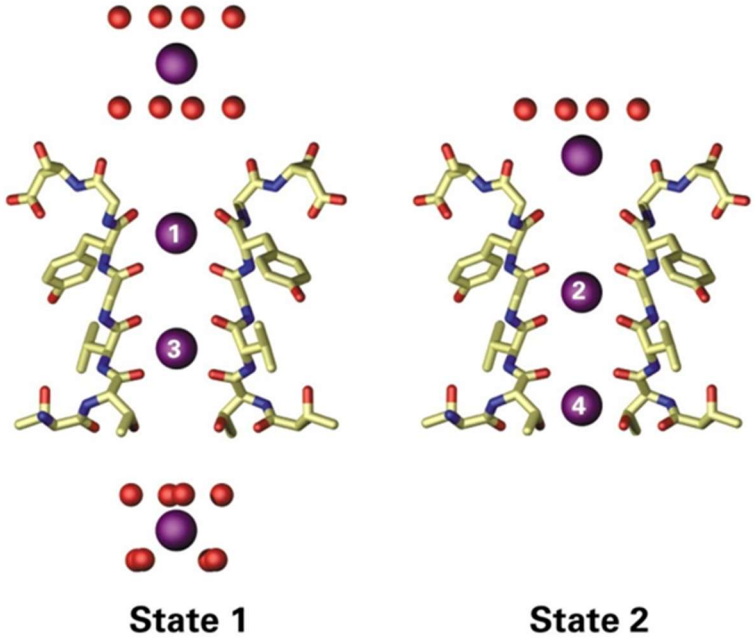

Figure 1.3: The two alternating states by which K^+ ions move through a potassium channel. In state 1, K^+ ions occupy positions 1 and 3 within the selectivity filter and there is a fully hydrated K^+ ion within the vestibule. During transformation of state 1 into state 2, K^+ ions move forward to positions 2 and 4 and a formerly fully hydrated K^+ ion on the exoplasmic site loses four of its eight water molecules. During transformation of state 2 into state 1, the K^+ ion at position 4 moves into the vestibule and picks up eight water molecules, while the K^+ ion on the exoplasmic site moves into position 1. (Lodish, 5th edition)

The potassium channel subunits of mammals can be subdivided into four families based on their structure and functional properties: (i) Channel subunits with six or seven transmembrane domains and one pore loop (6/7TM-1P) that form calcium-activated potassium channels which open in response to the presence of calcium ions and in response do depolarisation. (ii) Channel subunits with six transmembrane domains and one pore loop (6TM-1P) that form voltage-gated potassium channels which are regulated by changes in the membrane potential. (iii) Channel subunits with four transmembrane domains and two pore loops (4TM-2P) that form K2P channels. (iv) Channel subunits with two transmembrane domains and one pore loop (2TM-1P) that form inwardly rectifying potassium channels which conduct current more easily into than out of the cell.

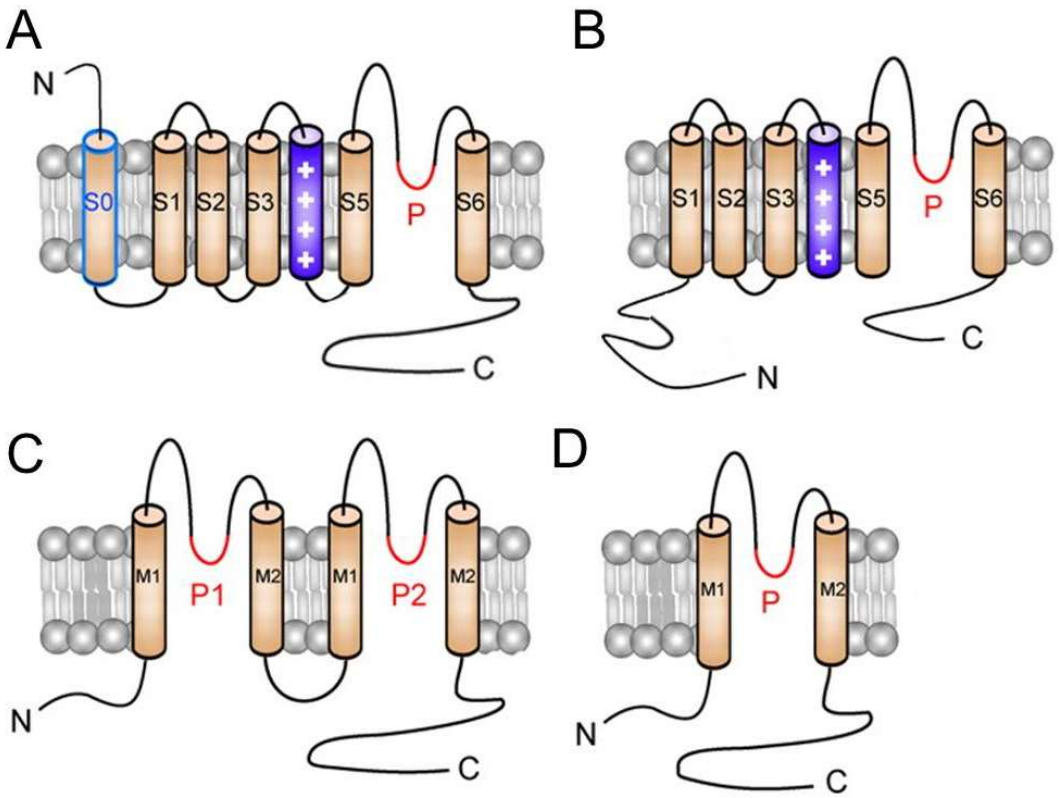

Figure 1.4: The four different classes of potassium channels. A) Calcium-activated potassium channels, **B)** voltage-gated potassium channels, **C)** K2P channels and **D)** Kir channels. The pore-domain is indicated in red; the voltage sensing helices are colored dark blue. (Benarroch 2009)

1.1.2 Inward rectifier channels

Inwardly rectifying (Kir) potassium channels are an important class of K^+ channels that regulates membrane excitability, heart rate, vascular tone, insulin release and salt flow across epithelia. Kir channels are characterized by their preference to conduct potassium ions into rather than out of the cell. Given an equal but oppositely directed chemical driving force, K^+ conductance into the cell considerably exceeds K^+ conductance out of the cell.

The family of inward rectifiers consists of seven subfamilies termed Kir1.x to Kir7.x that can further be classified into four functional groups. Classical Kir channels (Kir2.x), G-protein coupled channels (Kir3.x), ATP-sensitive channels (Kir6.x) and transport channels (Kir1.x, Kir4.x, Kir5.x and Kir7.x) (Figure 1.5).

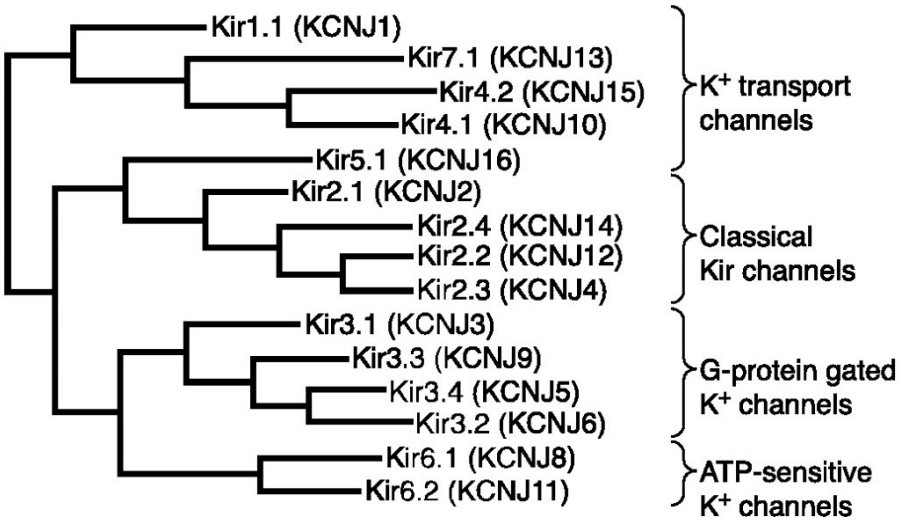

Figure 1.5: Amino acid sequence alignment and phylogenetic analysis of all known subunits of human Kir channels. The 15 known subunits can further be classified into four functional groups. (Hibino *et al.,* 2010)

A functional Kir channel is composed of four subunits and can either be homo- or heterotetrameric, although heteromerization generally occurs between members of the same subfamily. A single Kir channel subunit consists of two transmembrane domains, connected by a short pore loop that harbors the potassium selectivity filter and intracellularly located NH_2- and COOH-termini.

The characteristic inwardly rectifying properties of Kir channels are due to a potential dependent block of the channel pore by intracellular Mg^{2+} and polyamines. Upon depolarization, these substances bind to residues localized in transmembrane and cytoplasmic regions of the channel and mechanically block the channel pore (Kurachi 1985; Ficker *et al.,* 1994; Lopatin *et al.,* 1994). The cytoplasmic region is hereby thought to work as an intermediate binding site that increases the local concentration of polyamines which then plug the pore by binding to residues located in the transmembrane domain (Lopatin *et al.,* 1995; Lee *et al.,* 1999; Kubo and Murata 2001). In response to hyperpolarization, the inward current increases due to a fast, time-independent unblocking of the pore by Mg^{2+} that is followed by a slower, time dependent polyamine unblocking (Lopatin *et al.,* 1995).
However, not all Kir channels show the same degree of inward rectification. How strong a Kir channel acts as an inward rectifier depends on its binding affinity for blocking molecules. All strong inward rectifiers have a negatively charged aspartic acid in the TM2 helix, whereas the equivalent residue in weak inward rectifiers is uncharged. The negative charge in this position increases the affinity for Mg^{2+}, thereby increasing rectification (Lu and MacKinnon 1994; Stanfield *et al.,* 1994; Yang *et al.,* 1995).

The conductance of all inwardly rectifying potassium channels, except for Kir7.1 (Doring et al. 1997; Krapivinsky et al. 1998), increases with a rising extracellular potassium concentration $[K^+]_o$. This increase is roughly proportional to the square root of $[K^+]_o$ and is a property of the open channel pore (Hagiwara and Takahashi, 1974; Sakmann and Trube, 1984). Under physiological conditions, Kir channels therefore generate large K^+ currents at potentials negative to E_K but permit less current flow at potentials positive to E_K. Cells that exhibit a large Kir conductance show a resting membrane potential close to E_K (Hagiwara and Takahashi, 1974, Miyazaki et al. 1974, Noble et al. 1965).

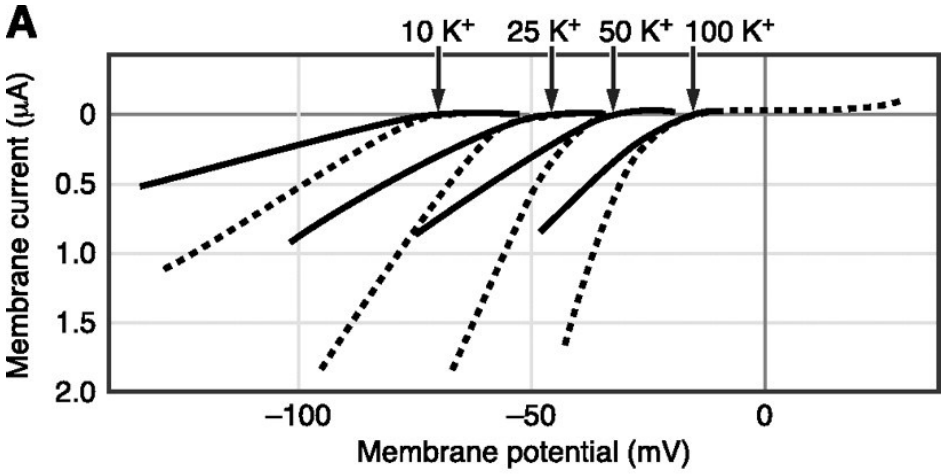

Figure 1.6: The dependence of inward rectification and conductance of Kir channels on $[K^+]_o$. I-V relationships of the starfish egg cell membrane at four different extracellular $[K^+]_o$ (10, 25, 50, and 100 mM) in Na^+-free medium. Continuous and dotted lines indicate instantaneous and steady-state currents, respectively. (Hibino *et al.,* 2010, data originally published by Hagiwara *et al.,* 1976)

The physiological function and activity of Kir channels can be modulated by regulation of pore opening, ion flux and intracellular localization of the channels. Major factors that regulate pore opening and ion flux through Kir channels include ions, polyamines, nucleotides, lipids, and a variety of intracellular proteins (Hilgemann and Ball 1996; Huang *et al.,* 1998). Gating is controlled by two distinct mechanisms, slow gating and fast gating, that have been linked to the bundle crossing (Trapp *et al.,* 1998; Yi *et al.,* 2001) and the selectivity filter (Guo and Kubo 1998; Choe *et al.,* 2000; Proks *et al.,* 2001), respectively. The majority of Kir channels can effectively be blocked by Ba^{2+} and Cs^+. The effect of Ba^{2+} and Cs^+ on Kir currents is dependent on the membrane potential and $[K^+]_o$. It increases with increasing hyperpolarization of the membrane and decreases as $[K^+]_o$ increases (Hagiwara *et al.,* 1976; Hagiwara *et al.,* 1978).

1.1.3 Kir2.2 channels

The Kir2.x family of potassium channels consists of five members, Kir2.1, Kir2.2, Kir2.3, Kir2.4 and Kir2.6, which can form functional homo- and hetero-tetramers (Preisig-Muller *et al.,* 2002; Schram *et al.,* 2002; Zobel *et al.,* 2003).
Kir2.2 plays a particularly important role in the heart. Together with Kir2.1 and Kir2.3, Kir2.2 channels represent the molecular basis of the inwardly rectifying potassium current I_{K1} which determines the stable resting potential of cardiac myocytes and is involved in shaping the action potential. During the plateau phase of the action potential the inward rectifiers are mostly closed, thus reducing the inward current required to maintain depolarization (Nichols *et al.,* 1996). The rapid, potential dependent unblock of inward rectifier channels during the initial phase of repolarization (Ishihara and Ehara 1998) contributes to the 'regenerative' phase of repolarization of the action potential (Shimoni *et al.,* 1992). Reduction of inward rectifier current is expected to increase the propensity for arrhythmias (Jongsma and Wilders 2001; Plaster *et al.,* 2001).
Kir2.2 activity is modulated through different mechanisms. The phosphoinositide PI(4,5)P2 activates the channel by initiating pore opening (Hansen *et al.,* 2012) and it was recently shown that this effect can be inhibited by CO (Liang *et al.,* 2014). PI(4,5)P2 binds to an interface between the transmembrane domain and the cytoplasmic domain of Kir2.2 and initiates a conformational change that leads to pore opening (Hansen *et al.,* 2012).

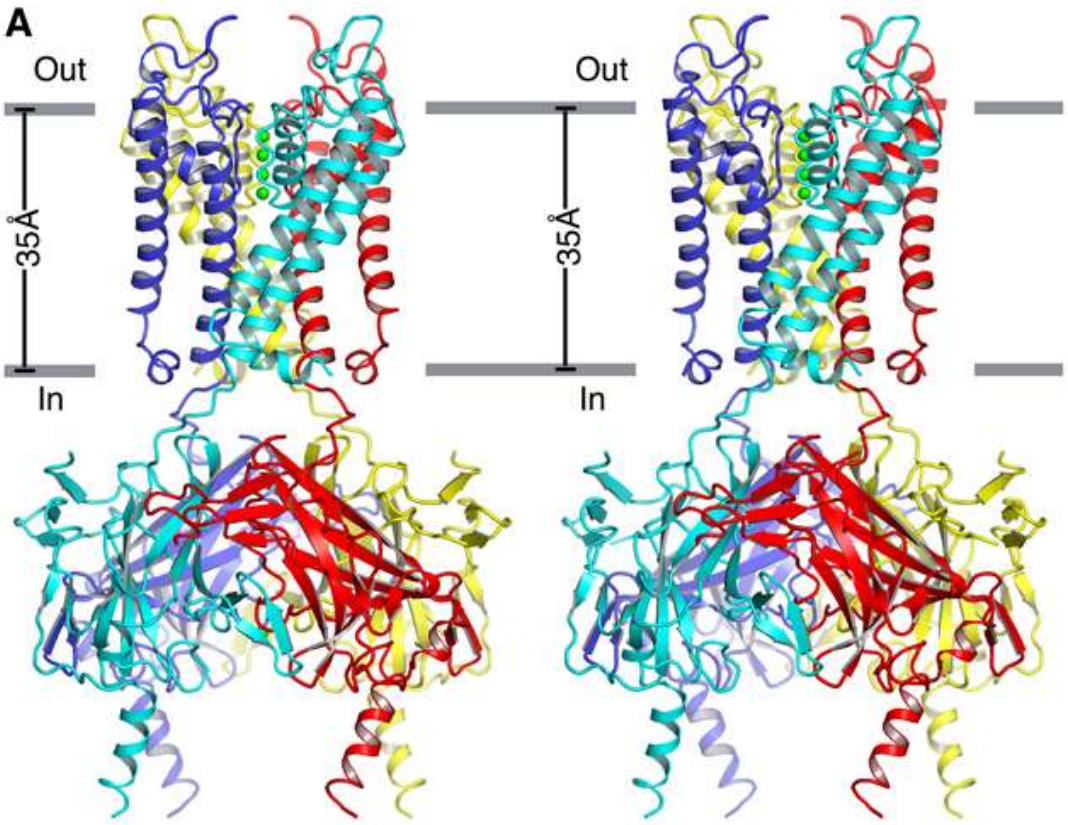

Figure 1.7: Crystal structure of eukaryotic Kir2.2. The four subunits of the Kir2.2 channel are shown in different colours. The approximate boundaries of the lipid bilayer are shown as grey bars, the four potential binding sites for potassium ions as green circles. (Tao et al., 2009)

In recent years, it has become obvious that in addition to direct modulation of the biophysical properties of an ion channels, the regulation of the intracellular traffic plays an equally important role in determining the current density at the cell surface and thus its functional role (Lai and Jan 2006; Welling 2013; Kilisch *et al.,* 2015). Anterograde transport, endocytosis rate and recycling of cargo are affected at multiple levels to fine-tune the amount of active plasma membrane resident proteins. Although several ER and Golgi export signals were found in the structure of Kir2.2 (Ma *et al.,* 2001; Tong *et al.,* 2001), little is known about the regulation of the channel density at the plasma membrane.

1.2 The family of serum- and glucocorticoid-inducible protein kinases (SGKs)

The family of serum- and glucocorticoid-inducible kinases consists of three members termed SGK1, SGK2 and SGK3. They are closely related to the PKB/Akt kinases, with which they share considerable sequence homology and the same mechanism of activation. While SGK1 and SGK3 are ubiquitously expressed, SGK2 mRNA is only present in epithelial tissues including liver, kidney and pancreas, and, at lower levels, in the brain (Kobayashi *et al.,* 1999). Even though the three SGK isoforms share about 80 % homology regarding their kinase domains, they also display important structural differences. The short C-terminal domains only share 44 - 68 % homology and the N-termini display hardly any similarities (Kobayashi *et al.,* 1999). SGK3 possesses a relatively long N-terminus containing a PX-domain that binds the phosphoinositide PI(3)P and thus localizes SGK3 to PI(3)P containing membranes in the cell (Virbasius *et al.,* 2001). In contrast, SGK1 and SGK2 possess short N-termini and were found to be localized both to the nucleus and the cytoplasm (Buse *et al.,* 1999 He et al). SGK1 supposedly translocates from the cytoplasm to the nucleus during S and G2/M phases of the cell cycle in response to growth factors or hormonal stimulation. This stimulus-induced nuclear import is mediated by a NLS-sequence that binds to importin-α and is localized in the kinase central domain (Buse *et al.,* 1999; Bell *et al.,* 2000). Similar NLS-like sites were found in the central domains of SGK2 and SGK3 (Maiyar *et al.,* 2003); however, the functional relevance of these sites has not been investigated yet.

1.2.1 Regulation of the serum- and glucocorticoid-inducible protein kinases

For full activation, the serum- and glucocorticoid-inducible kinases have to be phosphorylated at two conserved phosphorylation sites. One is in their kinase domain and the other one is in a hydrophobic motif (HM) at their C-terminus (SGK1: Thr^{256} and Ser^{422}, SGK2: Thr^{193} and Ser^{356}, SGK3: Thr^{253} and Ser^{419}).

The activation-loop threonine in the kinase domain is phosphorylated by the 3-phosphoinositide dependent kinase (PDK1) (Kobayashi *et al.,* 1999; Park *et al.,* 1999). The C-terminal hydrophobic domain of SGK1 is phosphorylated by the mTOR complex 2 (Garcia-Martinez and Alessi 2008), whereas the corresponding kinase for SGK2 and SGK3 remains to be discovered. It has been given the preliminary name PDK2. The phosphorylation of the C-terminal serine by PDK2/mTORC2 is the first crucial phosphorylation step and a prerequisite for the PDK1-catalysed phosphorylation of the activation-loop threonine (Figure 1.8). The interaction between SGK and PDK1 is mediated by a pocket in the kinase domain of PDK1 termed PDK1-interacting fragment (PIF)-binding domain. Phosphorylation of SGK at the HM domain promotes the binding of PDK1 to SGK via its PIF-binding domain and increases the subsequent phosphorylation rate of the activation loop (Biondi *et al.,* 2001).

Similar to Akt, phosphorylation and activity of the three serum- and glucocorticoid-inducible kinases in a mammalian expression system can be increased by treatment of cells with the PI3K class I agonists' insulin, IGF1 or exposure to oxidative stress. Preincubation of cells with the PI3K inhibitors wortmannin and LY 294002 strongly suppresses the activation, suggesting that it is mediated by PI3K class I. But in contrast to Akt, activation of SGKs via PI3K is independent of PDK1. The target of the PI3K signaling pathway therefore seems to be PDK2/mTORC2 (Kobayashi and Cohen 1999; Kobayashi *et al.,* 1999; Park *et al.,* 1999; Tessier and Woodgett 2006a).

The activation of Akt by PDK1 depends on the presence of $PI(3,4,5)P_3$. This phosphoinositide is localized to the plasma membrane and a product of PI3K class I. Both Akt and PDK1 contain a PH domain that interacts with $PI(3,4,5)P_3$, bringing them in close proximity and enabling the phosphorylation of PKB. It is likely that the SGKs, because they are lacking a PH domain that localizes them in close proximity to PDK1, rely more strongly than Akt on structural interactions with PDK1 to be phosphorylated. This hypothesis is supported by the observation that the scaffold protein Na^+/H^+ exchanger regulating factor 2 (NHERF2) promotes the interaction between PDK1 and SGK1. NHERF2 interacts with the PDZ binding motif of SGK1 via its PDZ domain and with the PIF binding pocket of PDK1 via its PIF tail and thus brings SGK1 and PDK1 in

spatial proximity and facilitates the phosphorylation of SGK1 (Chun *et al.,* 2002).

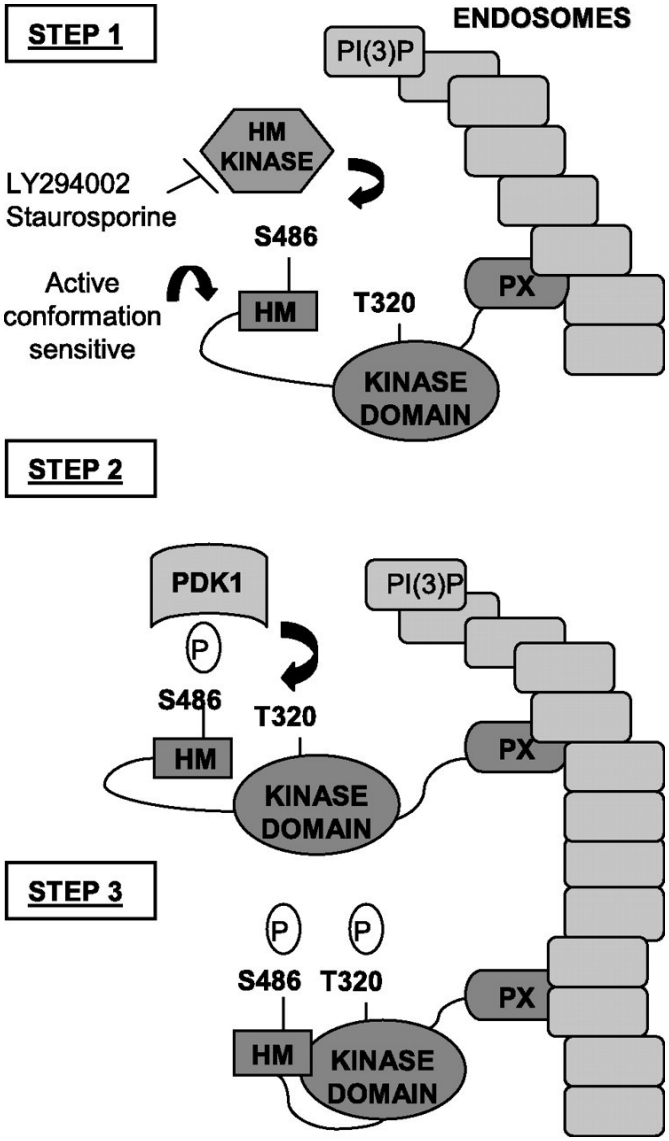

Figure 1.8: Mechanism of SGK3 activation. Upon PI3K activation, a kinase (PDK2) becomes activated which phosphorylates the SGKs at their HM-domain. This enables PDK1 to bind and phosphorylate the activation-loop. The doubly phosphorylated proteins adopt an active conformation (Tessier and Woodgett 2006a).

In contrast to SGK1 and SGK2, the activation of SGK3 was shown to depend on the subcellular localization of the kinase. When a mutation that abrogates the binding to PI(3)P was introduced into the PI binding pocket of SGK3, phosphorylation of both crucial phosphorylation sites was abolished. However,

the introduction of a phospho-mimicking mutation in the HM-domain made the second phosphorylation step independent of the localization of SGK3 in the cell (Tessier and Woodgett, 2006), indicating that only the phosphorylation of the HM-domain depends on the localization to PI(3)P containing membranes.
The activities of SGK1 and SGK3 are also regulated on the transcriptional level. SGK1 mRNA level was shown to increase greatly upon exposure to serum or glucocorticoids for 1 h in several cell lines (Webster *et al.,* 1993; Kobayashi and Cohen 1999). SGK3 can be transcriptionally induced by estrogen (Wang *et al.,* 2011) and androgen (Wang *et al.,* 2014). In addition to its transcriptional regulation, SGK1 is also regulated by polyubiquitination and subsequent degradation by the 26S proteasome (Bogusz *et al.,* 2006).

1.2.2 Role of SGK3 in the regulation of cellular functions

A number of studies have shown that SGK3 increases the current mediated by a broad range of ion transporters and channels, including glutamate transporter (Boehmer *et al.,* 2003; Böhmer *et al.,* 2010), Na^+ channels (Naray-Fejes-Toth *et al.,* 1999; Debonneville et al., 2001; Alvarez de la Rosa et al., 2004; Thomas et al., 2011), K^+ channels (Gamper *et al.,* 2002; Yun 2002; Embark *et al.,* 2003) and the Na^+ /K^+ -ATPase (Henke *et al.,* 2002).
However, the molecular mechanisms linking SGK3 activity and an increase in current amplitude are not yet fully understood (Lang *et al.,* 2006; Tessier and Woodgett 2006b). Several mechanisms have been proposed to be responsible for the increase in current caused by activation or co-expression of SGK3: (i) Phosphorylation of the ubiquitin ligase Nedd4-2 has been shown to affect the current amplitudes of KCNE/KCNQ, ENaC and hERG (Lamothe and Zhang 2013). (ii) Phosphorylation of the transcription factor FOXO3a has been shown to affect the transcription rate of several proteins (Xu *et al.,* 2009). (iii) Phosphorylation of the phosphoinositide kinase PIKfyve has been shown to increase the current amplitudes of Kir2.2 (Seebohm *et al.,* 2012b), TRPV6 (Sopjani *et al.,* 2010) and hERG (Pakladok *et al.,* 2013).
These observations indicate that SGK3 plays a role in a variety of cellular responses that require upregulation of certain channels and transporters; it may for example be involved in salt and glucose homeostasis (Lang *et al.,* 2006). A

possible function in glucose homeostasis is supported by observations made in SGK3 knockout mice: Although $SGK3^{-/-}$ mice had no defects in glucose homeostasis, characterization of SGK3/Akt double knockout mice revealed that these mice had a markedly worse glucose homeostasis than Akt single knockout mice. It was proposed that SGK3 might stimulate proliferation and insulin release in β-cells by controlling the expression and activity of β-catenin (McCormick *et al.,* 2004; Yao *et al.,* 2011).

Furthermore, SGK3 has been shown to phosphorylate a number of cellular target proteins that play a role for cell proliferation, survival and migration. The kinase recognizes and phosphorylates the consensus sequence R-X-R-X-XS/T-Φ (Kobayashi *et al.,* 1999; Park *et al.,* 1999), where X is any amino acid and Φ is a hydrophobic amino acid. SGK3 might affect cell proliferation by phosphorylating and thus inactivating the transcription factor Forkhead-Box-Protein O3 (FOXO3a). FOXO3a regulates the transcription of several members of the cell cycle machinery, thus SGK3-mediated downregulation of FOXO3a is likely to have an impact on cell cycle regulation at multiple levels (Bruhn *et al.,* 2013).

SGK3 can also phosphorylate and inactivate Glycogen synthase kinase 3 (GSK3β). GSK3β can in turn mark cyclin D1 for degradation by the proteasome; cyclin D1 is an important factor for cell cycle transition. The inactivation of GSK3β by SGK3 therefore allows cyclin D1 to continue its role in the cell cycle (Dai *et al.,* 2002; Vivanco and Sawyers 2002). The inactivation of GSK3β may also alter β-catenin dynamics, leading to the formation of adherens junctions and tight junction sealing (Failor *et al.,* 2007). These results indicate a role for SGK3 in the organization of cell polarity and migration. This hypothesis is supported by the characteristics of the SGK3 knockout mice. The $SGK3^{-/-}$ mice demonstrated a defect in hair follicle morphogenesis, producing a wavy hair phenotype. Further characterization showed a disorganization of hair follicles and cells in the outer root shear, suggesting a deregulation of cell polarity (McCormick *et al.,* 2004; Alonso *et al.,* 2005). The defect correlates with a reduced nuclear accumulation of β-catenin in hair bulb keratinocytes and in cultured keratinocytes; SGK3 is therefore thought to modulate activation of β-catenin/Lef-1-mediated gene transcription (McCormick *et al.,* 2004). The

relatively mild phenotype of the SGK3 knockout mouse suggests the presence of compensatory mechanisms; possibly SGK1 and SGK2 are partly able to compensate for SGK3. SGK3 has also been shown to be involved in cell survival signaling in estrogen receptor-positive breast cancer cells (Wang *et al.,* 2011), possibly via phosphorylation of Flightless-I (FLI-I). FLII acts as a co-activator for nuclear hormone receptors such as estrogen receptor (ER), enhancing receptor activity and promoting proliferation and survival (Xu *et al.,* 2009). Since SGK3 is also transcriptionally activated by estrogen, there may exist a positive feedback loop between SGK3 and the estrogen receptor.

1.2.3 Pathophysiological relevance of SGK3

In many human tumors, PI3K class I signaling is deregulated, leading to a hyper-activation of the PI3-K cascade. Akt is a major downstream effector of PI3K and is involved in cell transformation and tumorigenesis (Manning and Cantley 2007). Most studies investigating the mechanism by which deregulation of PI3K signaling drives the malignant transformation of cell have therefore focused on Akt. Nevertheless, it is now emerging that other downstream targets are also able to promote malignant transformation of cells independent of Akt. Given that it plays a role in cell survival, proliferation and growth, SGK3 has been proposed to be a candidate for PI3-K signaling to tumorigenesis (Bruhn *et al.,* 2013). Indicators for this theory were found in different solid tumor tissues.
As mentioned in chapter 1.2.2, SGK3 has been shown to be involved in cell survival signaling in estrogen receptor-positive breast cancer cells (Wang *et al.,* 2011), thereby driving tumorigenesis. Hepatocellular carcinoma cells demonstrated an increase in SGK3 transcript expression; enforced expression of SGK3 further resulted in increased cell growth, colony formation and anchorage-independent growth while SGK3 knockdown significantly decreased these processes (Liu *et al.,* 2012). SGK3 may therefore be a target for new therapeutic approaches in cancer treatment and a knockdown with small interfering RNA or specific inhibitors in malignant cells will give valuable insights in the precise function of SGK3 in oncogenic signaling in certain tumors.

1.3 Membrane trafficking

Cellular organelles involved in the exocytic and endocytic transport of proteins have a distinctive spatial distribution and their identity is determined by a specific combination of Rab GTPases, SNARE proteins and phosphoinositides.

1.3.1 Rab proteins

Rab proteins constitute the largest family of small GTPases. They function as molecular switches and alternate between two conformational states: a GTP bound and a GDP bound form. Rab GTPases exist both in a soluble form in the cytoplasm and specifically localized to distinct intracellular membranes. In the cytosol, they are kept in their GDP-bound form through association with GDP-dissociation inhibitors (GDI), which prevent the exchange of GDP for GTP (Matsui *et al.,* 1990; Ullrich *et al.,* 1993). Their reversible association with distinct membranes is mediated by geranylgeranyl-groups that are covalently attached to two conserved cysteine residues in the C-terminus by the enzyme geranylgeranyl transferase (GGT) (Chavrier and Zerial 1990; Sasaki *et al.,* 1990; Seabra 1991); freshly synthesized Rab proteins are presented to the GGT by the Rab escort protein (REP) (Alexandrov *et al.,* 1994). The relocalization of Rab GTPases from the cytoplasm to their target membrane is not completely understood. The membrane-bound GDI displacement factors (GDF) are thought to play a key role by recognizing specific Rab-GDI complexes and promoting the GDI release, thereby facilitating the interaction of the GTPase with its target membrane and making it available for the interaction with its GEF (Sivars *et al.,* 2003) (Figure 1.9).

Rab proteins undergo cycles of GTP binding and its subsequent hydrolysis to GDP. These exchange and hydrolysis reactions are catalyzed by guanine-nucleotide exchange factors (GEF) and GTPase activating proteins (GAP), which therefore play a key role as regulators of the GTP-GDP-cycle (Yoshimura *et al.,* 2010; Guo *et al.,* 2013; Wandinger-Ness and Zerial 2014). In their GTP bound form, Rab proteins can interact with numerous effector molecules including kinases, phosphatases, tethering factors and motor proteins and recruit them to the target membrane. The GTP bound form is therefore

considered to be the active form. However, the regular cycling between the GTP- and the GDP-bound state is equally important for the temporal and spatial regulation of membrane transport processes. These conformational changes are ‘decoded’ by their effector proteins and translated into the transient assembly of specific multiprotein machineries, which regulate membrane trafficking processes involving the sorting of cargo, the formation of functional transport vesicles, membrane tethering and fusion and also the transport of vesicles along the cytoskeleton (Somsel Rodman and Wandinger-Ness 2000; Park 2013).

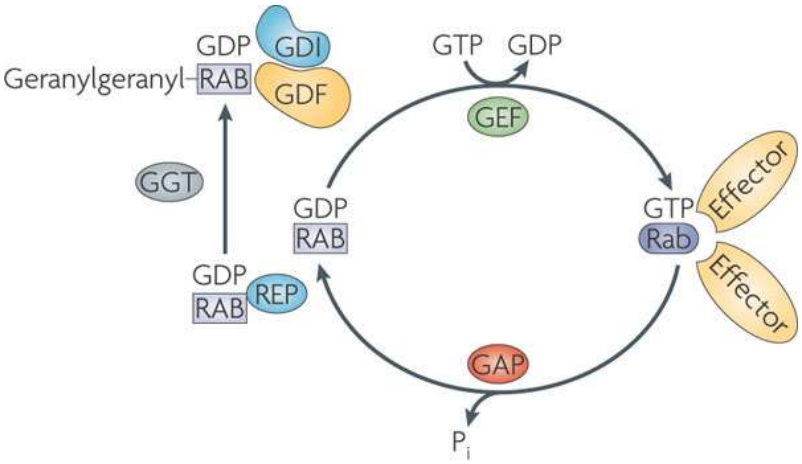

Figure 1.9: The alternation of Rab proteins between two conformational states. Freshly synthesized, GDP-bound Rab protein in the cytoplasm is recognized by a Rab escort protein (REP) that presents it to the geranylgeranyl transferase (GGT) which geranylgeranylates the GTPase. The GDP-dissociation inhibitor (GDI) keeps the Rab proteins in its soluble state. This GDI-Rab complex is targeted by the GDI displacement factor (GDF) to specific membranes where it is activated and the GDP is exchanged for GTP, a process that is catalyzed by guanine nucleotide exchange factors (GEFs). The GTP-bound form is recognized by a variety of effector proteins. It is converted back to the GDP-bound form by hydrolysis of GTP to GDP. This process is driven by intrinsic GTPase activity of the Rab protein and the GTPase activating proteins (GAPs). (Stenmark 2009)

About three quarters of all known Rab proteins have been associated with endocytic membranes and are localized to distinct organelles (Chavrier and Zerial 1990); Rab proteins localized to the same organelle occupy distinct membrane micro domains (Sönnichsen *et al.,* 2000) (Figure 1.10).

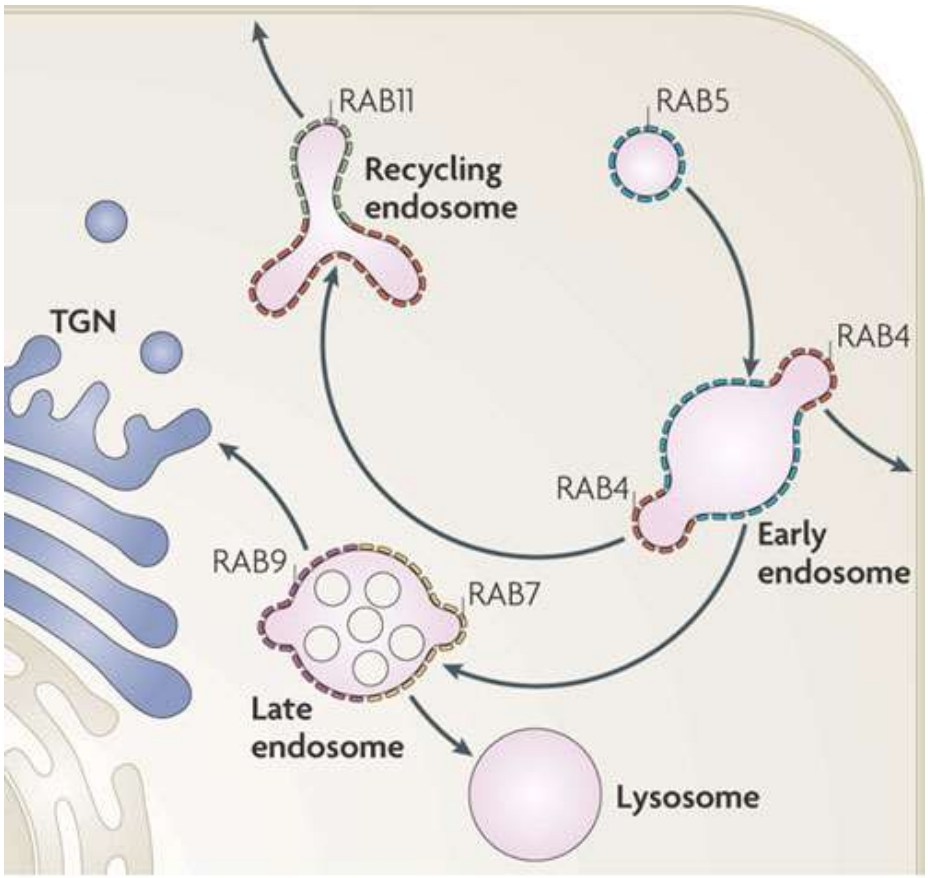

Figure 1.10: Typical intracellular distribution of Rab proteins to endosomal compartments. (Stenmark 2009)

The early endosome contains separate microdomains that are enriched in either Rab5 or Rab4. Rab5 is involved in the formation of clathrin coated vesicles (CCVs), in the fusion between CCVs and early endosomes and in the homotypic fusion between early endosomes (Gorvel *et al.,* 1991; Bucci *et al.,* 1992; McLauchlan *et al.,* 1998). Rab4 is involved in the fast recycling pathway which retrieves endocytosed proteins back to the plasma membrane within 2-3 min (Schmid *et al.,* 1988; van der Sluijs *et al.,* 1992; Mayor *et al.,* 1993). Proteins recycled via this pathway are sorted to Rab4-positive membrane domain patches in the early endosome by rabenosyn-5, an effector molecule that interacts with both Rab5 and Rab4 and causes merging of Rab4 and Rab5 positive domains (de Renzis *et al.,* 2002). In the current model, Rab4 positive domains bud from the early endosome and recycle back to the plasma membrane.

The pericentriolar recycling endosome contains domains that are enriched in Rab4 and Rab11. Rab4 is involved in vesicle trafficking from the early to the recycling endosome and Rab11 is involved in the further transport of vesicles to the plasma membrane via a slow recycling pathway (Ullrich *et al.,* 1996; Sönnichsen *et al.,* 2000). Rab11-positive late recycling endosomes are delivered to the cell surface along actin filaments, where these vesicles are tethered to the plasma membrane by binding of Rab11 to the exocyst component SEC15 (Guichard *et al.,* 2014).

The late endosome contains Rab7- and Rab9-positive domains that are responsible for the trafficking of cargo to the lysosome (Feng *et al.,* 1995; Méresse *et al.,* 1995) and the trans-Golgi network (TGN) (Lombardi *et al.,* 1993), respectively.

One important function that is common to these Rab proteins and their respective effector molecules is the regulation of phosphoinositide metabolism.

1.3.2 Phosphoinositides

Phosphoinositides are phosphorylated derivatives of phosphatidylinositol. The hydroxyl groups at the three, four and five carbon positions of the inositol ring can be phosphorylated, either singularly or in combination, resulting in seven different types of phosphoinositides (Figure 1.11). Although they have a low abundance in the cell, constituting only about 10 % of total cellular phospholipids, they are key components of cellular membrane signaling.

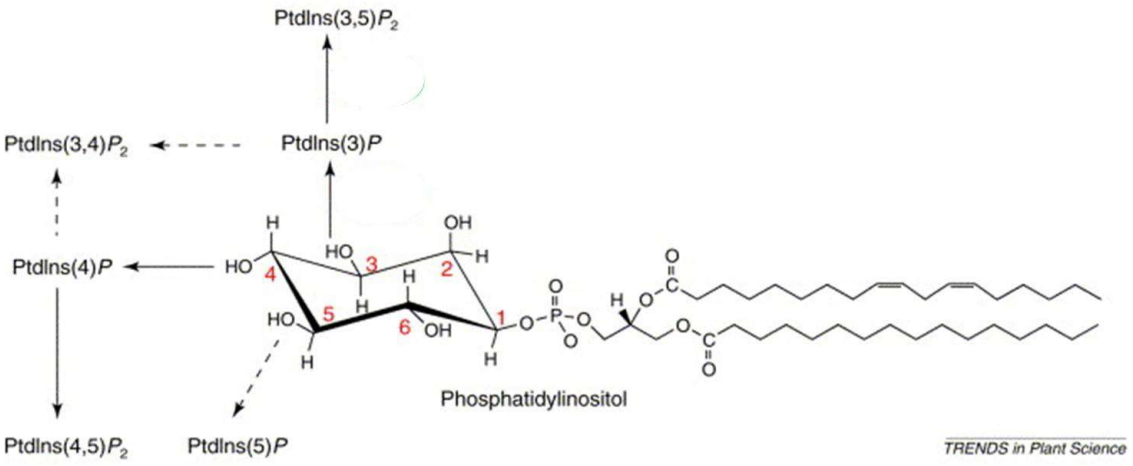

Figure 1.11: Structure of phosphatidylinositol and its seven phosphorylated derivates. (Drobak and Heras 2002)

The specific phosphoinositide composition of an intracellular compartment is determined by a tightly regulated network of specific phosphoinositide kinases and phosphatases. Although these regulatory circuits are poorly understood, for each phosphoinositide there exists at least one antagonistic lipid kinase and phosphatase pair forming a PI-cycle. They can either work in a direct or in an indirect antagonistic way; an example of both mechanisms is given in Figure 1.12 (Botelho 2009). Some of the phosphoinositide kinases and phosphatases are integral membrane proteins, but most enzymes are cytosolic proteins that are targeted to a specific membrane by binding domains that recognize small GTPases or other core components of the trafficking machinery.

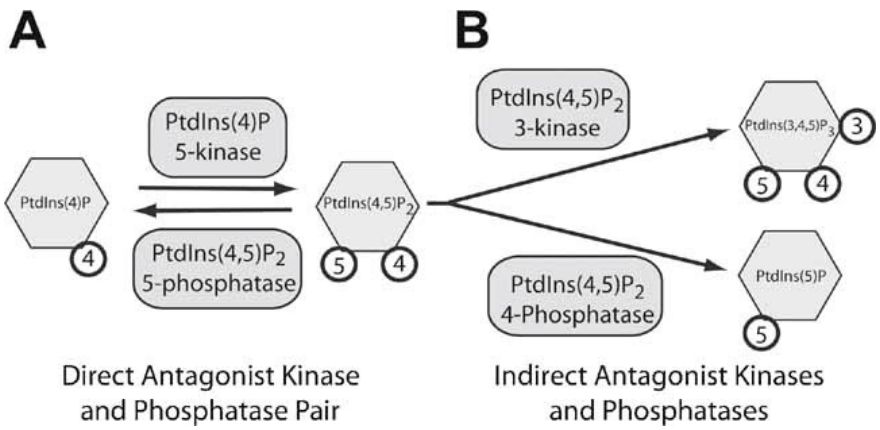

Figure 1.12: Phosphoinositide conversion mechanism through the example of PI(4,5)P_2. A) Direct antagonistic kinase-phosphatase pair. PI(4)P and PI(4,5)P_2 are interconverted by directly opposite enzymatic activities of a 5-kinase and a 5-phosphatase. **B)** Indirect antagonistic kinase-phosphatase pair. PI(4,5)P_2 is phosphorylated/dephosphorylated by a PI3-kinase or a PI4-phosphatase to generate PI(3,4,5)P_3 or PI(5)P, respectively. These enzymes both indirectly counteract the PI(4)P-5-kinase by acting on its product, PI(4,5)P_2. (Botelho 2009)

Phosphoinositides are concentrated in distinct membrane domains where they control the subcellular localization and activation of various effector proteins that possess PI-binding domains, such as the PH, FYVE, PX, ENTH, PH-GRAM, FERM and GLUE domains (Lemmon 2008, Krauss and Haucke 2011). Together with Rab proteins, they serve as markers of cell compartments and help to modulate a variety of functions including cytoskeletal organization, membrane fusion and fission, and signaling events particular to individual organelles.

PI(4,5)P_2 and PI(3,4,5)P_3 are concentrated in the plasma membrane (Martin 2001). Most surface PI(4,5)P_2 is generated from PI(4)P, which is the predominant phosphoinositide in the Golgi complex region. It is delivered to the cell surface by membrane carriers from the Golgi complex, but also produced locally at the plasma membrane. PI(4,5)P_2 is further converted to PI(3,4,5)P_2, mainly by class I PI3 kinase (Cantley 2002; Czech 2003). PI(3)P is present almost exclusively in early endosomes and internal vesicles of multivesicular bodies (Gillooly *et al.,* 2000). It is converted to PI(3,5)P_2 by the PI5-kinase PIKfyve during the maturation of early to late endosomes; PI(3,5)P_2 is present

on the membrane of late endosomes and lysosomes, where it is interconverted to PI(4,5)P_2.

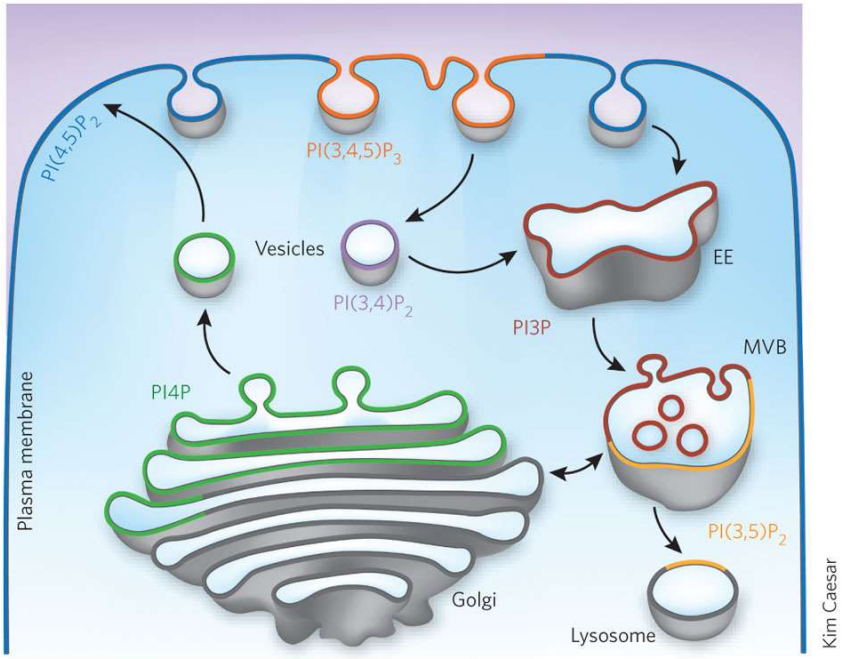

Figure 1.13: Typical intracellular distribution of different phosphoinositide species. EE: early endosome; MVB: multi vesicular body (Kutateladze 2010).

1.3.3 Rab GTPases and phosphoinositides cooperate in the organization of membrane trafficking

Rab proteins and phosphoinositides cooperate in determining the structural and functional identity of intracellular compartments and serve as organizers of membrane trafficking processes. On the one hand, phosphoinositides contribute to vesicular identity by recruiting specific proteins, for example Rab effectors, to restricted areas of cellular membranes. On the other hand, Rab proteins and other small GTPases contribute to vesicular identity by recruiting several PI kinases and phosphatases that regulate the metabolism of specific PIs and thus mediate a change in identity or maturation of the vesicles..

The small GTPase Rab5 defines the identity of early endosomes where it coordinates homotypic and heterotypic fusion events. It can also be detected on the plasma membrane (Chavrier and Zerial 1990), where it is involved in the formation of clathrin-coated vesicles (CCVs) (Gorvel *et al.,* 1991; Bucci *et al.,*

1992; McLauchlan *et al.,* 1998; Schmid and Mettlen 2013). Once Rab5 is activated and associated with the early endosomal membrane by a complex of the GEF Rabex-5 with Rabaptin-5, it recruits the class III PI3K complex, which then synthesizes the phosphoinositide PI(3)P (Christoforidis *et al.,* 1999). Rabaptin-5-Rabex-5 forms a complex with Rab5, thus stabilizing it on the membrane and initiating a positive feedback loop for the activation of Rab5 (Zerial and McBride 2001). Through a 'coincidence detection' mechanism (Carlton and Cullen 2005), Rab5 and PI(3)P cooperate in the recruitment of effector molecules including early endosome antigen 1 (EEA1) (Simonsen *et al.,* 1998; Christoforidis *et al.,* 1999; Lawe *et al.,* 2000), Rabenosyn-5 (Nielsen *et al.,* 2000), and Rabankyrin-5 (Schnatwinkel *et al.,* 2004). These effector proteins all contain a FYVE-domain that specifically binds to PI(3)P and binding motifs for GTP-bound Rab5; they are involved in early endosome membrane tethering and fusion. In addition to class III PI3K, Rab5 interacts with other enzymes involved in PI metabolism, including class I PI3K, which produces PI(3,4,5)P_2 from PI(4,5)P_2 at the plasma membrane and PI4- and PI5-phosphatases (Shin *et al.,* 2005; Hyvola *et al.,* 2005). Through the sequential activation of these enzymes, Rab5 can induce the dephosphorylation of PI(3,4,5)P_3 or PI(3,4)P_2 resulting in the formation of PI(3)P (Shin *et al.,* 2005).

In order for early endosomes to mature to late endosomes, the positive feedback loop activating Rab5 has to be disrupted. The identity of late endosomes is determined by Rab7 and the phosphoinositide PI(3,5)P_2, the maturation process therefore involves the exchange of Rab5 for Rab7 and the conversion of PI(3)P into PI(3,5)P_2. This process is called 'Rab conversion' and the SAND-1/Mon1 complex has been shown to play a crucial role. SAND-1/Mon1 displaces the Rab5 GEF Rabex5 from the membrane, thus abolishing the positive feedback loop of Rab5 activation. It further interacts with the CORVET/HOPS complex, which contains a GEF for Rab7, and thus recruits Rab7 to the membrane (Poteryaev *et al.,* 2010). PI(3,5)P_2 is synthesized by the 5-kinase, PIKfyve (Gary *et al.,* 1998), which is localized to the membrane by its PI(3)P-binding FYVE domain. Its activity is regulated by its activator ArPIKfyve/Vac14p and the PI(3,5)P_2 phosphatase Sac3/Fig4p, with which it forms a stable complex critical for both lipid kinase and phosphatases activities

(Sbrissa *et al.,* 2008; Ikonomov *et al.,* 2009). The PI conversion seems to be a necessary prerequisite for other endosome maturation steps. Some of the elements of the ESCRT machinery, which is responsible for the formation of intraluminal vesicles in multivesicular bodies, are recruited by both PI(3)P and $PI(3,5)P_2$ (Katzmann *et al.,* 2003; Whitley *et al.,* 2003;Teo *et al.,* 2006).

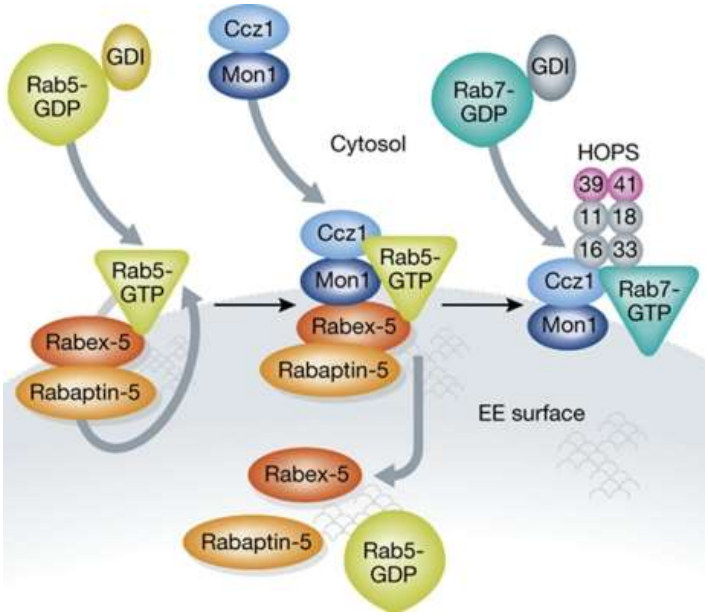

Figure 1.14: The Rab5/Rab7 conversion. Rab5 is recruited and activated to its GTP-bound by a complex of the GEF Rabex-5 and Rabaptin-5 by a positive feedback mechanism. To initiate the Rab switch, Mon1/SAND-1 complexed with Ccz1 binds to PI(3)P, causing the disassociation of Rabex-5 from the membrane and recruiting Rab7 through the HOPS complex (Huotari and Helenius 2011).

The observations described above gave rise to the current model, in which Rab GTPases that function sequentially are activated and inactivated in a 'cascade-like' manner. The recruitment of one GTPase leads to the recruitment of the next GTPase together with simultaneous inactivation of the upstream GTPase via a specific GAP and activation of the downstream GTPase via its GEF (Wandinger-Ness and Zerial 2014; Hutagalung and Novick 2011).

1.4 Goal of this study

The serum- and glucocorticoid-inducible kinase SGK3 has been shown to increase the surface expression of several channel and transporter proteins via phosphorylation of the ubiquitin ligase Nedd4-2, phosphorylation of the transcription factor FOXO3a and phosphorylation of the phosphoinositide kinase PIKfyve. However, for many of the target proteins, including the inward rectifier potassium channel Kir2.2, the underlying mechanism remains to be discovered.

The aim of this study was to investigate the mechanism underlying the SGK3 induced increase in Kir2.2 surface membrane expression in two heterologous expression systems, *Xenopus laevis* oocytes and mammalian COS-7 cells. For this purpose molecular-, cell- and electrophysiological methods as well as fluorescence microscopy were used.

2. Materials

2.2 Chemicals

All chemicals were purchased, if not mentioned separately in the text, from Sigma Aldrich, Carl Roth and Merck.

2.2 Media, Buffers and Solutions

All buffers and solutions were prepared with bidistilled water (ddH_2O) from a Milli-RO 12 Plus Water Filtration System (Merck Millipore). pH values were adjusted using a pH meter (Knick).

1 % Agarose-gel	1 g	agarose powder
	100 ml	1x TAE

The agarose was mixed with the TAE buffer and heated until the solution was boiling.

4 % paraformaldehyde	40 g paraformaldehyde
	1 l 1x PBS

The solution was heated to 60 °C and basidified with NaOH to dissolve the paraformaldehyde. When everything was dissolved, the pH was adjusted to 6.9 with HCl.

Anesthetic for the frog	0.6 g ethyl 3-aminobenzoate methanesulfonate salt was dissolved in 600 ml H_2O
Antibiotic stock solutions	100 mg / ml ampicillin in ddH_2O
	100 mg / ml kanamycin in ddH_2O

Cell culture medium	500 ml	DMEM
	10% (v/v)	FBS
	100 U/ml	penicillin
	100 U/ml	streptomycin

Collagenase solution: 40 mg Collagenase (C-6885, Sigma-Aldrich) were dissolved in 20 ml 1x OR2

LB medium (liquid)	10 g	NaCl
	10 g	peptone
	5 g	yeast extract
	ad 1 l	ddH_20

LB medium (solid)	10 g	NaCl
	10 g	peptone
	5 g	yeast extract
	15 g	Agar-Agar
	ad 1 l	ddH_20

The prepared LB-medium was autoclaved and supplemented with either ampicillin (100 µg / ml final concentration) or kanamycin (50 µg / ml final concentration).

ND96 buffer (10x)	960 mM	NaCl
	20 mM	KCl
	18 mM	$CaCl_2$
	10 mM	$MgCl_2$
	50 mM	HEPES

→ pH was adjusted to 7.5 with NaOH

ND96 storage solution	1 l of 1x ND96 was complemented with	
	2.5 mM	sodium pyruvate
	0.5 mM	theophylline
	50 mg	gentamicin
OR2 buffer (10x)	825 mM	NaCl
	20 mM	KCl
	10 mM	MgCl2
	50 mM	HEPES
	→ pH was adjusted to 7.5 with NaOH	
PBS (10x)	1.37 M	NaCl
	26.8 mM	KCl
	80 mM	Na_2HPO_4
	14.7 mM	KH_2PO_4
	→ pH was adjusted to 7.4 with NaOH	
TAE buffer (50x)	40 mM	TRIS
	1 mM	EDTA
	20 mM	glacial acetic acid
	→ pH was adjusted to 8.3 with NaOH	
TFB1	30 mM	potassium acetate
	10 mM	$CaCl_2$
	50 mM	$MnCl_2$
	100 mM	RbCl
	15 %	glycerol
	→ pH was adjusted to 5.8 with 1 M acetic acid	

TFB2	100 mM	MOPS
	75 mM	$CaCl_2$
	10 mM	RbCl
	15 %	glycerol

→ pH was adjusted to 6.5 with 1 M KOH

Both TFB1 and TFB2 were filter sterilized through a 0.2 µm filter before usage.

2.3 Enzymes, Antibodies and Reagents

Enzymes

BamHI (FastDigest)	Thermo Scientific
EcoRI (FastDigest)	Thermo Scientific
NheI (FastDigest)	Thermo Scientific
SalI (FastDigest)	Thermo Scientific
DpnI (10 U / µl)	Thermo Scientific
T7 RNA Polymerase	Life Technologies
T4 DNA Ligase (10 U / µl)	Thermo Scientific
AmpliTaq Gold® DNA polymerase (5 U / µl)	Life Technologies
Pfu DNA Polymerase (2.5 U / µl)	Thermo Scientific
Turbo Pfu DNA Polymerase (2.5 U / µl)	Agilent Technologies
SuperScript® II Reverse Transcriptase (200 U / µl)	Life Technologies

Primary Antibodies

Anti-HA IgG_1 from rat (#11867423001)	Roche Diagnostics
Anti-HA IgG_1 from mouse (H9658)	Sigma-Aldrich
Rab4, rabbit anti-human (#2167)	Cell Signaling Technology®
Rab5 IgG, rabbit anti-human (#3547)	Cell Signaling Technology®
Rab7 IgG, rabbit anti-human (#9367)	Cell Signaling Technology®
Rab11 IgG, rabbit anti-human (#5589)	Cell Signaling Technology®

Secondary Antibodies

F(ab')$_2$ fragment IgG, goat anti-rat (#112-036-072)	Jackson ImmunoResearch
IgG-Alexa Fluor® 488, goat anti-mouse (A11001)	Life Technologies
IgG-Alexa Fluor® 594, goat anti-mouse (A11005)	Life Technologies

Reagents

GelRed	Phenix Research Products

Markers

GeneRuler^{TM} 1 kb Plus DNA Ladder	Thermo Scientific
6x MassRuler Loading Dye	Thermo Scientific

Transfection Reagent

jetPRIME®	polyplus transfection^{TM}

Surface Assay Substrate

SuperSignal ELISA Femto Maximum Sensitivity Substrate	Thermo Scientific

Chemicals

Brefeldin A (B5936)	Sigma Aldrich
Cyclohemximide (C7698)	Sigma Aldrich
YM 201636 (Cay13576-5)	Biomol

2.4 Vectors

The following vector backbones were used:

pSGEM(-KS)	Constructed by Michael Hollmann, derived from pGEMHE vector
pEGFP-C1 (#6084-1)	Clontech
pmCherry-C1 (#632524)	Clontech
pCDNA3.1(+/-)	Invitrogen™ Life Technologies

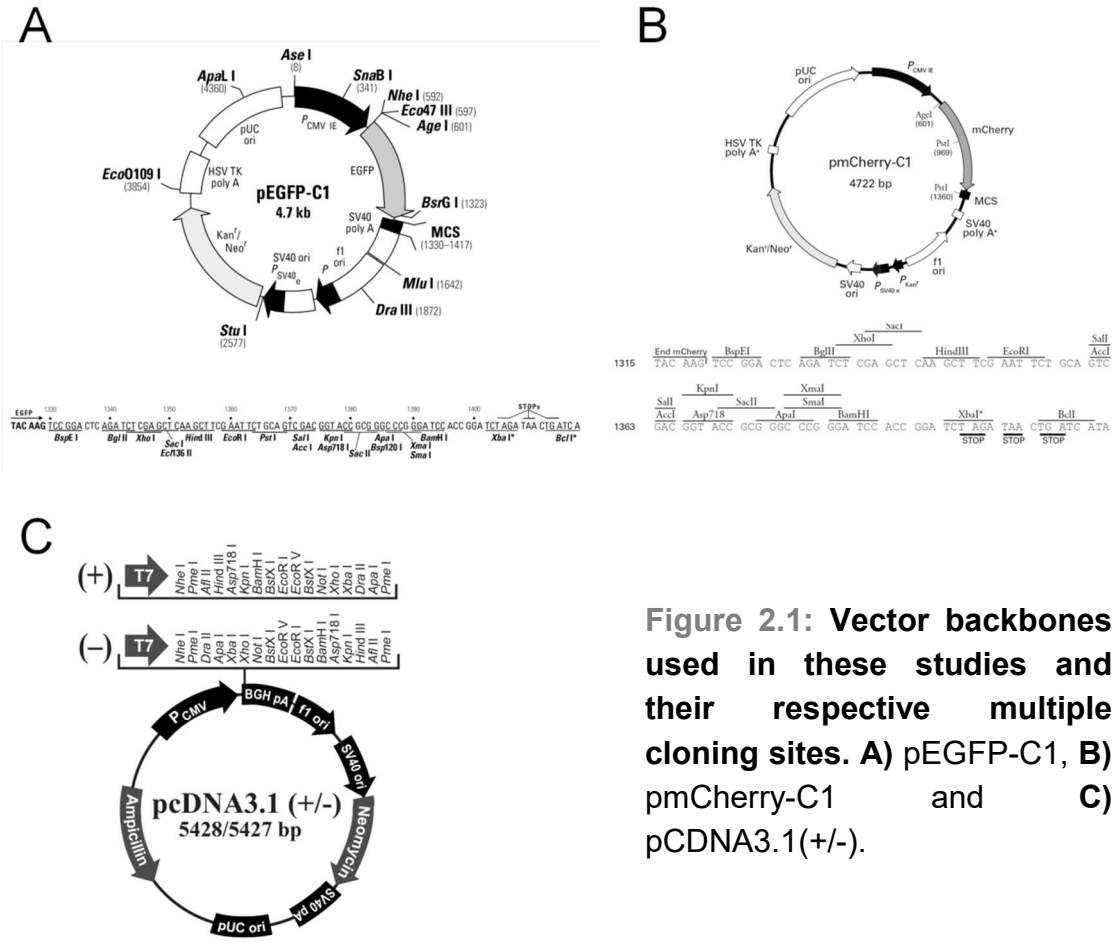

Figure 2.1: Vector backbones used in these studies and their respective multiple cloning sites. A) pEGFP-C1, **B)** pmCherry-C1 and **C)** pCDNA3.1(+/-).

The following constructs were used for the generation of cRNA:

Gene	Vector	Restriction Enzyme sites
hKir2.1	pSGEM	
hKir2.1-HA	pSGEM	
gpKir2.2	pSGEM	EcoRI, BamHI
pgKir2.2-HA	pSGEM	EcoRI, BamHI
hKv1.5		
hSGK1	pSGEM-KS	EcoRI, BamHI
hSGK2	pSGEM-KS	EcoRI, BamHI
hSGK3	pSGEM-KS	SalI, BahmHI
hNedd4-2	pSGEM	HindIII, SalI
AP180C	pSGEM-KS	

The following constructs were used for the transfection of COS-7 cells:

Gene	Vector	Restriction Enzyme sites
hKir2.1	pEGFP-C1	
gpKir2.2	pEGFP-C1	EcoRI, BamHI
	pmCherry-C1	EcoRI, BamHI
	pCDNA3.1-	EcoRI, BamHI
gp-Kir2.2-HA	pEGFP-C1	EcoRI, BamHI
	pCDNA3.1-	EcoRI, BamHI
hSGK1	pEGFP-C1	EcoRI, BamHI
	pCDNA3.1-	EcoRI, BamHI
hSGK1-K127N	pCDNA3.1-	EcoRI, BamHI
hSGK1-S422D	pCDNA3.1-	EcoRI, BamHI
hSGK2	pEGFP-C1	EcoRI, BamHI
hSGK3	pEGFP-C1	SalI, BamHI
	pmCherry-C1	SalI, BamHI
	pCDNA3.1-	NotI, BamHI
hSGK3-K191N	pEGFP-C1	SalI, BamHI
	pCDNA3.1-	NotI, BamHI

hSGK3-PRK2	pEGFP-C1	SalI, BamHI
	pmCherry-C1	SalI, BamHI
	pCDNA3.1-	NotI, BamHI
hSGK3-R90A	pmCherry-C1	SalI, BamHI
	pCDNA3.1-	NotI, BamHI
hSGK3-R90A-PRK2	pmCherry-C1	SalI, BamHI
	pCDNA3.1-	NotI, BamHI
hRab4	pEGFP-C1	EcoRI, BamHI
	pmCherry-C1	EcoRI, BamHI
hRab5	pEGFP-C1	EcoRI, BamHI
	pmCherry-C1	EcoRI, BamHI
hRab7	pEGFP-C1	EcoRI, BamHI
	pmCherry-C1	EcoRI, BamHI
hRab11	pEGFP-C1	EcoRI, BamHI
	pmCherry-C1	EcoRI, BamHI
	pCDNA3.1-	EcoRI, BamHI

Some of the vectors used in this thesis were generous gifts from other groups: SGK3-pCMV was obtained from AddGene (plasmid 24650). hNedd4-2-pXOOM was a kind gift from Thomas Jespersen; hSGK3-PRK2-pCMV was a kind gift from Jim Woodgett; hKv1.5-pSGEM, Rab4-pCDNA3.1, Rab5-pCDNA3.1, Rab7-pCDNA3.1 and Rab11-pCDNA3.1 were kind gifts from Guiscard Seebohm.

2.5 Oligonucleotides

The following oligonucleotides were used to introduce restriction enzyme cleavage sites into the listed genes:

Kir2.2-EcoRI-for	AAT GAA TTC ATG ACT GCT GCC AGT CGG
Kir2.2- BamHI-rev	TAT GGA TCC TCA GAT CTC TGA CTC TCG
hSGK1-EcoRI-for	TAT GAA TTC ATG ACG GTG AAA ACT GAG
hSGK1-BamHI-rev	AAT GGA TCC TCA GAG GAA AGA GTC CGT
hSGK2-EcoRI-for	TAT GAA TTC TAC AGA ATG AAC TCT AGC CCA
hSGK2-BamHI-rev	TAA GGA TCC CTA GCA ATC CAA GAT GTC ATC
hSGK3-SalI-for	ATA GTC GAC ATG CAA AGA GAT CAC ACC

hSGK3-NotI-for	AT AGC GGC CGC ATG CAA AGA GAT CAC ACC
hSGK3-BamHI-rev	TA TGG ATC CCG CAA AAA TAA GTC TTC TGA
Nedd4-2-HindIII-for	TA CAA GCT TCG ATG GCG ACC GGG CTC GGG
Nedd4-2-SalI-rev	ATT GTC GAC TTA ATC CAC CCC TTC AAA TCC
Rab4-for-EcoRI	A AAG AAT TCT ATG TCC GAA ACC TAC GAT
Rab4-rev-BamHI	TAT GGA TCC TCA ACA ACC ACA CTC CTG AGC
Rab5-for-EcoRI	A AAG AAT TCT ATG GCT AGT CGA GGC GCA
Rab5-rev-BamHI	ATA GGA TCC TCA GTT ACT ACA ACA CTG ATT
Rab7-for-EcoRI	A AAG AAT TCT ATG ACC TCT AGG AAG AAA GTG
Rab7-rev-BamHI	TAT GGA TCC TCA GCA ACT GCA GCT TTC TGC
Rab11-for-EcoRI	A AAG AAT TCT ATG GGC ACC CGC GAC GAC
Rab11-rev-BamHI	ATA GGA TCC CTA GAT GTT CTG ACA GCA CTG

The following oligonucleotides were used to introduce mutations:

hSGK3-K191N-for	TAT GCT GTC AAC GTG TTA CAG
hSGK3-K191N-rev	CTG TAA CAC GTT GAC AGC ATA
hSGK3-R90A-for	TT ATT AAA CAA GCA CGA GCA GGA CTA
hSGK3-R90A-rev	TAG TCC TGC TCG TGC TTG TTT AAT AA
hSGK3- S486D-for	TTC GTT GGT TTC GAC TAT GCA CCT CCT
hSGK3- S486D-rev	AGG AGG TGC ATA GTC GAA ACC AAC GAA

The following oligonucleotides were used for RT-PCR:

SGK1:	sense:	5’-AAACTGAGGCTGCTAAGGGC-3‘,
	antisense:	5’-CAGTGAATGCAGGTAGCCCA-3‘.
SGK2:	sense:	5’-CCTGACTGGGAAGGTTGCTT-3‘,
	antisense:	5’-AGAACGCCCCATCAGACTTG-3‘.
SGK3:	sense:	5’-TGCCCGAAGGTTGCATGAT-3’,
	antisense:	5’-ACGGTCCCAGGTTGATGTTC-3‘.
GAPDH:	sense:	5′-CATCACCATCTTCCAGGAGCGA-3′;
	antisense:	5′-GTCTTCTGGGTGGCAGTGATGG-3′.

2.6 Kits

peqGOLD Cylce-Pure Kit	Peqlab
peqGOLD Gel Extraction Kit	Peqlab
T7 mMESSAGE mMACHINE®-Kit	Life Technologies
E.Z.N.A.® Plasmid DNA Mini Kit	VWR International
Plasmid Plus Midi Kit (25)	Quiagen
High Pure RNA Isolation Kit	Roche Diagnostics

2.7 Cell lines and microorganisms

DH5α [Genotyp: F^-φ80*lac*ZΔM15Δ (*lac*ZYA-*arg*F) 169*deo*R*rec*A1*end*A1*hsd*R19 (r_{K-},m_{K+}) *pho*A*sup*E44*thi*1*gyr*A96*rel*A1λ-)]
Invitrogen™ Life Technologies (Darmstadt)

COS-7 (African green monkey kidney fibroblast-like cell line, CRL-1651)
ATCC (Middlesex, UK)

HeLa (human epithelial carcinoma cell line, CCL2.2)
ATCC (Middlesex, UK)

2.8 Instruments

60x objective	Plan Apo VC Oil WD 0.13, Nikon
100x objective	Plan Apo VC Oil DIC N2, Nikon
Agarose gel electrophoresis system	savant
Amplifier	TurboTec-10C, npi electronic
Auto-nanoliter injector	Nanoject II, Drummond Scientific Company
Cabinet incubator	Function line, Heraeus instruments
Cell culture incubator	Hera cell 240, Heraeus instruments
	cytoperm 2, Heraeus instruments
Camera	DU-885, Andor Technology
Centrifuge	Biofuge 28 RS, Thermo Scientific
	5804 R, eppendorf
	Fresco 17, Heraeus instruments
Fluorescence Microscope	Eclipse Ti microscope, Nikon

Laminar flow hood	Hera Safe, Heraeus instruments
Light microscope	Zeiss
Luminometer	Glomax 20/20, Promega
Nikon Eclipse Ti microscope	Nikon
Puller	DMZ-Universal, Zeitz
Scale	Sartorius
Shaker incubator	WiseCube, PMI-Labortechnik
Spectrometer	nanodrop 2000c, Thermo Scientific
Thermocycler	T100 Thermal Cycler, Biorad
Thermomixer	5463, eppendorf
UV-transilluminator	MWG-Biotech
Water Filtration System	Milli-RO 12 Plus, Merck Millipore

3. Methods

3.1 Molecular Biology

3.1.1 Bacterial strains and culture conditions

The *Escherichia coli* strain DH5α [genotype: F$^-$φ80*lac*ZΔM15Δ (*lac*ZYA-*arg*F) 169*deo*R*rec*A1*end*A1*hsd*R19 (r_{K-},m_{K+}) *pho*A*sup*E44*thi*1*gyr*A96*rel*A1λ$^-$)] was used for the amplification of plasmids. *E. coli* liquid cultures were grown under aerob conditions in LB medium shaking with 200 rpm at 37 °C. Bacteria on solid LB agar plates were incubated in a cabinet incubator at 37 °C.

3.1.1.1 Antibiotics

All plasmids used contained genes conferring resistance to either ampicillin or kanamycin. After transformation of *E. coli* with the respective plasmid, bacteria were cultivated in medium supplemented with ampicillin (100 µg / ml) or kanamycin (50 µg / ml), depending on the resistance gene of the plasmid.

3.1.1.2 Preparation of competent E. coli cells for electro-transformation

4 ml LB medium were inoculated with 2 µl DH5α and this preparatory culture was grown overnight at 37 °C and 200 rpm. The next morning, 0.4 l LB medium in a 1 l flask were inoculated with the pre-culture. Cells were grown with aeration at 37 °C until OD A_{600} ≈ 0.6 was reached. All following steps were performed on ice or at 4 °C. The cells were centrifuged for 10 min at 3,500 rpm in 50 ml falcons and the pellets were resuspended in altogether 200 ml ice cold H_2O. The centrifugation step and the resuspension of the pellet were repeated with 200 ml and 60 ml ice cold 10% glycerol. After the final centrifugation step, the supernatant was discarded and the pellets were resuspended in the liquid still contained in the falcon. Aliquots of 100 µl were distributed into 1.5 ml polypropylene tubes and the tubes were stored at -80 °C.

3.1.1.3 Preparation of competent E. coli cells for heat shock transformation

2 ml LB medium were inoculated with 2 µl DH5α and this preparatory culture was grown overnight at 37 °C and 220 rpm. The next morning, the entire overnight culture was used to inoculate 200 ml LB medium supplemented with 20 mM $MgSO_4$. The cells were grown in a 1 l flask until OD A_{600} = 0.4 - 0.6 was reached. All following steps were performed on ice or at 4 °C. The culture broth was distributed on four 50 ml falcons and bacteria were collected by centrifugation at 4,000 rpm for 10 min. Each pellet was then resuspended in 20 ml TBF1 and incubated for 15 min on ice. This was followed by another centrifugation step and the pellets were subsequently resuspended in altogether 8 ml TFB2. After 30 min incubation on ice, aliquots of 100 µl were distributed into 1.5 ml polypropylene tubes and stored at -80°C.

3.1.2 Molecular Cloning

3.1.2.1 Polymerase chain reaction (PCR)

Polymerase chain reaction (PCR) was used for the amplification of DNA fragments and the introduction of restriction enzyme cleavage sites. The primers that were used are listed in chapter 2.5. All PCR reactions were performed using the following reaction mixture and cycling program, elongation time was adjusted to the template length.

Reaction mixture:

Reaction buffer (10x)	5 µl
dNTP mix (10 mM)	1 µl
5’ Primer (10 mM)	5 µl
3’ Primer (10 mM)	5 µl
Template	50 – 200 ng
Pfu DNA Polymerase (2.5 U / µl)	0.5 µl
ddH_2O	ad 50 µl

Cycling program:

95 °C	1 min	
95 °C	30 sec	26 cycles
54 °C	1 min	
72 °C	1.5 - 3 min	
2 °C	5 min	
12 °C	∞	

3.1.2.2 Site-directed mutagenesis

Mutations were introduced using a PCR based approach. For each mutagenesis specific primers were designed that contained the desired mutation (compare chapter 2.6).

Reaction mix:

Reaction buffer (10x)	1.5 µl
dNTPs (10 mM)	0.75 µl
DMSO	1.5 µl
5’ Primer (10 mM)	0.45 µl
3’ Primer (10 mM)	0.45 µl
Template	100 ng
Turbo Pfu DNA Polymerase (2.5 U / µl)	0.3 µl
ddH_2O	ad 15 µl

Cycling program:

96 °C	30 sec	
96 °C	30 sec	18 cycles
55 °C	1 min	
68 °C	18 min	
68 °C	2 min	
12 °C	∞	

3.1.2.3 DNA purification after polymerase chain reaction

To purify single DNA fragments amplified by polymerase chain reaction, ‘peqGOLD Cylce-Pure Kit’ (Peqlab) was used according to the manufacturer’s instructions. The purified fragments were eluted in 20 µl ddH_2O.

3.1.2.4 Agarose gel electrophoresis

For the electrophoretic separation of DNA fragments, 1 % agarose gels were used. For one gel 0.5 g agarose powder were mixed with 50 ml 1x TAE buffer and heated in the microwave until the agarose was completely resolved and the solution was boiling. The agarose solution was then complemented with 5 µl GelRed (Phenix Research Products), poured into a gel chamber containing a sample comb and allowed to solidify at room temperature. The solid gel was inserted into an electrophoresis chamber and covered with 1x TAE buffer. DNA samples were mixed with 6x MassRuler Loading Dye solution (Thermo Scientific) and then applied to the agarose gel with a DNA ladder (GeneRuler^{TM} 1 kb Plus DNA ladder, Thermo Scientific). DNA fragments were separated according to length for 30 min at 85 mV and then made visible using an UV-transilluminator.

3.1.2.5 DNA extraction from agarose gels

To isolate DNA fragments after a restriction digest resulting in two or more fragments, the digested DNA was separated by gel electrophoresis. DNA bands were made visible by exposing the gel to UV-light using an UV-transilluminator and then rapidly cut from the gel. Extraction was performed using the ‘peqGOLD Gel Extraction Kit’ (Peqlab) and following the manufacturer’s instructions. The purified fragments were eluted in 20 µl ddH_2O.

3.1.2.6 Enzymatic digestion with restriction endonucleases

The hydrolytic cleavage of template DNA with restriction endonucleases was performed using FastDigest enzymes (Thermo Scientific) according to the manufacturer’s instructions. The volume of restriction endonucleases did not exceed 1/10 of the complete reaction mix and the reaction mix was incubated for 0.5 to 1.5 h at 37 °C. Restriction enzymes were used to introduce matching

cleaving sites in vector DNA and inserts that could thereupon be fused in a ligation reaction.

3.1.2.7 Ligation of vectors and inserts

The ligation of DNA vectors and inserts with compatible ends was performed with the T4 DNA Ligase (Thermo Scientific). The molar ration between insert and vector was 6:1 and following reaction mixture was used:

vector and insert	1 : 6 ratio, 10 – 100 ng insert
Ligase buffer (10x)	1 µl
T4 DNA ligase (10 U / µl)	1 µl
H_2O	ad 10 µl

The reaction mixture was incubated for 1 h at RT and then directly used for the transformation of chemical competent *E. coli* cells.

3.1.2.8 Heat-shock transformation of chemically competent E. coli

The ligation reaction was added to 100 µl chemical competent *E. coli* cells and incubated for 30 min on ice. Cells were then heated to 42 °C for 1 min followed by 1 min incubation on ice. 900 µl LB medium were added and cells were grown at 37 °C for 0.5 to 1.5 h. Subsequently, cells were spinned down (1 min, 1,000 rpm), 900 µl of the supernatant were discarded and the pellet was resuspended in the remaining ~100 µl medium. The cell suspension was plated on an agar plate containing the particular antibiotic and incubated overnight at 37 °C.

3.1.2.9 Plasmid Isolation – Mini

Single colonies were picked from LB agar plates and cultured overnight in 2 ml LB medium at 37 °C and 200 rpm. The next morning, cells were collected by centrifugation and the supernatant was discarded. The pellet was used to isolate the plasmid according to the manufacturer's instructions using an 'E.Z.N.A.® Plasmid DNA Mini Kit' (VWR International).

3.1.2.10 Electroporation of electrocompetent E. coli

Transformation of electrocompetent *E. coli* with electroporation was used to amplify cloned plasmids. 100 ng plasmid and 100 µl competent cells were transferred to an electroporation cuvette (peqlab). The cuvette was exposed to an electrical impulse, washed with 1 ml LB medium and the transformed cells in the medium were transferred to a sterile 1.5 ml polypropylene tube. They were incubated for 0.5 to 1.5 h at 37 °C and then used to inoculate 50 ml LB medium in a 250 ml flask. The culture was incubated overnight at 37 °C shaking with 200 rpm.

3.1.2.11 Plasmid Isolation – Midi

After electrical transformation with the plasmid that was to be amplified, *E. coli* cells were grown in 50 ml LB medium overnight. The next morning, the bacteria were collected by a 10 min centrifugation step at 5300 rpm and the supernatant was discarded. The plasmid was isolated according to the manufacturer's instructions using a 'Plasmid Plus Midi Kit' (Quiagen).

3.1.3 Quality control

3.1.3.1 Quantification of DNA and RNA concentrations

The concentration of DNA and RNA solutions was determined by measuring the absorbance at λ = 260 nm using the nanodrop 2000c (Thermo Scientific). OD_{260} = 1 corresponds to a RNA concentration of 40 ng / µl and a DNA concentration of 50 ng / µl.
The ratio of the readings at 260 nm and 280 nm was used to estimate the purity of the nucleic acid. For pure DNA, A260/280 is ~1.8 and for pure RNA, A260/280 is ~2. An appreciably lower ratio indicates the presence of protein, phenol or other contaminants that absorb strongly at or near 280 nm.

3.1.3.2 DNA sequencing

Seqlab GmbH (Göttingen) was commissioned with the sequencing of all DNA plasmids.

3.1.4 In vitro cRNA synthesis

cRNA was synthesized in vitro using the 'T7 mMESSAGE mMACHINE®-Kit' (Life Technologies). pSGEM or pSGEM-KS vectors containing the gene of interest were linearized with NheI (Thermo Scientific). cRNA synthesis was then performed using the following reaction mix:

NTP/Cap (2x)	7.5 µl
Reaction buffer (10x)	2 µl
Linearized plasmid	~0.8 µg
T7 enzyme mix	1.5 µl
H_2O	ad 20 µl

The reaction mix was incubated for 2 h at 37 °C. 1.5 µl DNAse were added for the last 15 min to digest the vector DNA. Subsequently, 20 µl LiCl and 20 µl H_2O RNAse free were added and the reaction mix was incubated for at least 30 min at -20 °C, followed by a 30 min centrifugation step at 13,000 rpm and 4 °C. The supernatant was discarded and the pellet was resolved in 100 µl 80 % ethanol, followed by another centrifugation step. The pellet was dried for 5 min at 37 °C, then solved in 20 µl RNAse free H_2O (3 min, 37 °C, 2,000 rpm).

3.1.5 Reverse transcriptase polymerase chain reaction

The total RNA of COS-7 cells was isolated using 'High Pure RNA Isolation Kit' (Roche Diagnostics). mRNA was transcribed into cDNA using SuperScript® II Reverse Transcriptase (Life Technologies) and the following protocol:

RNA	1 µl
Hexanucleotide	0.5 µl
ddH_2O	8.5 µl

The reaction mix was incubated for 10 min at 70 °C and then placed on ice. The following components were added:

RT buffer (5x)	5 µl
DNTP (2 mM)	6 µl
DTT	2.5 µl
SuperScript® II (200 U / µl)	1 µl

The mix was incubated for 50 min at 42 °C, followed by a 10 min incubation step at 72 °C, and subsequently placed on ice.

RT-PCR expression analysis was performed with AmpliTaq Gold® DNA polymerase (Life Technologies) using the following, intron-spanning, gene specific primers:

SGK1:	sense:	5'-AAACTGAGGCTGCTAAGGGC-3',
	antisense:	5'-CAGTGAATGCAGGTAGCCCA-3'.
SGK2:	sense:	5'-CCTGACTGGGAAGGTTGCTT-3',
	antisense:	5'-AGAACGCCCCATCAGACTTG-3'.
SGK3:	sense:	5'-TGCCCGAAGGTTGCATGAT-3',
	antisense:	5'-ACGGTCCCAGGTTGATGTTC-3'.
GAPDH:	sense:	5′-CATCACCATCTTCCAGGAGCGA-3′;
	antisense:	5′-GTCTTCTGGGTGGCAGTGATGG-3′.

Reaction mixture:

PCR buffer (10x) + 15 mM $MgCl_2$	3 µl
dNTPs (10 nM)	0.6 µl
5'primer (10 mM)	3 µl
3'primer (10 M)	3 µl
cDNA	1 µl
DMSO	1.2 µl
AmpliTaq Gold® (5 U / µl)	1 µl
ddH_2O	ad 30 µl

Cycling program:

96 °C	5 min	
96 °C	30 sek	35 cycles, 5 min
53 °C	1 min	
72 °C	3 min	
12 °C	∞	

3.2 Cell Culture

3.2.1 Maintenance of cells

All cell culture works were carried out under sterile conditions under a laminar air flow hood. Only sterile materials were used and the hood was cleaned thoroughly with terralin® (Schülke) before and after usage.
COS-7 cells were cultured in high glucose DMEM containing 10 % fetal bovine serum (Life Technologies) and 1% penicillin/streptomycin (PAA Laboratories) at 37 °C and 5 % CO_2. 25 cm^2 and 75 cm^2 cell culture flasks (Sarstedt) were used. Cells were split every two to three days. Cells were therefore washed with 1x PBS and then detached with trypsin/EDTA for ~4 min at 37 °C. The reaction was stopped by addition of full medium, cells were spinned down for 2 min at 1,500 rpm and 4 °C and the pellet was resuspended in 1 ml full medium. Cells were then split 1:4 and freshly plated in a new cell culture flask.

3.2.2 Thawing and freezing of cells

The cryopreservation of cells was carried out in liquid nitrogen. The cells were thawed in a water bath at 37 °C, transferred to 9 ml prewarmed full medium and centrifuged for 2 min at 1,500 rpm. The pellet was resuspended in 5 ml medium and plated in a new cell culture flask (25 cm^2).
For freezing, 5-10 x 10^6 cells were sedimented for 5 min at RT and 1,200 rpm, resuspended in 0.5 ml of freezing solution I (DMEM medium + 30% FCS) and transferred to a cryogenic vial. Afterwards, 0.5 ml of freezing solution II (DMEM medium + 20% DMSO) was added drop-wise. The cells were frozen overnight at -80 °C in a Freezing Container and finally stored in liquid nitrogen.

3.2.3 Transfection of cells

For all experiments, cells were transfected 24 h after seeding with the indicated construct using jetPRIME® transfection reagent (Polyplus) according to the manufacturer's instructions.

3.2.4 Surface expression analysis in COS-7 cells

$2x10^5$ COS-7 cells were seeded in 35 mm cell culture dishes (Thermo Scientific) and transfected one day later with the indicated constructs. Surface expression of HA-tagged Kir2.x constructs was measured 24 h after transfection. Cells were fixed with 4 % paraformaldehyde (PFA) for 20 min and subsequently blocked for 30 min with 1 % FBS / 1x PBS. To label surface membrane resident Kir2.x channels, cells were incubated with 100 ng / ml rat anti-HA antibody (clone 3F10, Roche Diagnostics) in blocking solution for 1 h, washed with 1 % FBS / 1x PBS six times for a total of 1 h and then incubated with 800 ng / ml peroxidase-conjugated goat anti-rat antibody (Jackson Immuno Research) in 1 % BSA / 1x ND96 for 60 min. Cells were then washed thoroughly for 1 h with blocking solution (6 steps a 10 minutes) followed by 6 washing steps with 1x PBS for 2.5 min each. Each dish was covered with 550 µl SuperSignal ELISA Femto solution (Thermo Scientific) which was enzymatically converted by the horse radish peroxidase, generating detectable chemo-luminescence. The luminescence signal was quantified with a luminometer (Glomax20/20). The peak of each measured signal was evaluated for surface quantification. The luminescence of mock-transfected cells was used as a reference (negative control).

3.2.5 Antibody Uptake Assay

$2x10^4$ COS-7 cells were seeded in 35 mm glass bottom dishes (ibidi) and transfected with Kir2.2-HA-pCDNA3.1- together with SGK3-K191N-pCDNA3.1- or SGK3-PRK2-pCDNA3.1- one day later. The antibody-uptake assay was performed 24 h after the transfection. Cells were blocked with 5 % FBS in 1x PBS for 30 min at room temperature, followed by a 1 h incubation on ice with anti-HA primary antibody (Sigma-Aldrich) 1:1000 in blocking solution to label membrane resident channels. Cells were then heated to 37 °C for 0 min, 15 min

or 30 min, allowing surface channels to undergo endocytosis, and subsequently fixed with 4 % paraformaldehyde on ice. Channels in the membrane were labeled with Alexa Fluor® 488-conjugated anti-mouse antibody (Life Technologies) 1:1000 in blocking solution for 1.5 h at RT. After permeabilization of the membrane with 0.1 % Triton X-100 for 5 min at RT, the internalized channels were labeled with Alexa Fluor® 594-conjugated anti-mouse antibody (Life Technologies) 1:2000 in blocking solution for 30 min at RT. Cells were then washed extensively with 1x PBS buffer and covered with the anti-fade agent Mowiol 4-88 (Carl Roth; containing 25 µg / µl DABCO). The cells were visualized using an inverted Nikon Eclipse Ti microscope equipped with a 60x objective (Plan Apo VC 60x Oil WD 0.13, Nikon) and a 100x objective (Plan Apo VC 100x Oil DIC N2, Nikon) and the corresponding filters for the fluorescent dyes. Images were acquired and analyzed with NIS Elements AR 4 software (Nikon). Channel endocytosis was quantified by taking the ratio between the fluorescence of the Alexa Fluor® 594-conjugated secondary antibody (internalized channels) and the fluorescence of the Alexa Fluor® 488-conjugated secondary antibody (channels at the cell surface).

3.2.6 Recycling Assay

$2x10^4$ COS-7 cells were seeded in 35 mm glass bottom dishes and transfected with Kir2.2-HA-pCDNA3.1- together with SGK3-K191N-pCDNA3.1- or SGK3-PRK2-pCDNA3.1- one day later. The recycling assay was performed 24 h after transfection. Cells were blocked with 5 % FBS in 1x PBS for 30 min at room temperature, followed by a 1 h incubation with anti-HA primary antibody (Sigma-Aldrich) 1:1000 in blocking solution on ice to label membrane resident channels. Cells were then heated to 37 °C for 30 min, allowing surface channels to undergo endocytosis. The channels still remaining in the plasma membrane after this incubation period were removed using a low pH high salt stripping buffer (50 mM glycine, 150 mM NaCl, pH 2.5) for 2 x 2 min. Cells were heated to 37 °C again for 15 or 30 min, allowing internalized channels to recycle back to the plasma membrane. Subsequently, the cells were fixed with 4 % paraformaldehyde on ice. Channels that were endocytosed during the first incubation period at 37 °C and recycled back to the plasma membrane during the second incubation period at 37 °C were labeled with Alexa Fluor® 488-

conjugated anti-mouse antibody (1:1000 in 1x PBS, 30 min). Finally cells were washed extensively with 1x PBS buffer and covered with the anti-fade agent Mowiol 4-88 (Carl Roth; containing 25 µg / µl DABCO).

3.3 Electrophysiology

3.3.1 Preparation of Xenopus laevis oocytes

For experiments involving *Xenopus* oocytes, adult female African clawed frogs (*Xenopus laevis*) were used. *X. laevis* frogs were anaesthetized by putting them in water containing 1 g / l tricaine and then placed on ice for surgery. A small abdominal incision (1 – 2 cm) was made and the ovaries containing the oocytes were partly removed. The wound was subsequently closed with reabsorbable suture.

Anesthesia and operation were carried out in accordance with the principles of German legislation with approval of the animal welfare officer of the Medical Faculty of Marburg University under the governance of the Regierungspräsidium Giessen (the regional veterinary heath authority).

To defollicate the oocytes, they were incubated for 1 h with 40 mg fresh collagenase (C-6885, Sigma-Aldrich) in 20 ml 1x OR2 solution. After one hour of incubation, the oocytes were separated manually and washed thoroughly, first with 1x OR2 solution and then with1x ND96. Stage V oocytes were sorted and subsequently stored in storage solution in 6 well plates at 18 °C.

3.3.2 Injection of cRNA into Xenopus laevis oocytes

cRNA for injections was transcribed in vitro as described in chapter 3.1.4. The cRNA solution was injected with glass capillaries (3,5" Drummond Replacement Tubes, Drummond Scientific Company) that were manufactured on a DMZ-Universal Puller (Zeitz). 50.6 nl of the prepared cRNA solution were injected into the cytoplasm of the oocytes using a Nanoject II microinjector (Drummond Scientific Company). The following amounts were injected per oocyte: 1 ng or 0.1 ng Kir2.2/Kir2.2-HA were injected alone or together with 1.5 ng SGK1, SGK2 or SGK3, 6 ng AP180C and 5 ng Nedd4-2. 0.75 ng Kv1.5 were injected alone or together with 6.5 ng SGK3, 1.25 ng Nedd4-2 and 5 ng AP180C. 0.025 ng Kir2.1 were injected alone or together with 1.5 ng SGK1, SGK2 or SGK3.

3.3.3 Two electrode voltage clamp measurements

Two-microelectrode voltage clamp measurements were performed 48 h after injection with a TurboTec-10C amplifier (npi electronic); data acquisition and analysis were performed with software developed in our laboratory (PC.DAQ1.2). Data were recorded at a sampling rate of 120 Hz. Before the measurements, oocytes were incubated at 18 °C. Patch pipettes were made from glass capillaries (GB150TF-8P, Science Products) using a DMZ-Universal puller (Zeitz); they were filled with 3 M KCl as pipette solution. The pipettes had resistances between 0.5 and 2 MΩ. For the voltage clamp measurements, the oocytes were placed in a small-volume perfusion chamber and superfused with physiological salt solution. For the initial current measurements, oocytes were injected with 1 ng Kir2.2 per oocyte and 1x ND96 solution containing 2 mM K^+ was used. For later measurements, oocytes were injected with 0.1 ng Kir2.2 and the extracellular potassium concentration was elevated to 24 mM by equimolar replacement of Na^+ by K^+. Currents were recorded with a ramp-shaped voltage command (Figure 3.1A). For quantification of the current amplitude, Kir2.2 mediated currents were evaluated at -100 mV. Kv1.5 channels were measured in 1x ND96 solution containing 2 mM K^+ using a step protocol (Figure 3.1B). Kv1.5 mediated currents were evaluated at +40 mV. All electrophysiological experiments were carried out at room temperature (20–23 °C).

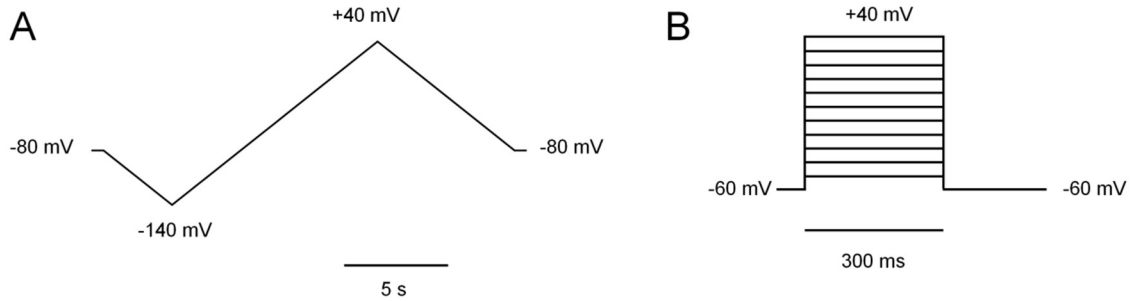

Figure 3.1: A) Ramp shaped voltage command that was used for the measurement of Kir channels. **B)** Step Protocol that was used for the measurement of Kv1.5 channels.

3.3.4 Statistical evaluation

The arithmetic mean was calculated for each batch of oocytes that was measured on one day and the values were normalized to the control group of

that day. The normalized values for three to five measuring days were then pooled and the standard error of the mean (SEM) was calculated. All data are reported as mean ± SEM. Statistical significance was determined using Student's t-test. In the Figures, statistically significant differences to control values are identified by asterisks (*, $p<0.05$; **, $p<0.01$; ***, $p<0.001$) while n.s. indicates non-significant differences ($p>0.05$).

3.3.5 Surface Expression analysis in Xenopus oocytes

Surface expression of HA-tagged Kir2.x constructs in *Xenopus* oocytes was measured 48 h after injection of cRNA. The following amounts of cRNA were injected per oocyte: 0.1 ng Kir2.2-HA, 0.025 ng Kir2.1-HA, 1.5 ng SGK1, SGK2 and SGK3, 6 ng AP180C. All steps were performed on ice. Injected Oocytes were blocked for 30 min in 1 % BSA / 1x ND96 solution, and then incubated for 60 min with 1 µg/ml primary anti-HA antibody (clone 3F10, Roche Diagnostics) in blocking solution to label Kir2.x channels in the surface membrane. To remove unbound antibody, oocytes were washed six times for 10 minutes with 1 % BSA / 1x ND96. Then they were incubated with 1.6 µg / ml peroxidase-conjugated goat anti-rat antibody (Jackson ImmunoResearch) in blocking solution for 60 min and washed thoroughly. First with 1 % BSA / 1x ND96 for 60 min, then with 1x ND96 for 45 min. Individual washing steps were performed for five to ten minutes. Each oocyte was placed in 20 µl SuperSignal Elisa Femto solution (ThermoScientific) and the emitted chemoluminescence was quantified with a luminometer (Glomax20/20, Promega). The luminescence produced by water injected oocytes was used as a reference signal (negative control).

3.4 Fluorescence Microscopy

3.4.1 Set up of the microscope

Both still images and time lapse recordings were captured with an inverted Nikon Eclipse Ti microscope equipped with a 100x (Plan Apo VC 100x Oil DIC N2, Nikon) and a 60x objective (Plan Apo VC 60x Oil WD 0.13, Nikon). Single images and image sequences were acquired and analyzed with NIS Elements AR 4 software (Nikon). When EGFP and mCherry channels were acquired separately, the images were merged afterwards using the NIS Elements AR 4

software. When both channels were acquired simultaneously, a dual camera port system composed of custom-made excitation/emission filters, a dual-band beam splitter and two cooled 14 bit EMCCD cameras (DU-885, Andor Technology) was used.

3.4.2 Live cell imaging

$2x10^4$ cells were seeded in a µ-slide (ibidi) and transfected one day later with the particular constructs. Images were taken 24 – 48 h after the transfection. For live-cell imaging experiments the cells were maintained at 37 °C by means of a stage heater (ibidi) with a temperature control system (TC 20, npi) and an objective heater (PeCon).

3.4.3 Imaging of fixed cells

$2x10^4$ cells were seeded in 35 mm glass bottom dishes (ibidi) and transfected one day later with the particular constructs. Images were taken 24 – 48 h after the transfection. Cells were fixed in 4 % PFA for 10 min, washed extensively with 1x PBS and then covered with 1x PBS for the recording of images.

3.4.4 Immunocytochemistry

Cells were grown on coverslips and transfected with the respective plasmids one day before the immunocytochemical assay was performed.
Cells were fixed with 4 % PFA for 15 min, followed by three washing steps with 1x PBS for 2 min. The cells were then permeabilized with 0.1 % Triton X-100 for 8 min, washed extensively with 1x PBS and incubated for 1 h in blocking buffer (0.2 % BSA and 1 % FBS in 1x PBS). The proteins of interest were then labeled by incubation with the respective primary antibody in blocking solution for 1 h, followed by incubation with secondary antibody in blocking solution for 1 h. After three washing steps with 1x PBS the coverslips were mounted on microscope slides (Superfrost™ Plus Gold Slides, Thermo Scientific) with Mowiol (~10 µl), dried overnight and images were taken the next day.

4. Results

It has been shown recently that the current amplitude of the potassium channel Kir2.2 is increased by coexpression of the channel with each of the three members of the serum- and glucocorticoid-inducible kinase family (Seebohm *et al.,* 2012a). In the present study the underlying mechanism was investigated.

4.1 Effects of the serum- and glucocorticoid-inducible kinases (SGKs) on the inwardly rectifying potassium channel Kir2.2

4.1.1 SGK1, SGK2 and SGK3 increase Kir2.2 current amplitude in Xenopus laevis oocytes

To study the effect of the serum- and glucocorticoid-inducible kinases on Kir2.2 current amplitude, the channel was coexpressed with SGK1, SGK2 and SGK3 in *Xenopus laevis* oocytes. The two-electrode voltage clamp technique was used to measure the Kir2.2 current-voltage relation. The currents were measured in the range -140 to +40 mV using a ramp-shaped voltage command (Figure 4.1A). The inward current at -100 mV was analyzed and the arithmetic mean was calculated.

When oocytes were injected with 1 ng Kir2.2-cRNA, coexpression of SGK1, SGK2 and SGK3 did not lead to a change in the Kir2.2 current amplitude (Figure 4.1B). The Kir2.2-cRNA concentration was therefore gradually decreased to determine whether the high initial concentration of the channel had prevented a stimulatory effect of the kinases. When 0.1 ng Kir2.2-cRNA were injected together with 1.5 ng of the respective kinase, all kinase isoforms had a stimulatory effect on the current amplitude of the potassium channel. SGK3 increased the current by 165 %, SGK1 by 125 % and SGK2 by 76 % (Figure 4.1 D).

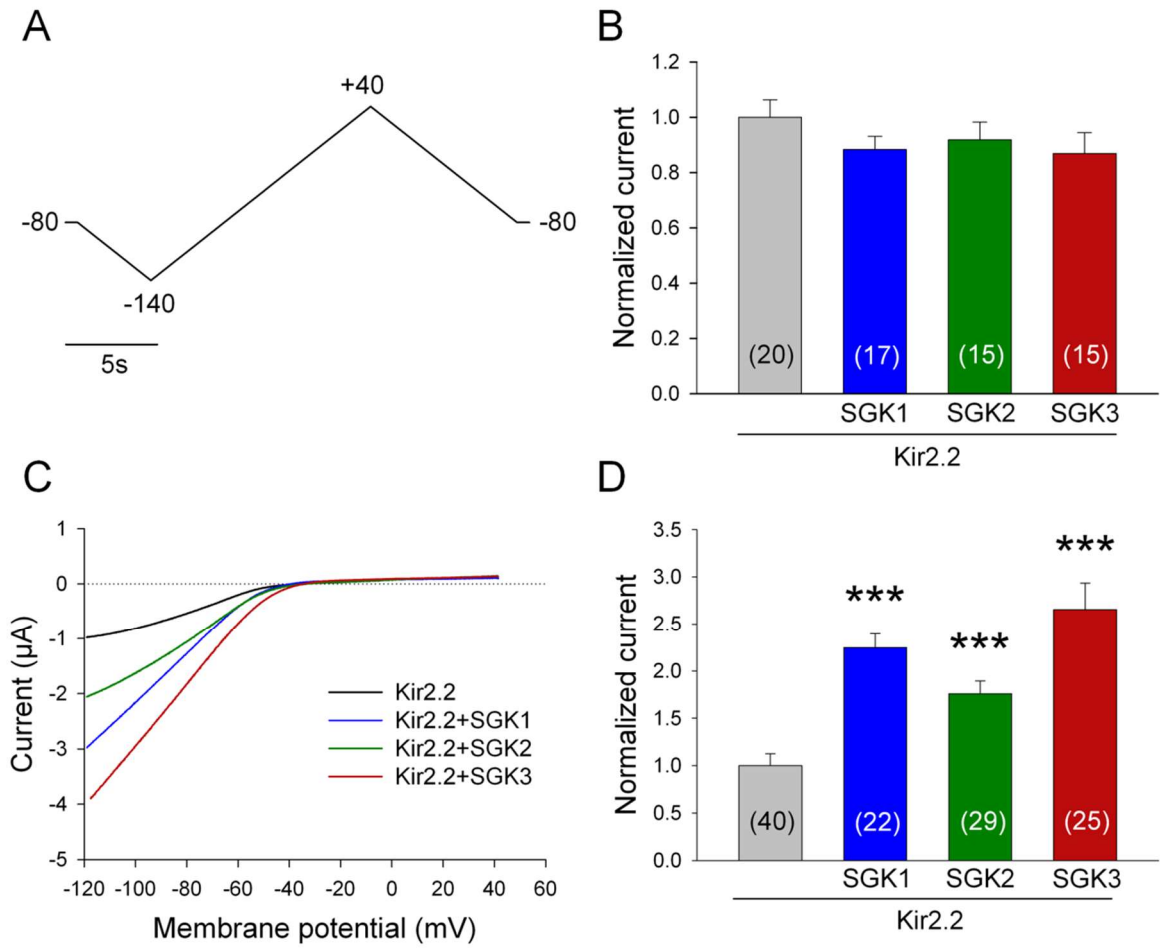

FIGURE 4.1: Serum- and glucocorticoid-inducible kinases elevate Kir2.2 current amplitude in *Xenopus laevis* oocytes. *Xenopus* oocytes were injected with Kir2.2 alone or together with SGK1, SGK2 and SGK3, respectively. **A)** The Oocytes were clamped to a given voltage using a ramp shaped voltage command and the resulting current amplitude was recorded. **B)** Mean inward current at -100 mV after injection of *Xenopus* oocytes with 1 ng Kir2.2-cRNA, alone or together with SGK1, SGK2 or SGK3, using an extracellular potassium concentration $[K^+]_o$ of 2 mM. **C)** Representative current-voltage relations of Kir2.2 (0.1 ng), alone or together with SGK1, SGK2 or SGK3, in *Xenopus* oocytes using an extracellular potassium concentration $[K^+]_o$ of 24 mM. **D)** Mean inward currents at -100 mV after injection of *Xenopus* oocytes with 0.1 ng Kir2.2 cRNA, alone or together with SGK1, SGK2 or SGK3, using an extracellular potassium concentration $[K^+]_o$ of 24 mM. All values were normalized to the expression of the channel alone, the number of oocytes from which the data were obtained is given in brackets; mean ± SEM; *** $p<0.001$.

Representative current-voltage relations are shown in Figure 4.1C, illustrating the typical inward current mediated by Kir2.2 when the membrane potential of the oocyte is clamped to values negative of the potassium equilibrium potential. Only the current amplitude but not the current-voltage relation of the channel was changed by coexpression with the serum- and glucocorticoid-inducible

kinases. While a bath solution containing 2 mM K^+ was used to measure the Kir2.2 current in oocytes injected with 1 ng Kir2.2-cRNA, the extracellular potassium concentration had to be elevated to 24 mM K^+ to induce measurable Kir-currents in the oocytes injected with 0.1 ng Kir2.2-cRNA. As mentioned in section 1.1.2, Kir2.2 is an inwardly rectifying channel and its conductance increases with an increasing extracellular potassium concentration $[K^+]_o$ (Hagiwara *et al.,* 1976; Sakmann and Trube 1984).

Taken together, these observations indicate that the serum- and glucocorticoid-inducible kinases SGK1, SGK2 and SGK3 have a stimulatory effect on Kir2.2 current amplitude in *Xenopus* oocytes. However, this effect is obscured by a high initial concentration of the channel protein in the cell.

4.1.2 SGK3 increases Kir2.2 surface expression in Xenopus oocytes

An increase in current amplitude can be caused by (i) an elevated single channel conductance, (ii) an increased open probability of the channel or (iii) a larger number of channels in the plasma membrane. To investigate the mechanism underlying the observed change in Kir2.2 current amplitude after coexpression with SGK1, SGK2 and SGK3, I performed a chemoluminescence based surface expression assay that allowed me to determine the amount of channel molecules in the plasma membrane (Margeta-Mitrovic 2002).

For this assay, I used a Kir2.2 construct containing an HA-tag introduced into the extracellular domain at position 116 (Figure 4.2A). To make sure that the HA-tag did not alter the channel properties, the tagged channel was compared to the wild type channel in two-electrode voltage clamp measurements. I found that neither the current amplitude nor the current-voltage relation was changed (Figure 4.2, B and C). Subsequently, the surface membrane expression of Kir2.2-HA in *Xenopus* oocytes, alone and in presence of SGK1, SGK2 and SGK3, was compared.

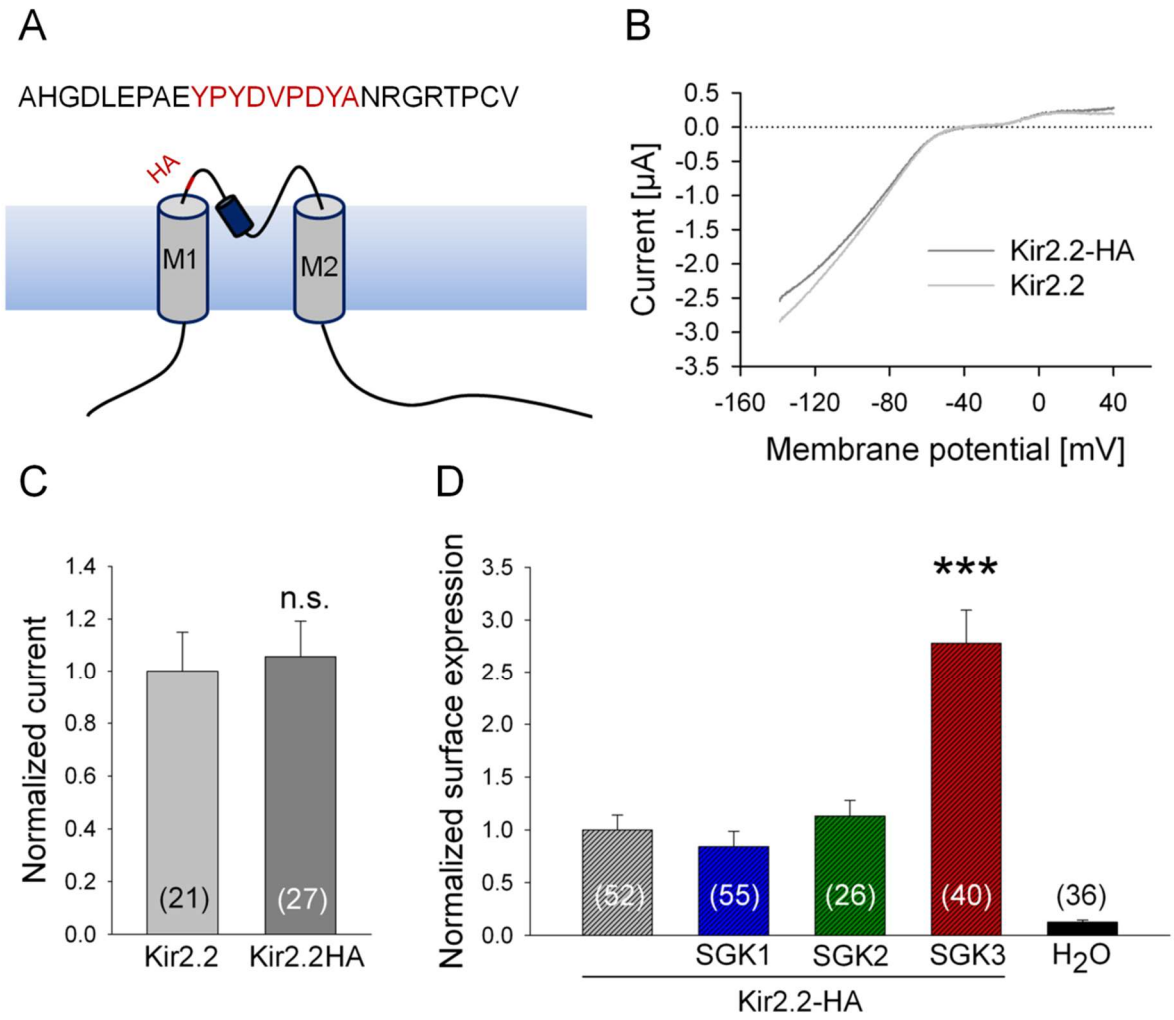

Figure 4.2: SGK3 elevates Kir2.2 surface expression in *Xenopus laevis* oocytes. **A)** A hemagglutinin epitope was introduced into the extracellular domain of Kir2.2 at position 116. **B)** Shape of the current-voltage relation and **C)** current amplitude at -100 mV of wild type Kir2.2 was compared to the HA-tagged Kir2.2 construct in *Xenopus* oocytes. **D)** Surface membrane expression of HA-tagged Kir2.2 channels, injected alone or together with SGK1, SGK2 or SGK3, was quantified using a chemoluminescence based surface expression assay. All values were normalized to the expression of the channel alone, the number of oocytes from which the data were obtained is given in brackets; mean ± SEM; *** $p<0.001$.

When coexpressed with SGK3, the number of Kir2.2 channels in the plasma membrane was increased by 178% (Figure 4.2D), i.e. to approximately the same extent as the current amplitude (Figure 4.1D). These findings suggest that the increase in Kir2.2 current amplitude induced by coexpression with SGK3 is due to an elevated membrane abundance of Kir2.2 rather than a change in the conductance or the gating of the channels. In contrast, SGK1 and SGK2 had no statistically significant effect on the amount of Kir2.2 channels in the surface membrane, indicating that there are differences in the molecular mechanism of

action between the three serum- and glucocorticoid-inducible kinases. A possible conclusion from these observations would be that SGK1 and SGK2 affect the biophysical properties of the channel.

4.1.3 Kir2.2 and SGK3 are colocalized in COS-7 cells

To investigate whether the subcellular localization of Kir2.2 and the three serum- and glucocorticoid-inducible kinases could provide an indication why only SGK3 had an effect on Kir2.2 surface expression, mCherry-tagged Kir2.2 channels were coexpressed with EGFP-tagged SGK1, SGK2 or SGK3 protein in COS-7 cells. In accordance with published data, SGK1 and SGK2 displayed a diffuse distribution in the cytoplasm data (Buse *et al.,* 1999; He *et al.,* 2011) and SGK2 was also localized to the nucleus (Figure 4.3, A and B). SGK3, however, showed a clear localization to distinct vesicular structures throughout the cytoplasm (Figure 4.4C). This is due to the fact that only SGK3, but not SGK1 and SGK2, possesses a phox homology (PX) domain in its N-terminus (Virbasius *et al.,* 2001) that binds to phosphatidylinositol-3-phosphate [PI(3)P] and thus localizes SGK3 to PI(3)P containing endosomal membranes (Sato *et al.,* 2001). Kir2.2 is a non-soluble membrane protein and its localization is thus restricted to the cell surface and membrane containing structures within the cell. Accordingly, a localization of Kir2.2 to vesicular structures in the cell as well as a homogeneous staining of the entire cell was observed (Figure 4.3). In COS-7 cells, which are extremely flat, a weak homogeneous staining of the entire cells indicates localization to the plasma membrane.

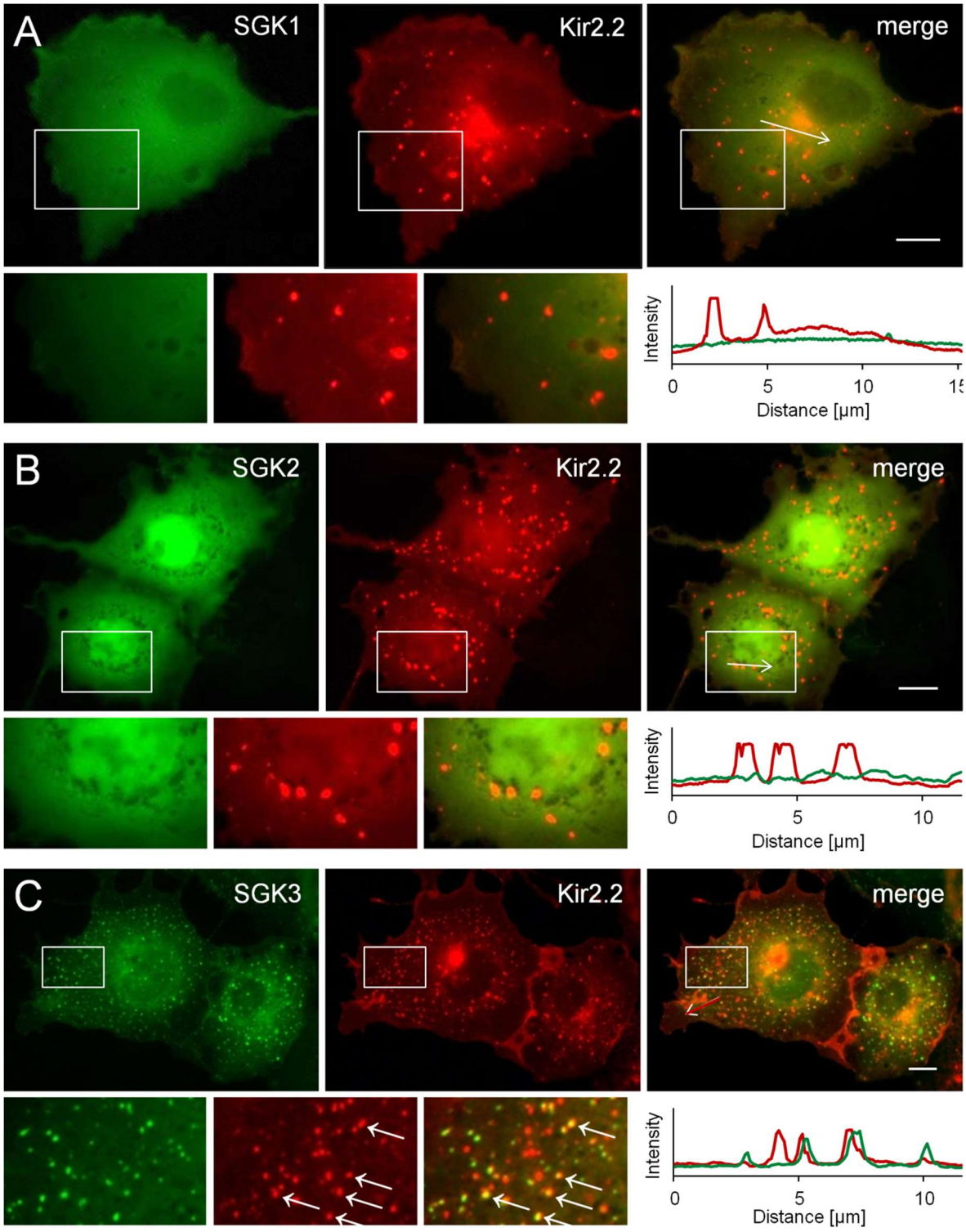
A
SGK1
Kir2.2
merge
Intensity
0
5
10
15
Distance [µm]
B
SGK2
Kir2.2
merge
Intensity
0
5
10
Distance [µm]
C
SGK3
Kir2.2
merge
Intensity
0
5
10
Distance [µm]

Figure 4.3: Kir2.2 is colocalized with SGK3 but not SGK1 and SGK2. Coexpression of mCherry-tagged Kir2.2 channels with **A)** EGFP-tagged SGK1, **B)** EGFP-tagged SGK2 or **C)** EGFP-tagged SGK3 in COS-7 cells. Selected regions of interest (white rectangles) are shown at higher magnification. The intensity profiles of EGFP and mCherry along the large white arrows are shown in the panels below the pictures. Small white arrows indicate structures that were positive for both Kir2.2 and SGK3. All pictures were taken 24 h after transfection, the scale bars are 10 µm.

While no colocalization of Kir2.2 with SGK1 or SGK2 was observed, a large number of vesicles were positive for both the channel and SGK3. The localization to the same intracellular compartment indicates that the spatial proximity of the two proteins might play a role in mediating the activation of Kir2.2. I therefore concentrated my subsequent studies on SGK3.

4.1.4 SGK3 increases Kir2.2 surface expression in COS-7 cells

To further explore the stimulating effect of SGK3 on Kir2.2 in a mammalian expression system, both proteins were coexpressed in COS-7 cells, and surface membrane expression of Kir2.2 was determined with a chemoluminescence-based surface expression assay. To investigate whether the serum- and glucocorticoid-inducible kinases are expressed endogenously in COS-7 cells, a RT-PCR analysis was performed on COS-7 whole cell lysate. Both SGK1 and SGK3 mRNA could be detected using intron-spanning primers (Figure 4.4).

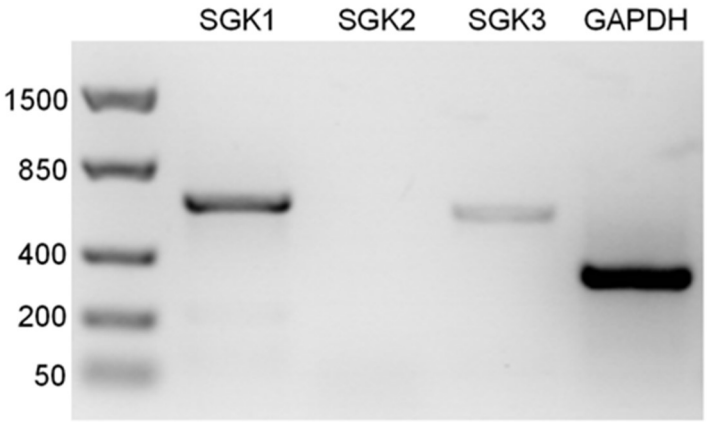

Figure 4.4: COS-7 cells endogenously express SGK1 and SGK3. RT-PCR was performed on whole cell lysate of COS-7 cells using intron-spanning primers for SGK1, SGK2, SGK3 and GAPDH as a control.

To rule out an increase in surface expression of Kir2.2 by endogenous SGK3, Kir2.2 was coexpressed with a dominant negative mutant of SGK3 (SGK3-DN). This dominant negative SGK3-construct harbors a mutation in the ATP-binding site (K191N) and is kinase-dead; it is therefore expected to outcompete the endogenous enzymes. It was used as a negative control in all following surface expression experiments in COS-7 cells. Somewhat surprisingly, coexpression of wild-type SGK3 did not increase the surface expression of Kir2.2-HA in comparison to the kinase-dead mutant. One explanation for this finding is that in COS-7 cells the transfected wild-type SGK3 protein was present in a dephosphorylated and thus inactive state. To be fully active, SGK3 has to be phosphorylated at two distinct phosphorylation sites: Thr320 and Ser486. Since transient transfection of SGK3 does not necessarily lead to a phosphorylated and thus active protein in COS-7 cells, I used a constitutively active mutant for my further experiments.

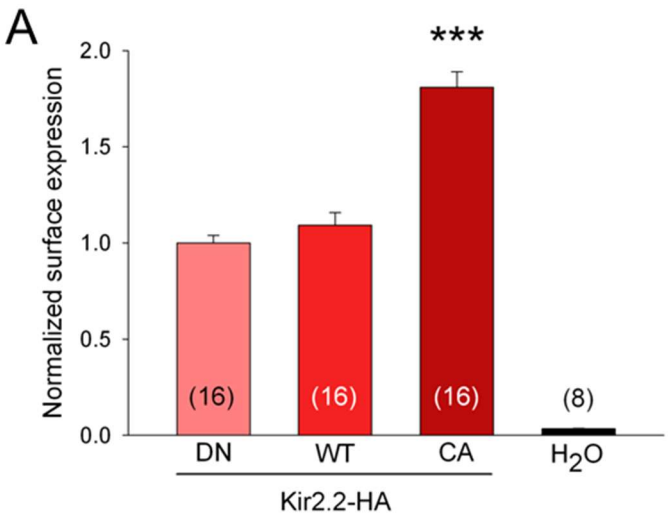

Figure 4.5: Overexpression of a constitutively active (CA) mutant of SGK3 increases the abundance of Kir2.2 in the plasma membrane of COS-7 cells. Surface membrane expression of HA-tagged Kir2.2 coexpressed with wild type (WT) and constitutively active (CA) SGK3 was compared to coexpression with a dominant negative mutant (DN). Surface expression was quantified by chemoluminescence based assay. Values were normalized to the channel coexpressed with the dominant negative mutant, the number of cells that were measured is given in brackets; mean ± SEM; *** $p<0.001$.

In this mutant, the HM-domain in the extreme C-terminus of SGK3 that harbors the first mandatory phosphorylation site was replaced with the HM of PKC-related kinase 2 (PRK2), a potent mimic of a phosphorylated HM (Tessier and Woodgett 2006a), leading to a constitutively active kinase (SGK3-CA). When coexpressed with SGK3-CA, Kir2.2-HA surface expression was increased by 80% compared to SGK3-DN (Figure 4.5), confirming the results obtained in *Xenopus* oocytes. These findings suggest that SGK3 is not constitutively active in COS-7 cells. The activation of the kinase possibly depends on the presence of extracellular stimuli that induce its phosphorylation.

To make sure that the intracellular localization of SGK3 was not disturbed by introduction of the activating and inactivating mutations, both mutants and the wild type SGK3 protein were attached to EGFP. Each construct was expressed in COS-7 cells and live-cell imaging was performed. As illustrated in Figure 4.6, no differences regarding the subcellular localization were observed between the three proteins; they all showed localization to distinct vesicular compartments.

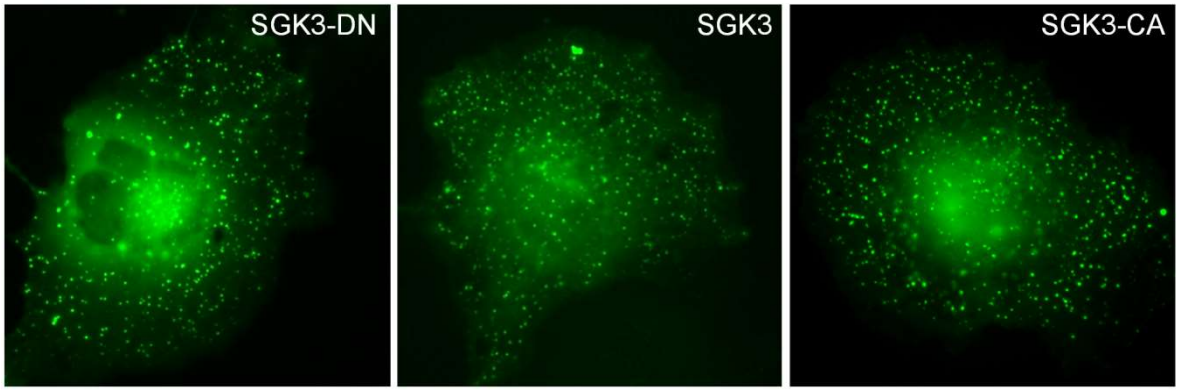

Figure 4.6: The intracellular distribution of a constitutively active (CA) and a dominant negative (DN) mutant of SGK3 in comparison to the wild type. Pictures were taken 24 h after transfection; the kinases were tagged with EGFP.

I also coexpressed each EGFP-tagged SGK3-mutant with mCherry-tagged Kir2.2 channel (Figure 4.7). Here, too, I did not observe any differences regarding the expression pattern of the channel or the amount of colocalization between Kir2.2 and SGK3.

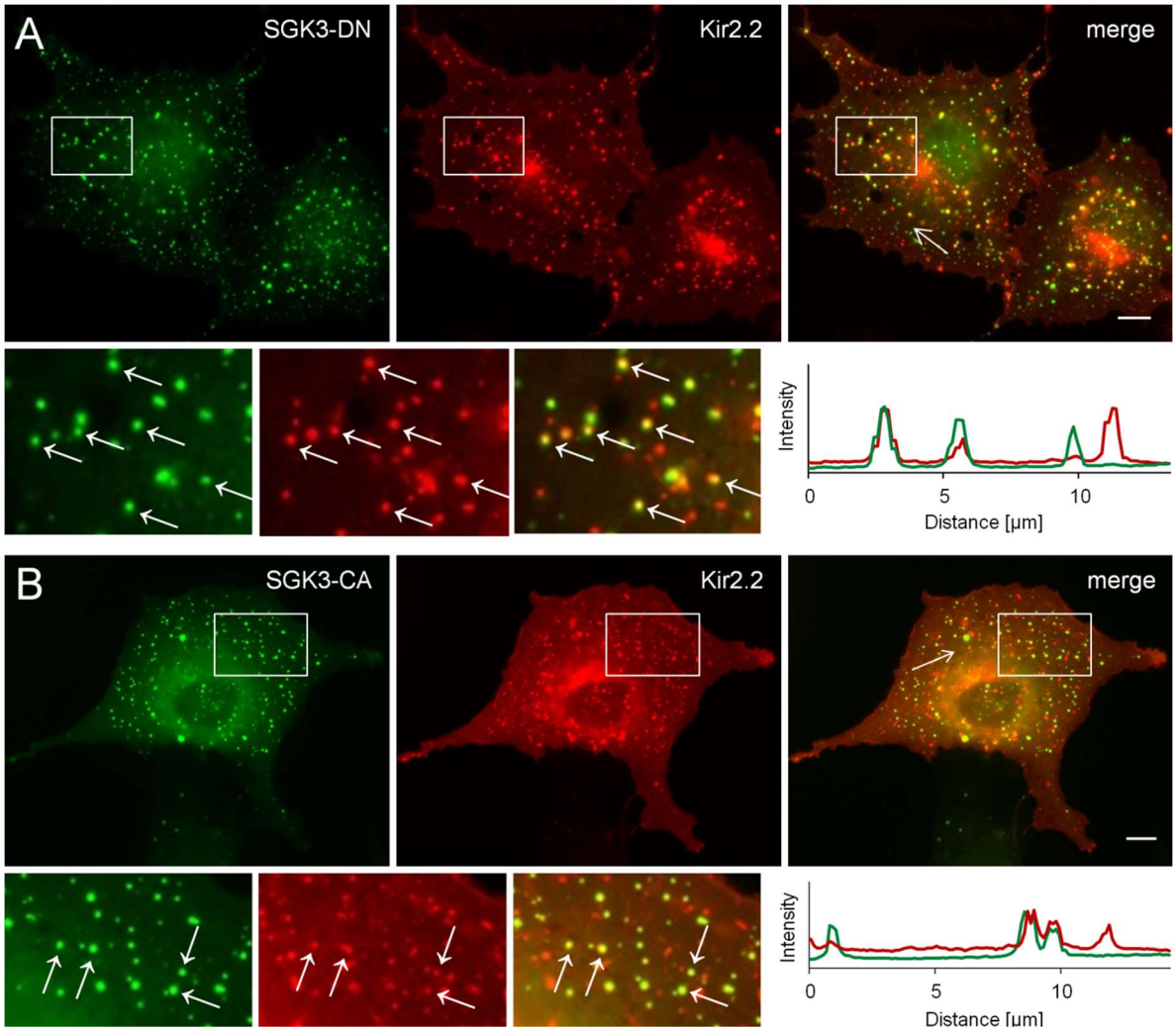

Figure 4.7: Kir2.2 shows the same amount of colocalization with dominant negative (DN) and constitutively active (CA) mutants of SGK3. MCherry-tagged Kir2.2 was coexpressed with **A)** an EGFP-tagged dominant negative mutant of SGK3 and **B)** an EGFP-tagged constitutively active mutant of SGK3. Selected regions of interest (white rectangles) are shown at higher magnification. Intensity profiles of EGFP and mCherry along the large white arrows are shown in the panels below the merged images. Small arrows indicate structures that are positive for both proteins. All pictures were taken 24 h after transfection; the scale bars are 10 µm.

4.2 Investigation of the molecular mechanism underlying the increase in Kir2.2 surface expression mediated by SGK3

An increased number of channels in the surface membrane could be due to: i) reduced endocytosis and retrograde transport of channel molecules; ii) an increased number of newly synthesized channels or iii) an increased recycling rate of channels. To further elucidate the mechanism underlying the increase in membrane expression observed in this study, I explored a number of possible pathways.

4.2.1 SGK3 does not affect protein biosynthesis of Kir2.2

One possible mechanism by which SGK3 might elevate the membrane abundance of Kir2.2 is by interfering with protein biosynthesis. By increasing the overall amount of synthesized channel, the kinase could lead to an increased insertion of Kir2.2 channels into the plasma membrane. SGK3 has, for instance, been shown to affect the transcription rate of proteins by phosphorylating the transcription factor FOXO3a (Xu *et al.,* 2009).

To block biosynthesis of Kir2.2 I applied cycloheximide. Cycloheximide is a glutaramide antibiotic that inhibits eukaryotic protein biosynthesis by inhibiting translation elongation. It binds to the E-site of the 60S ribosomal subunit and interferes with deacetylated tRNA (Schneider-Poetsch *et al.,* 2010).

When *Xenopus* oocytes injected with Kir2.2 alone or together with SGK3 were incubated with 10 µM cycloheximide for 16 h, a marked reduction of current amplitude to 50 – 60 % of the untreated control group was observed. Although the absolute current was smaller, block of protein translation with cycloheximide did not affect the extent to which SGK3 increased Kir2.2 current amplitude (Figure 4.8). These data therefore suggest that SGK3 does not affect protein biosynthesis of Kir2.2

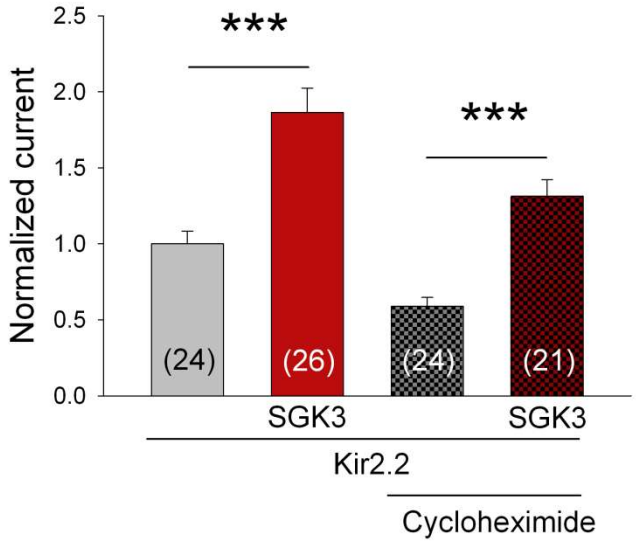

Figure 4.8: SGK3 does not affect translation of Kir2.2. *Xenopus* oocytes were injected with Kir2.2 alone or together with SGK3 and incubated with 10 µM Cycloheximide for 16 h. All values were normalized to the expression of the channel alone, the number of oocytes from which the data were obtained is given in brackets; mean ± SEM; *** p<0.001.

4.2.2 SGK3 does not affect anterograde transport of Kir2.2

As a membrane protein, Kir2.2 is transported from the endoplasmic reticulum to the Golgi apparatus, where it is posttranslationally modified before it is inserted into the plasma membrane. To determine whether SGK3 promotes the anterograde transport of the channel I used the lactone antibiotic Brefeldin A. It interferes with the anterograde transport of cargo from the ER to the Golgi apparatus, leading to the accumulation of proteins in the ER and eventually to a collapse of Golgi stacks. As a result, proteins are held back in the ER and can no longer be transported forward to the plasma membrane (Klausner *et al.,* 1992). Treatment of oocytes for 6 h with 5 µM Brefeldin A resulted in a significant reduction of Kir2.2 mediated current by 50%. However, the relative increase in channel activity through SGK3 remained unchanged (Figure 4.9).

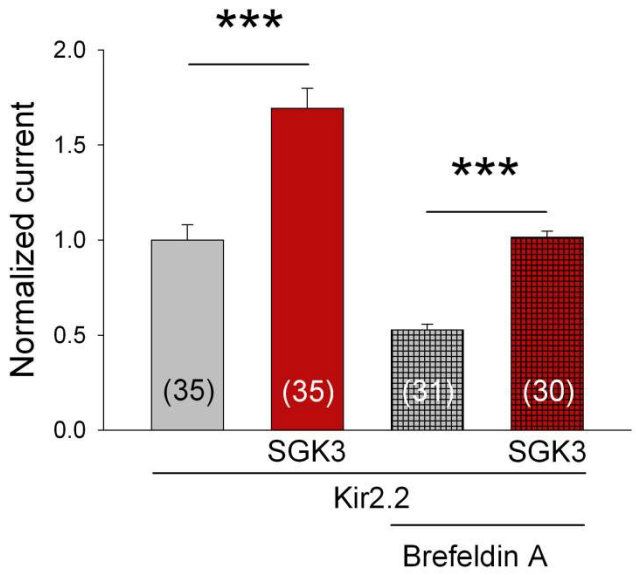

Figure 4.9: SGK3 does not affect export of Kir2.2 from the ER. *Xenopus* oocytes were injected with Kir2.2 alone or together with SGK3 and incubated with 5 µM Brefeldin A for 6 h. All values were normalized to the expression of the channel alone, the number of oocytes from which the data were obtained is given in brackets; mean ± SEM; *** p<0.001.

These results indicate that SGK3 does not promote anterograde transport of Kir2.2 to the plasma membrane. A possible interpretation for our data is that SGK3 interferes with a pool of channel molecules that has successfully passed the Golgi complex. SGK3 could either (i) inhibit the endocytosis and retrograde transport of channel molecules that have already been inserted into the plasma membrane or (ii) promote the recycling of a pool of Kir2.2 channels residing in the endosomal system back to the plasma membrane.

4.2.3 Kir2.2 is not affected by the ubiquitin ligase Nedd4-2

It has been shown for several ion channels whose surface expression is upregulated by SGK3, for instance hERG and Kv1.5, that this effect is mediated by inactivation of Nedd4-2 (Boehmer *et al.,* 2008; Lamothe and Zhang 2013). Nedd4-2 is an E3 ubiquitin-ligase that transfers ubiquitin to substrate molecules, leading to their internalization from the membrane and subsequent degradation. The serine/threonine kinase SGK3 inhibits Nedd4-2 activity by phosphorylating it at Ser444. The phosphorylated ligase is then bound by 14-3-3, which decreases its abundance at the plasma membrane (Bhalla *et al.,* 2005; Chandran *et al.,* 2011). As a result, SGK3 reduces the amount of ubiquitinated and internalized Nedd4-2 substrates and thus increases their expression at the cell surface.

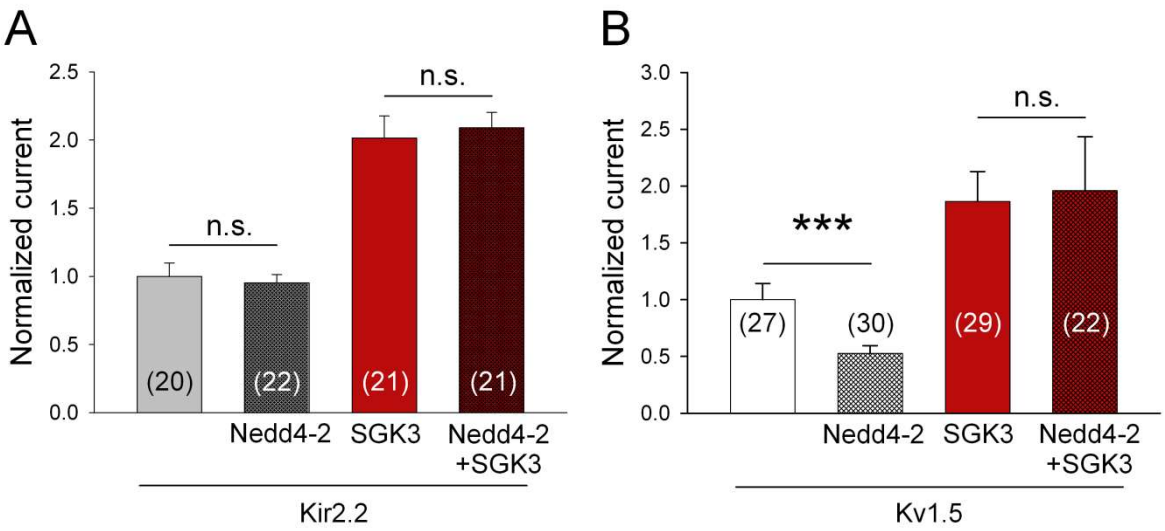

Figure 4.10: The ubiquitin ligase Nedd4-2 does not modify the effect of SGK3 on Kir2.2 currents measured in *Xenopus* oocytes. **A)** Coexpression of Kir2.2 with SGK3 and/or Nedd4-2. **B)** Coexpression of the voltage-activated potassium channels Kv1.5 with SGK3 and/or Nedd4-2 served as a positive control. All values were normalized to the respective channel alone; the number of oocytes from which the data were obtained is given in brackets; mean ± SEM; *** p<0.001.

To investigate whether Nedd4-2 is involved in the SGK3 mediated upregulation of Kir2.2 surface expression, the potassium channel and the ubiquitin ligase were coexpressed in *Xenopus* oocytes with and without SGK3. Nedd4-2 had no effect on the current amplitude of Kir2.2, neither in absence nor in presence of SGK3 (Figure 4.10A).

To ensure that under our experimental conditions the Nedd4-2 construct was properly expressed and functional in oocytes, the voltage gated potassium channel Kv1.5 was used as a positive control. It was shown previously that the channel is ubiquitinated and downregulated by Nedd4-2 and that this effect can partly be restored by SGK1 (Boehmer *et al.,* 2008). In the present study, coexpression with Nedd4-2 reduced the current amplitude of Kv1.5 by approximately 50%, whereas coexpression of SGK3 caused a twofold increase in Kv1.5 current, independent of the additional coexpression of Nedd4-2 (Figure 4.10B). These results are in agreement with previous results and with the hypothesis outlined above. From these data it can be concluded that SGK3 elevates Kir2.2 membrane abundance through a pathway that is independent of the ubiquitinase Nedd4-2.

4.2.4 SGK3 does not inhibit clathrin mediated endocytosis

In the next step, it was tested whether SGK3 might impede the endocytosis of Kir2.2 through clathrin-mediated endocytosis via a mechanism unrelated to Nedd4-2. To this end the potassium channel was coexpressed with AP180C in the absence and presence of SGK3 in *Xenopus* oocytes. AP180C is the C-terminal part of the clathrin adaptor AP180 and efficiently blocks clathrin mediated endocytosis (Doherty and McMahon 2009). Coexpression of Kir2.2 with AP180C led to an increase in current amplitude by a factor of 2.5, consistent with the idea that Kir2.2 is constantly endocytosed via a clathrin dependent mechanism and that endocytosis can effectively be blocked by AP180C. However, the relative increase in current amplitude caused by SGK3 was roughly the same in absence and presence of AP180C (Figure 4.11A), indicating that the effect of SGK3 on Kir2.2 current amplitude is not mediated by inhibition of endocytosis. These observations were corroborated by a surface expression assay which also showed that SGK3 caused an additional increase in surface expression on top of the effect of AP180C (Figure 4.11B).

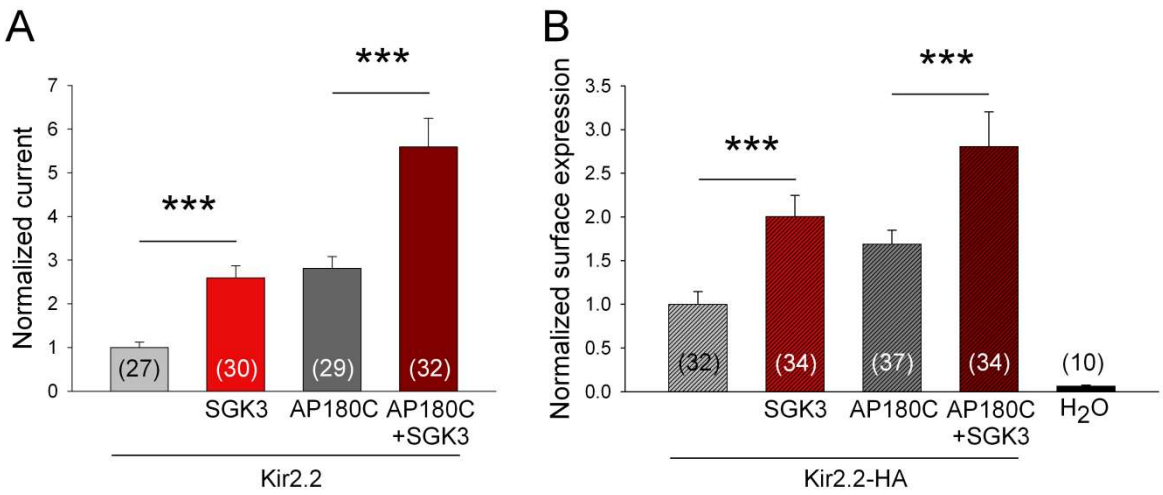

Figure 4.11: SGK3 does not impair clathrin dependent endocytosis of Kir2.2. Effect of SGK3 on **A)** Kir2.2 current amplitude and **B)** Kir2.2 surface expression measured in *Xenopus* oocytes in the absence and presence of AP180C. A P180C is the C-terminus of the clathrin adaptor AP180 and a potent inhibitor of clathrin-mediated endocytosis. All values were normalized to the respective channel alone; the number of oocytes from which the data were obtained is given in brackets; mean ± SEM; *** $p<0.001$.

To confirm the results obtained in *Xenopus* oocytes in a mammalian expression system, an antibody uptake assay was performed in COS-7 cells (Zadeh *et al.,* 2008). The amount of endocytosed channel in the presence of either the kinase dead SGK-DN or the constitutively active SGK3-CA after 0 min, 15 min and 30 min was monitored (Figure 4.12). Channel proteins that were internalized after the indicated time period are shown in red, channel proteins that remained in the plasma membrane are shown in green. To compare the amount of channel protein that was internalized in the presence of SGK3-DN and SGK3-CA, the ratio between internalized and membrane resident channels was determined for each cell. The evaluation of 38-53 cells for each construct revealed that the fraction of channels that was internalized after 0 min, 15 min and 30 min was the same, regardless whether it was coexpressed with the dominant-negative or with the constitutively active mutant of SGK3. Taken together, these experiments confirm that SGK3 does not affect clathrin mediated endocytosis of Kir2.2.

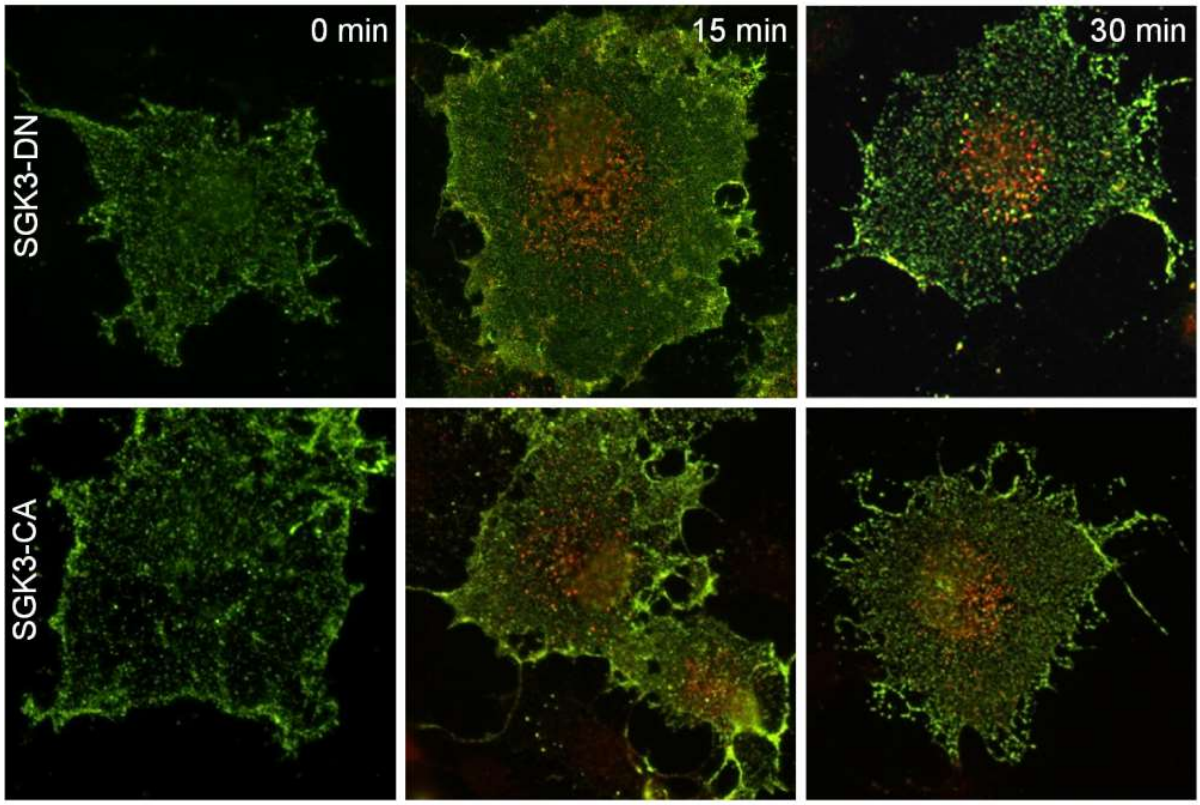

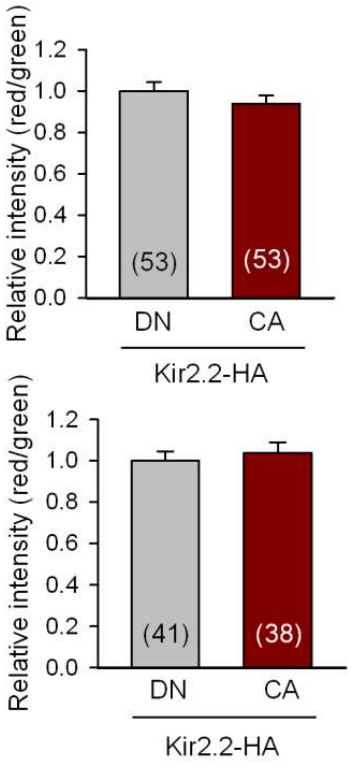

Figure 4.12: SGK3 does not impair endocytosis of Kir2.2. Coexpression of HA-tagged Kir2.2 with SGK3-DN or SGK3-CA in COS-7 cells. Channels in the plasma membrane were labeled with mouse anti-HA antibody at t=0 and 4 °C, followed by a 0 min, 15 min or 30 min internalization period at 37 °C. Cells were then fixed and channels that had remained in the plasma membrane were stained with Alexa Fluor® 488-conjugated anti-mouse antibody (green). After permeabilization of the membrane, the internalized channels were stained with Alexa Fluor® 594-conjugated anti-mouse antibody (red). To determine the rate of endocytosis, the ration between internalized channels (red) and surface membrane resident channels (green) was calculated. The fluorescence intensity of the red and the green dyes was determined and the ratio is shown in the bar graphs at the left (normalized to SGK3-DN). Cells were stained 24 h after transfection; the number of cells analyzed is indicated in brackets.

4.2.5 Internalized Kir2.2 channels are recycled back to the plasma membrane

Since the results described in the preceding chapters suggest that SGK3 (i) neither affects the number of newly synthesized channels (ii) nor the rate of endocytosis, the third possibility was investigated, namely that SGK3 may promote the recycling of a pool of Kir2.2 channels residing in the endosomal system.

To test whether Kir2.2 is recycled to the plasma membrane, I performed an antibody-based recycling assay in COS-7 cells. In this assay, the cells were transfected with Kir2.2-HA and either SGK3-DN or SGK3-CA. Membrane resident channels were labeled with a primary anti-HA antibody and subsequently allowed to undergo endocytosis for 30 min at 37 °C. The HA-tagged channels still present in the surface membrane were then labeled with a secondary antibody conjugated to a green fluorescent dye. This was followed by a second incubation at 37 °C for 30 min to allow previously internalized channels to recycle back to the plasma membrane. Subsequently, cells were fixed and incubated with a secondary antibody conjugated to a red fluorescent dye, labeling the channels that were recycled back to the plasma membrane. Figure 4.13 illustrates that a considerable number of Kir2.2 channels is endocytosed and recycled back to the plasma membrane during two incubation periods of 30 min. Although it was not possible to precisely quantify the amount of recycled Kir2.2 channels, analysis of the images indicated that co-transfection of SGK3-CA substantially increased the number of recycled Kir2.2 channels compared to the dominant negative mutant.

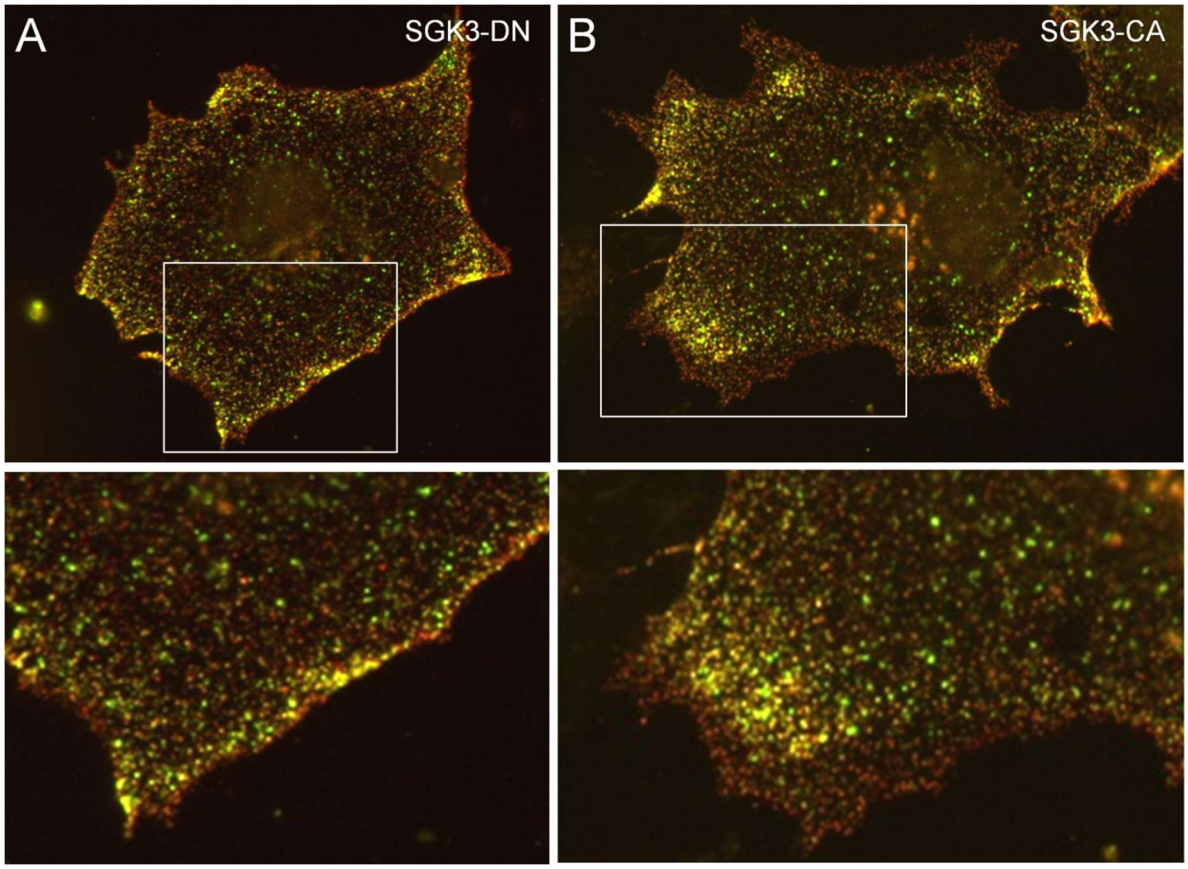

Figure 4.13: Recycling of endocytosed Kir2.2 channels to the plasma membrane. COS-7 cells transfected with Kir2.2-HA and either **A)** SGK3-DN or **B)** SGK3-CA were cooled to 4 °C and membrane resident Kir2.2-HA channels were labeled with a primary mouse anti-HA antibody. Cells were then re-warmed to 37 °C for 30 min and the channels were allowed to undergo endocytosis. Subsequently, cells were cooled to 4 °C and HA-tagged channels still present in the surface membrane were labeled with Alexa Fluor® 488-conjugated anti-mouse antibody (green). This was followed by a second incubation step at 37 °C for 30 min to allow previously internalized channels to recycle back to the plasma membrane. Cells were then fixed with 4 % paraformaldehyde on ice and channels that had been endocytosed during the first incubation period at 37 °C and had been recycled back to the plasma membrane during the second incubation period at 37 °C were labeled with Alexa Fluor® 594-conjugated anti-mouse antibody (red). Cells were stained 24 h after transfection; selected regions of interest (white rectangles) are shown at higher magnification.

4.2.6 The PI5-kinase PIKfyve is not involved in the stimulating effect of SGK3

In a previous study it has been proposed that the effect of SGK3 on Kir2.2 current amplitude is mediated by the effect of SGK3 on the PI5-kinase PIKfyve (Seebohm *et al.,* 2012b). PIKfyve contains a FYVE domain that localizes it to PI(3)P containing membranes where it produces PI(3,5)P_2 by phosphorylating

PI(3)P. The Seebohm lab published data indicating that PIKfyve is phosphorylated by SGK3 at residue Ser318 and may be involved in mediating the effect of SGK3 on Kir2.2 current amplitude.

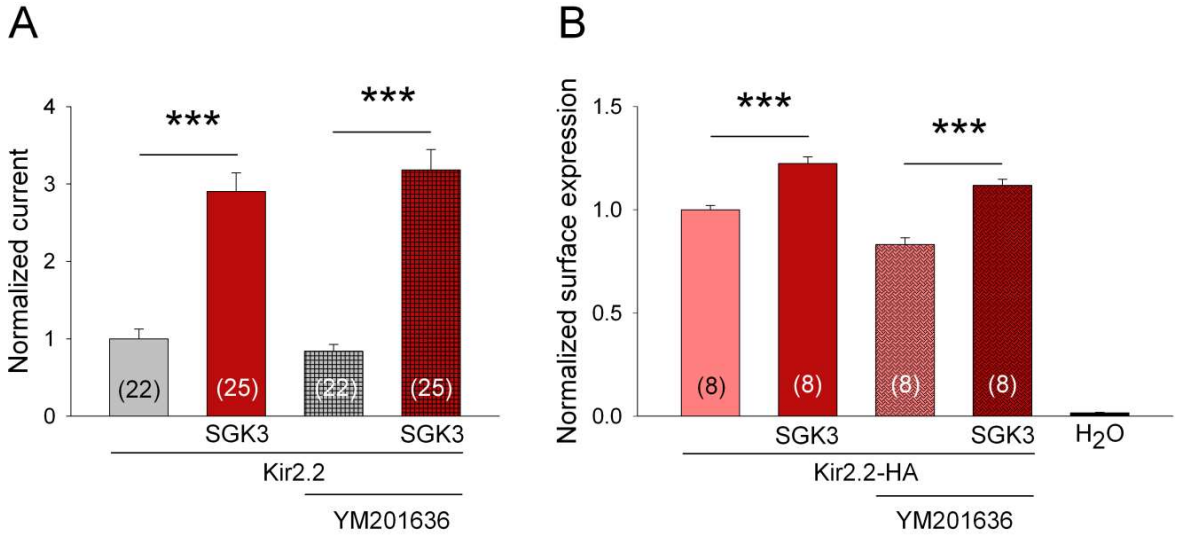

Figure 4.14: The PI5-kinase PIKfyve is not involved in mediating the SGK3 effect. **A)** *Xenopus* oocytes injected with Kir2.2 alone or together with SGK3 were incubated with 5 µM of the PIKfyve inhibitor YM201636 for 16 h and the current amplitude was determined. **B)** COS-7 cells were transfected with Kir2.2-HA alone or together with SGK3 and incubated with the PIKfyve Inhibitor YM201636 (800 nM, 4 h). Mean surface expression was determined. The number of cells from which the data were obtained is given in brackets; mean ± SEM; *** $p<0.001$.

This hypothesis was tested using the PIKfyve inhibitor YM201636 (Jefferies *et al.,* 2008; Sbrissa *et al.,* 2012). When oocytes injected with either Kir2.2 cRNA alone or together with SGK3 cRNA were incubated with 5 µM of the inhibitor for 16 h, no significant differences in current amplitude could be observed between treated and untreated oocytes (Figure 4.14A). This observation was corroborated by a surface expression assay in COS-7 cells. The mean surface expression of Kir2.2-HA was slightly, but not significantly, reduced after incubation with 800 nM YM201636 for 4 h (Figure 4.14B), and the stimulatory effect of SGK3 on surface expression was not changed by incubation of the cells with YM201636. These results indicate that the effect of SGK3 on Kir2.2 is not mediated by PIKfyve.

4.3 Role of the intracellular localization of Kir2.2 and SGK3

4.3.1 Abrogating the endosomal localization of SGK3 reduces the effect on Kir2.2

To study the relevance of the endosomal localization of SGK3 for its effect on Kir2.2 surface expression, a mutation was introduced into the PX domain of the kinase. An arginine residue at position 90 was mutated to alanine; this mutation has previously been shown to abolish binding of SGK3 to phosphoinositides (Xing *et al.,* 2004). When tagged with EGFP and coexpressed with Kir2.2 in COS7 cells, the $SGK3^{R90A}$ mutant showed a diffuse cytoplasmic localization; colocalization with the potassium channel was completely abolished (Figure 4.15A). $SGK3^{R90A}$ was then coexpressed with Kir2.2 in *Xenopus* oocytes. The effect on both current amplitude and surface expression of the potassium channel was significantly reduced compared to the wild type (Figure 4.15, B and C). These results were corroborated by a surface expression assay in COS-7 cells. Here, too, the surface expression of Kir2.2 coexpressed with $SGK3^{R90A}$-CA was significantly decreased in comparison to SGK3-CA (Figure 4.15D). Nevertheless, the R90A mutant still caused a significant increase in current amplitude and surface expression of the channel in comparison to control in both expression systems.

These findings indicate that the endosomal localization of SGK3 contributes to the effect on the surface expression of Kir2.2 channels; however it is not essential for the effect on the intracellular traffic of Kir2.2.

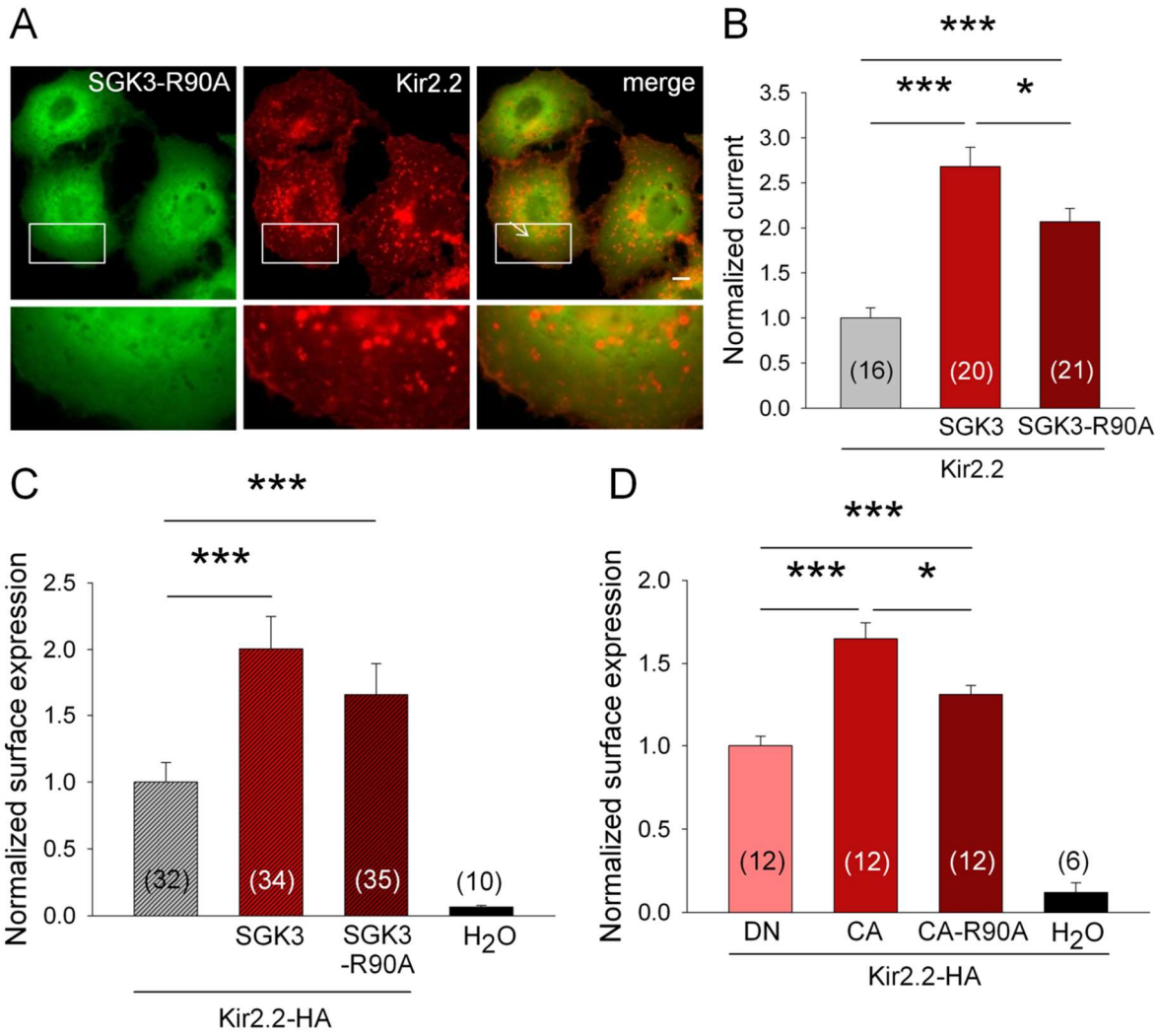

Figure 4.15: Abrogating the endosomal localization of SGK3 abolishes colocalization with Kir2.2 and reduces the effect of SGK3 on Kir2.2 current amplitude and surface expression. A) A mutant of SGK3 harboring a mutation in its PX domain ($SGK3^{R90A}$) was coexpressed with Kir2.2 in COS7 cells. The R90A mutation abolishes binding of SGK3 to phosphoinositides and therefore its endosomal localization. Pictures were taken 24 h after transfection; Kir2.2 was tagged with mCherry and $SGK3^{R90A}$ with EGFP. Selected regions of interest (white rectangles) are shown at higher magnification. **B)** Kir2.2 currents measured in *Xenopus* oocytes after coexpression of Kir2.2-HA with $SGK3^{R90A}$. **C)** Surface expression of HA-tagged Kir2.2 channels measured in *Xenopus* oocytes after coexpression of Kir2.2 with $SGK3^{R90A}$. **D)** Mean surface expression of Kir2.2 coexpressed with $SGK3^{R90A}$-CA in COS7 cells was compared to the surface expression of Kir2.2-HA coexpressed with SGK3-DN or SGK3-CA. The number of cells from which the data were obtained is given in brackets; mean ± SEM; * $p<0.05$, *** $p<0.001$.

4.3.2 SGK3 and Kir2.2 are both localized to PI(3)P and Rab7 containing compartments

The results obtained in the preceding experiments strongly suggest that SGK3 affects a pool of functional Kir2.2 channels residing in an endosomal compartment. To more precisely identify the subcellular compartments in which SGK3 and Kir2.2 reside, both proteins were coexpressed with the small GTPases Rab5, Rab7, Rab4, and Rab11 and the biosensor 2xFYVE.

Rab proteins constitute the largest family of small GTPases and are reversibly associated with distinct intracellular membranes. Together with a group of highly specific phosphoinositide (PI) kinases and phosphatases, the Rab-GTPases serve as organizers of membrane trafficking processes and determine the identity of intracellular compartments. They are therefore well-suited as markers for specific endosomal compartments. In the following experiments, Rab5 served as a marker for the early endosome, Rab7 as a marker for the late endosome, Rab11 as a marker for the recycling endosome and Rab4 as a marker for a fast recycling pathway. 2×FYVE is a biosensor that contains two PX domains which specifically bind the phosphoinositide PI(3)P; it was used as a marker of PI(3)P containing membranes.

Kir2.2 was highly colocalized (virtually to the same extent) with 2xFYVE (Figure 4.16A) and Rab7 (Figure 4.16C). It showed only a very limited localization to early endosomes containing Rab5 (Figure 4.16 B). As expected, a nearly perfect colocalization was observed for SGK3 and 2xFYVE (Figure 4.17A). The kinase was also clearly localized to compartments positive for Rab5 (Figure 4.17B) and, somewhat surprisingly, to a compartment positive for Rab7 (Figure 4.17C).

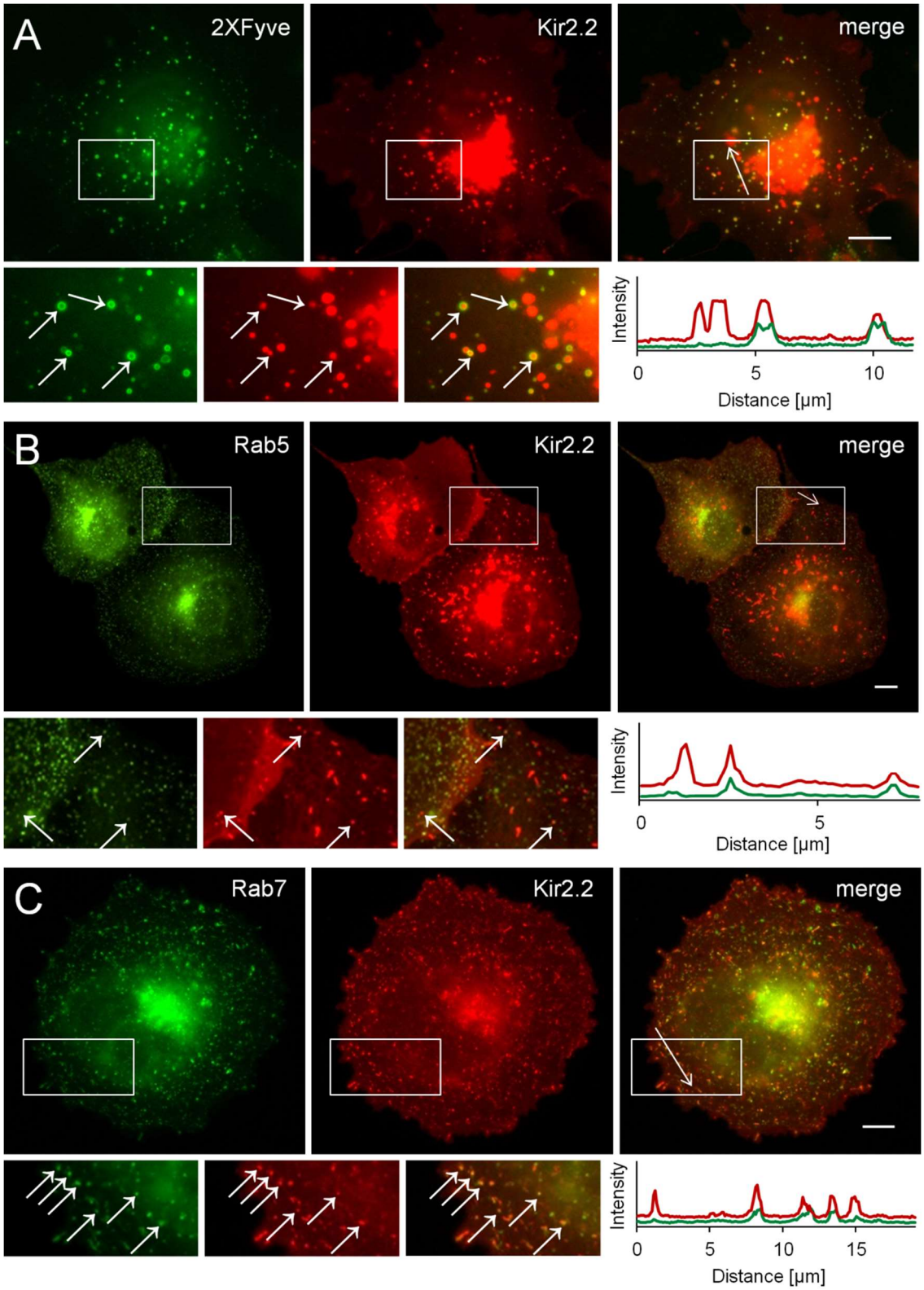

Figure 4.16: Kir2.2 is localized to the early endosome and the late endosome. Coexpression of mCherry-tagged Kir2.2 with **A)** EGFP-tagged 2XFYVE, **B)** EGFP-tagged Rab5 and **C)** EGFP-tagged Rab7 as markers for PI(3)P containing membranes, the early endosome and the late endosome, respectively. Selected regions of interest (white rectangles) are shown at higher magnification. Small arrows indicate structures that are positive for both proteins. Intensity profiles of EGFP and mCherry along the large white arrows are shown in the panels below the merged images. All pictures were taken 24 h after transfection; the scale bars are 10 µm.

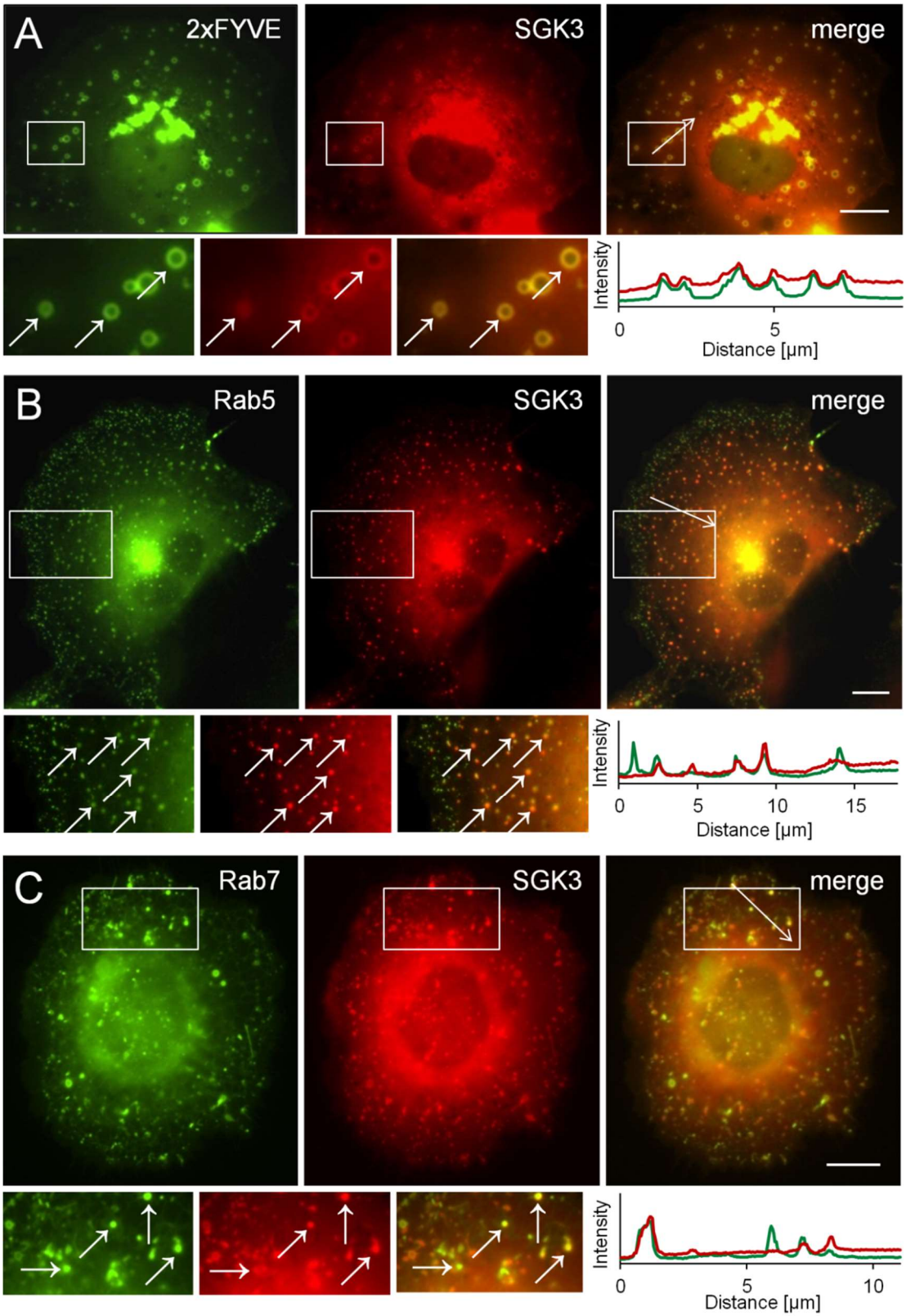

Figure 4.17: SGK3 is localized to the early endosome and the late endosome. Coexpression of mCherry-tagged SGK3 with **A)** EGFP-tagged 2XFYVE, **B)** EGFP-tagged Rab5 and **C)** EGFP-tagged Rab7, which were used as markers of PI(3)P containing membranes, the early endosome and the late endosome, respectively. Selected regions of interest (white rectangles) are shown at higher magnification. Small arrows indicate structures that are positive for both proteins. Intensity profiles of EGFP and mCherry along the large white arrows are shown in the panels below the merged images. All pictures were taken 24 h after transfection; the scale bars are 10 µm.

Since I could show in preceding experiments that Kir2.2 is constantly endocytosed in a clathrin dependent manner (compare Figures 4.11, 4.12 and 4.13), it would be expected that a certain fraction of the channel is localized to Rab5 positive endosomes. The coexpression of mCherry-tagged Kir2.2 with GFP-tagged Rab5 did not result in a substantial colocalization; I therefore performed an antibody-staining in COS-7 cells transfected with Kir2.2-HA for endogenous Rab5 protein (Figure 4.18). The staining demonstrated a clear localization of Kir2.2 to Rab5 positive endosomes, indicating that the marginal colocalization that was observed with the EGFP-tagged Rab5-construct might be due to the overexpression of the GTPase and does not necessarily reflect the intracellular distribution of Kir2.2 under normal circumstances.

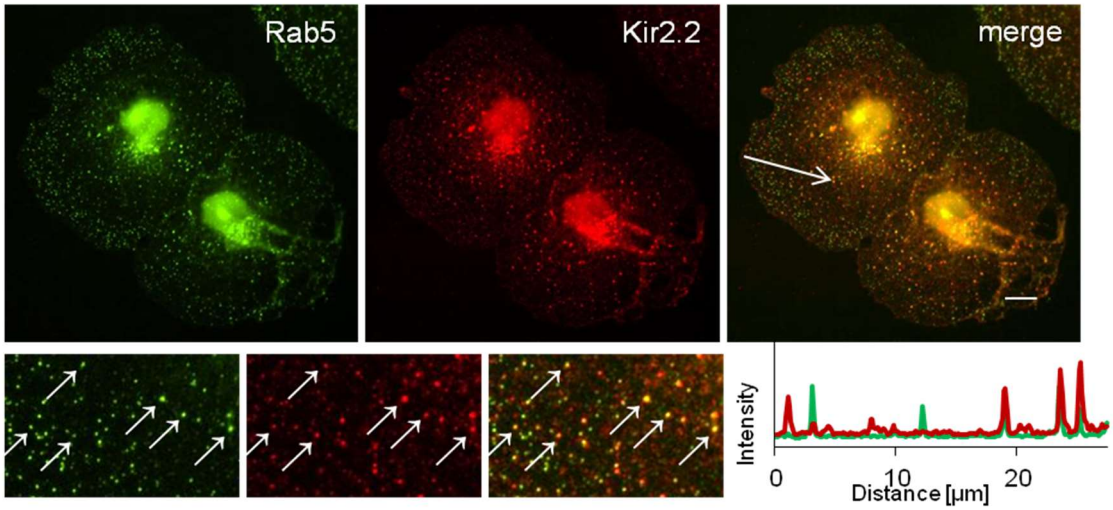

Figure 4.18: Kir2.2 is localized to Rab5 positive endosomes. Kir2.2-HA was expressed in COS-7 cells. Kir2.2-HA channels were labeled with anti-HA (mouse) primary antibody and Alexa Fluor® 594-conjugated anti-mouse secondary antibody (red); Rab5 was labeled with anti-Rab5 (rabbit) primary antibody and Alexa Fluor® 488-conjugated anti-rabbit secondary antibody (green). Selected regions of interest (white rectangles) are shown at higher magnification. Small arrows indicate structures that are positive for both proteins. Intensity profiles of EGFP and mCherry along the large white arrows are shown in the panels below the merged images. All pictures were taken 24 h after transfection; the scale bars are 10 µm.

The interaction between vesicles containing Kir2.2, SGK3, Rab5 and Rab7 was studied in more detail using live-cell imaging sequences. After transfection of COS-7 cells with mCherry-tagged SGK3 and EGFP-tagged Rab5, I observed the fusion of SGK3 positive vesicles (diameter, ~0.8-1.6 µm) with Rab5 positive vesicles that were distinctly smaller (diameter: ~0.3-0.5 µm; n = 9) (Figure 20A). Similar observations could be made in cells transfected with EGFP-tagged SGK3 and mCherry-tagged Kir2.2. In this case, too, somewhat larger SGK3-positive vesicles (diameter, 0.8-0.9 µm) fused with smaller Kir2.2-positive vesicles which had a diameter of 0.4-0.5 µm (n = 9) (Figure 19A). I further observed what appeared to be the recruitment of cytoplasmic Rab7 protein (green) to the membrane of SGK3 positive vesicles (red) (Figure 20B); these vesicles usually exhibited a ring-like structure. Similar ring-like endosomes positive for Rab7 (green) were found to interact with smaller vesicles containing Kir2.2 (Figure 19B).

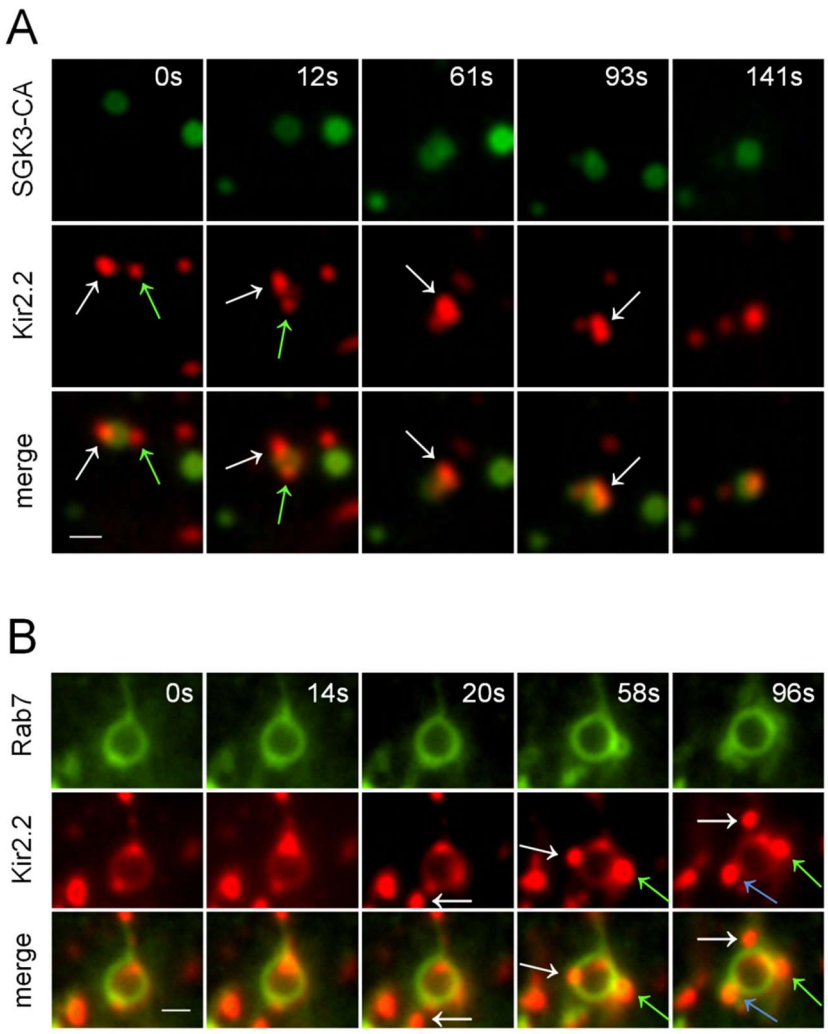

Figure 4.19: Kir2.2-positive vesicles interact with SGK3-positive vesicles and with Rab7-positive vesicles. Live-cell imaging of COS-7 cells transfected with mCherry-tagged Kir2.2 together with **A)** EGFP-tagged SGK3-CA or **B)** EGFP-tagged Rab7. The panels show the magnification of one characteristic event. The panels show the magnification of one characteristic event at different time points. The small arrows indicate the endosomal vesicles involved in the interaction. The images were recorded 24 h after transfection; the scale bars are 1 µm.

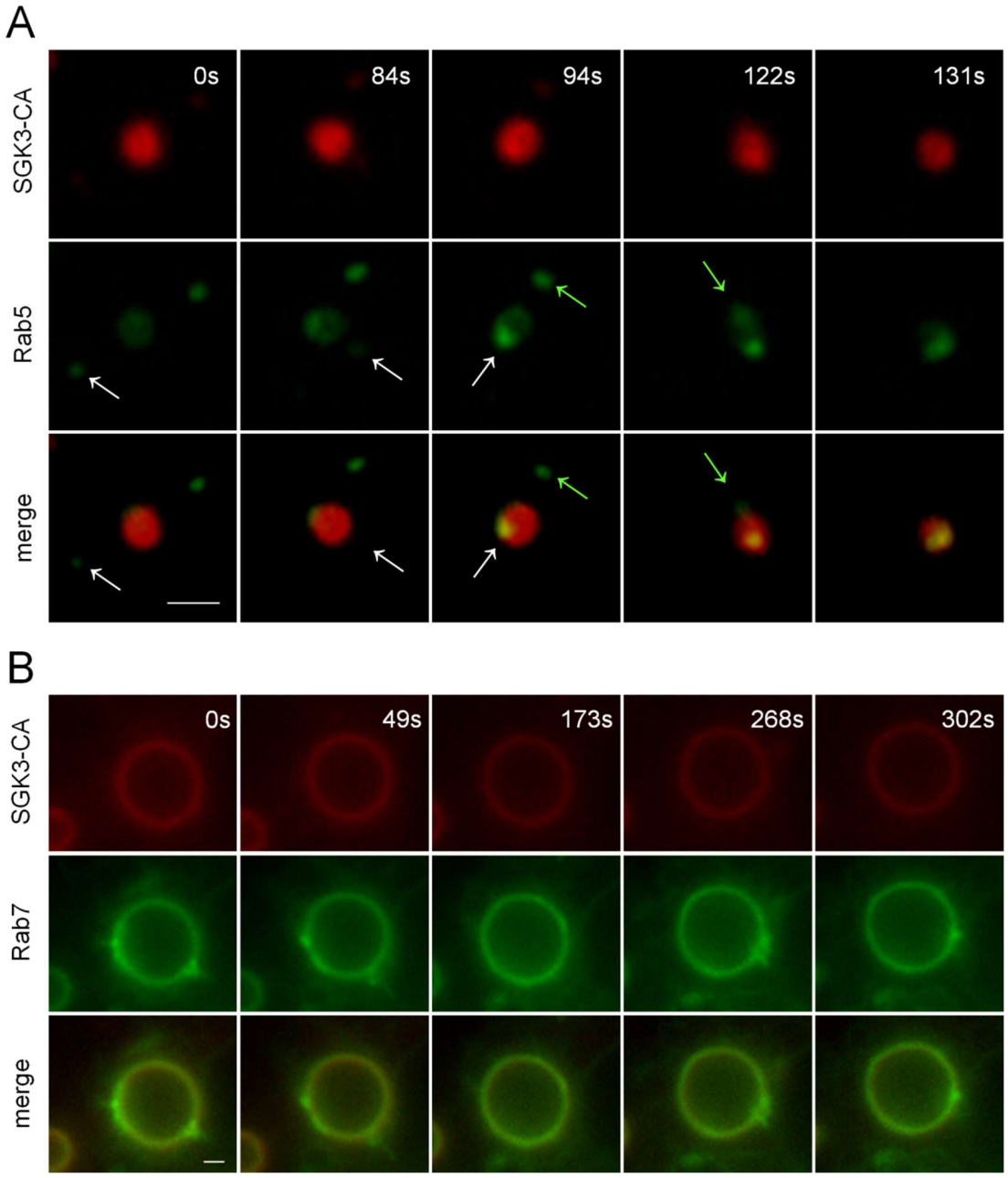

Figure 4.20: SGK3-positive vesicles interact with Rab5-positive vesicles and with Rab7-positive vesicles. Live-cell imaging of COS-7 cells transfected with mCherry-tagged SGK3-CA together with **A)** EGFP-tagged Rab5 or **B)** EGFP-tagged Rab7. The panels show the magnification of one characteristic event at different time points. The small arrows indicate the endosomal vesicles involved in the interaction. The images were recorded 24 h after transfection; the scale bars are 1 µm.

Taken together, these results indicate that the colocalization of Kir2.2 and SGK3 occurs mainly in PI(3)P and Rab7 positive structures in the endosomal pathway that could represent maturing early endosomes.

To investigate more precisely through which compartment Kir2.2 channels are recycled back to the plasma membrane, I coexpressed Kir2.2 and SGK3 with

Rab4 and Rab11, which served as markers for a slow and a fast recycling pathway, respectively. Neither Kir2.2 nor SGK3 was localized to Rab4 positive vesicles (Figures 4.21B and 4.22B). However, both proteins showed a certain amount of colocalization with Rab11 (Figures 4.21A and 4.22A). When I analyzed this putative colocalization more closely using live-cell imaging sequences, I observed that Kir2.2 and SGK3 positive vesicles (red) were not colocalized permanently with Rab11 but rather showed extensive ‘kiss-and-run’ interactions with the Rab11 positive recycling endosomes (green) (Figure 4.23, A and B). A similar pattern was visible when EGFP-tagged Rab11 was coexpressed with mCherry-tagged Rab7; the highly mobile recycling endosomes interacted with the more static and larger Rab7 positive endosomes (Figure 4.23C). These results indicate that the Kir2.2-SGK3-Rab7 positive compartment might interact with the Rab11 positive recycling endosomes, which might be involved in the transport of Kir2.2 channels back to the plasma membrane.

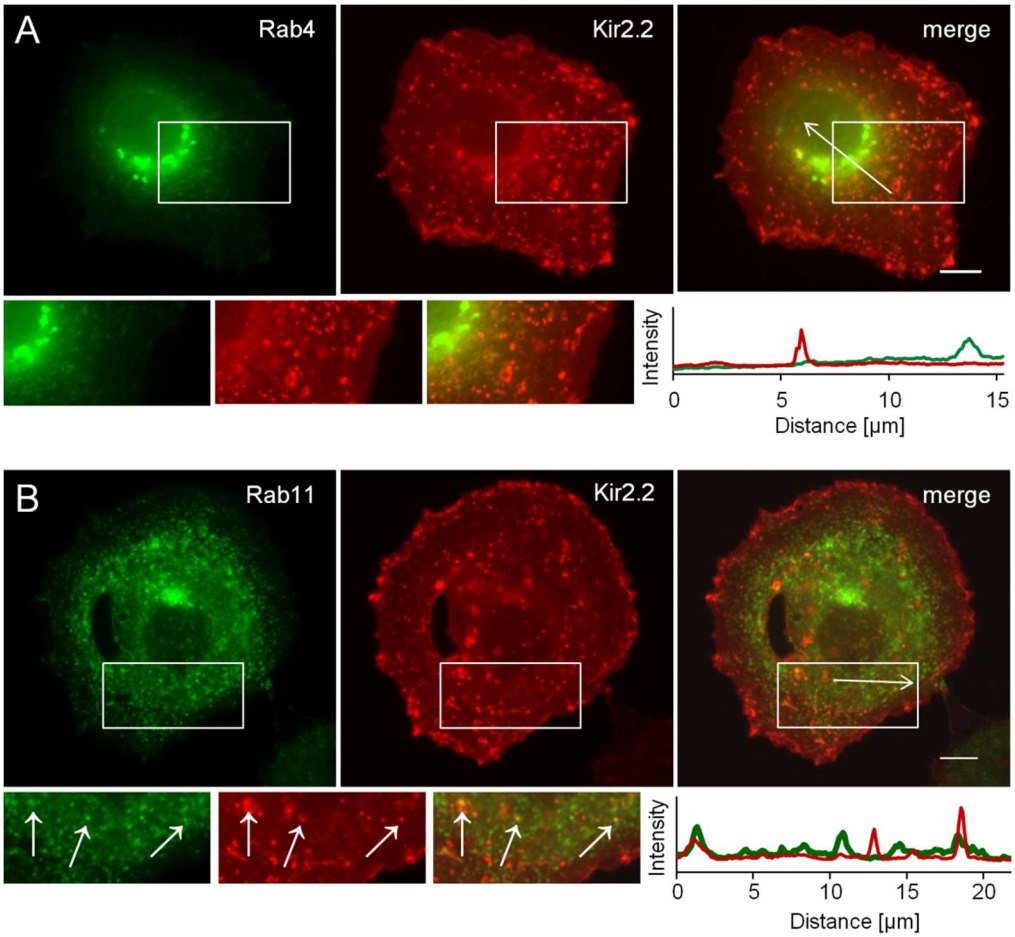

Figure 4.21: Kir2.2 is colocalized with Rab11 but not with Rab4. A) Coexpression of EGFP-tagged Rab4 and mCherry-tagged Kir2.2. **B)** Coexpression of EGFP-tagged Rab11 and mCherry-tagged Kir2.2. Selected regions of interest (white rectangles) are shown at higher magnification. Small arrows indicate structures that are positive for both proteins. Intensity profiles of EGFP and mCherry along the large white arrows are shown in the panels below the merged images. All pictures were taken 24 h after transfection; the scale bars are 10 µm.

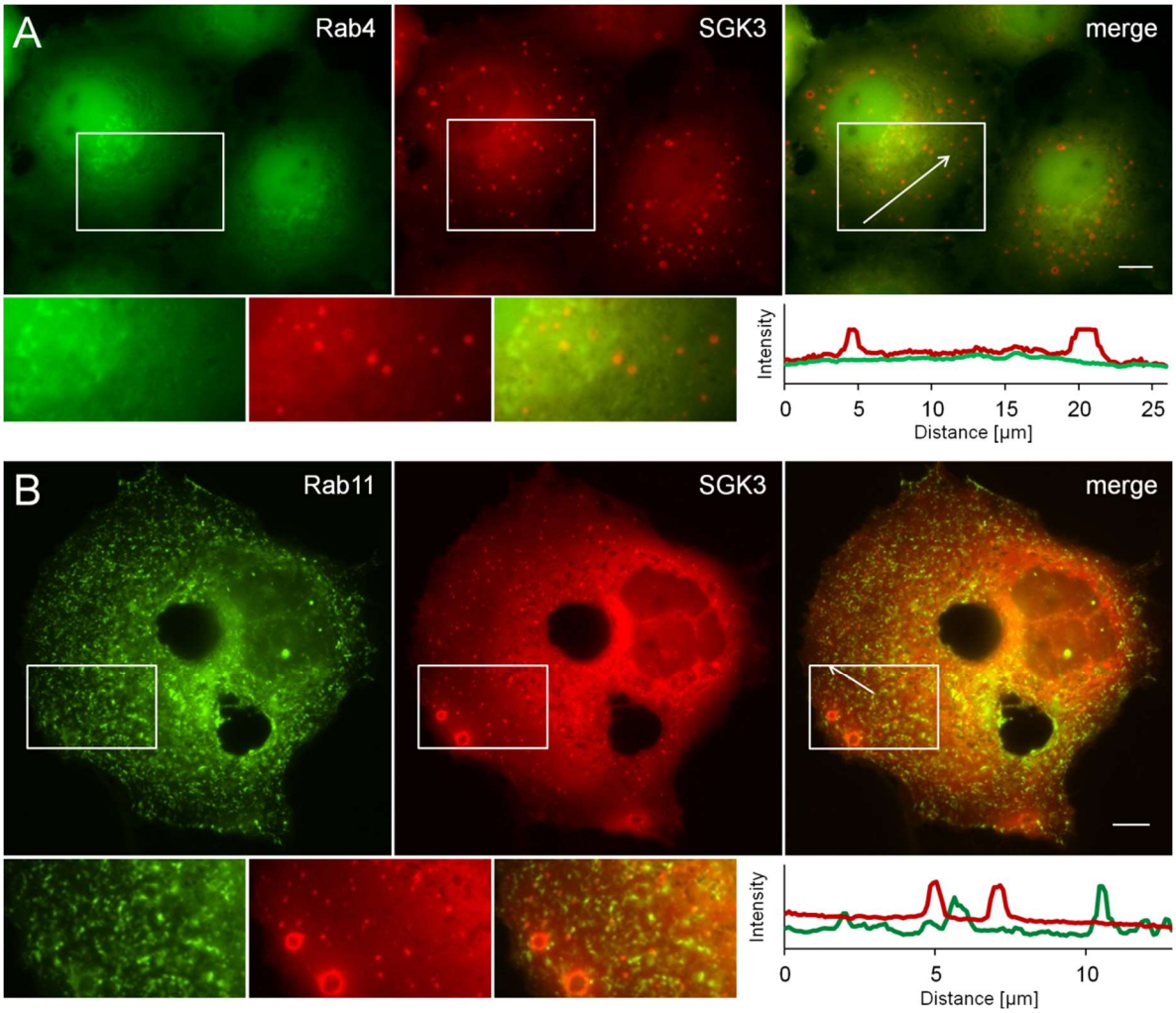

Figure 4.22: SGK3 is colocalized with Rab11 but not with Rab4. A) Coexpression of EGFP-tagged Rab4 and mCherry-tagged SGK3. **B)** Coexpression of EGFP-tagged Rab11 and mCherry-tagged SGK3. Selected regions of interest (white rectangles) are shown at higher magnification. Intensity profiles of EGFP and mCherry along the large white arrows are shown in the panels below the merged images. All pictures were taken 24 h after transfection; the scale bars are 10 µm.

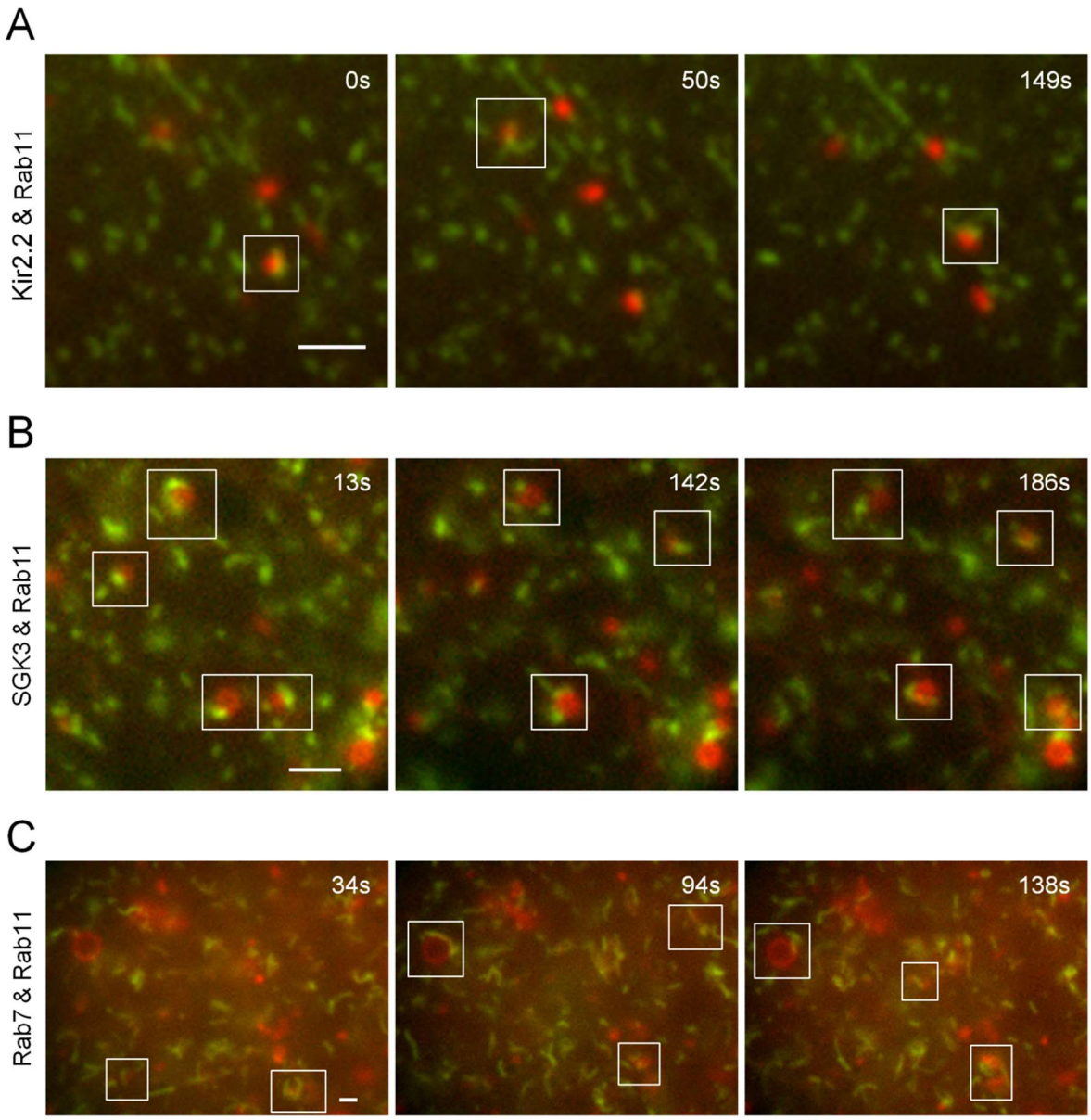

Figure 4.23: Rab11-positive endosomes interact with Kir2.2-positive, SGK3-positive and Rab7-positive endosomes. Live-cell imaging of COS-7 cells transfected with EGFP-tagged Rab11 together with **A)** mCherry-tagged Kir2.2, **B)** mCherry-tagged SGK3 or **C)** mCherry-tagged Rab7. The panels show magnified areas of one cell at different points of time. The white rectangles indicate interacting vesicles. Pictures were taken 24 h after transfection; scale bars are 1 µm.

In summary, the live-cell imaging experiments presented in this chapter suggest that we can discriminate at least three stages of endosomal maturation. (i) One of the earliest events after fission of endocytic vesicles is the recruitment of Rab5 to very small uncoated vesicles (Figure 4.17B, Rab5 positive and SGK3 negative vesicles). (ii) In the second stage, the synthesis of PI(3)P and the recruitment of SGK3 (and other PX-domain or FYVE-domain containing membrane associated proteins) occurs (Figure 4.17B, Rab5 and SGK3 positive vesicles). (iii) In the third stage of endosomal maturation, the Rab5/Rab7 switch and the sorting to different endosomal compartments take place (Figures 4.16, 4.17 and 4.23).

5. Discussion

Kir2.2 channels are crucial for stabilizing the resting membrane potential of many excitable and non-excitable cell types and they are active during the terminal repolarization phase of neuronal and cardiac action potentials. In the present study, I tried to clarify the molecular mechanism by which SGK3 increases the surface expression of Kir2.2 channels.

5.1 SGK3, but not SGK1 and SGK2, increases the surface expression of Kir2.2

The results obtained in this study show that SGK3 increases both Kir2.2 mediated currents and Kir2.2 surface expression in frog oocytes (from *Xenopus laevis*) and a mammalian cell line (COS-7). The increase in Kir2.2 current in *Xenopus* oocytes could be fully accounted for by the increase in surface expression (Figures 4.1, 4.2 and 4.5).

However, there was also a striking difference between the two expression systems. While in *Xenopus* oocytes expression of wild type SGK3 was sufficient to increase the surface expression of Kir2.2, a constitutively active mutant of SGK3, SGK3-CA, had to be coexpressed in COS-7 cells to increase Kir2.2 membrane expression. These findings suggest that the two kinases necessary for the activation of SGK3, PDK1 and PDK2, are constitutively active in *Xenopus* oocytes, while they need to be induced by some stimulus in COS-7 cells.

When Kir2.2 was coexpressed with SGK1 or SGK2, neither kinase increased the surface expression of the channel, although both significantly increased Kir2.2 mediated currents (Figures 4.1 and 4.2). The most likely explanation for this observation is that SGK1 and SGK2 change the open-state probability of the channel rather than affect the number of channels in the plasma membrane. This hypothesis is consistent with results obtained with other ion channels; SGK1, for example, has been shown to modulate the open probability of the epithelial sodium channel (ENAC) (Vuagniaux *et al.,* 2002; Wesch *et al.,* 2010). The notion that the three SGK isoforms act on Kir2.2 via different mechanisms is supported by the observation that only SGK3, but not SGK1 and SGK2, exhibits a distinct colocalization with Kir2.2 in vesicular structures when

coexpressed in COS-7 cells (Figure 4.3). When the binding of SGK3 to PI(3)P was abolished by the introduction of a mutation into the PX domain ($SGK3^{R90A}$), colocalization with Kir2.2 was completely abolished. Furthermore, when coexpressed with the channel in *Xenopus* oocytes or COS-7 cells, $SGK3^{R90A}$ had a smaller effect on the surface expression of Kir2.2 than SGK3-wt or SGK3-CA, respectively (Figure4.15). These results suggest that the localization of SGK3 to early endosomes is important for its effect on the surface membrane expression of Kir2.2. It may well be that the residual effect of $SGK3^{R90A}$ on Kir2.2 currents is attributable to the overexpression of the enzyme and that in vivo the PX domain is a prerequisite for the effect of SGK3 on membrane proteins.

Taken together, these findings show that SGK3, possibly due to its unique localization to PI(3)P containing structures in the cell, is the only member of the serum- und glucocorticoid-inducible kinase family that increases the surface expression of Kir2.2 channels.

5.2 The surface expression of Kir2.2 is not upregulated by any of the known mechanisms

A multitude of studies have shown a stimulating effect of SGKs on a broad range of different channels and transporters. Some of these effects appear to be of great pathophysiological relevance (Wulff *et al.,* 2002; Rangone *et al.,* 2004; Ullrich *et al.,* 2005; Xu *et al.,* 2005).

However, despite all efforts, the molecular mechanisms linking SGK3 activity and membrane trafficking are not yet fully understood. Different mechanisms of action have been proposed that include (i) phosphorylation of the E3 ubiquitin ligase Nedd4-2. Nedd4-2 possesses WW protein-protein interaction domains that bind to PPxY motifs and, to a lesser degree, to LPSY motifs in its substrates; this interaction enables the transfer of ubiquitin residues (Kamynina *et al.,* 2001). SGK3 phosphorylates Nedd4-2 at Ser444, the phosphorylated ligase is bound by 14-3-3 and subsequently downregulated from the plasma membrane (Bhalla *et al.,* 2005; Chandran *et al.,* 2011). Thus, SGK-mediated downregulation of Nedd4-2 activity inhibits ubiquitination and subsequent endocytosis of some of its target molecules, including channel proteins like

Kv1.5 and hERG, and thus increases their surface expression and current amplitude (Boehmer *et al.,* 2008; Wiemuth *et al.,* 2010; Lamothe and Zhang 2013). (ii) Phosphorylation of the transcription factor FOXO3a, thus induces the exit of FOXO3a from the nucleus and represses the transcription of FOXO3a-dependent target genes (Brunet *et al.,* 2001). (iii) Phosphorylation of the phosphoinositide kinase PIKfyve. It has been proposed that phosphorylation of PIKfyve may activate the kinase and that this activation may increase the current amplitude of several channel proteins in *Xenopus* oocytes, including Kir2.2 (Seebohm *et al.,* 2012b), TRPV6 (Sopjani *et al.,* 2010) and hERG (Pakladok *et al.,* 2013). This effect may be mediated by phosphorylation of PIKfyve, which induces the formation of PI(3,5)P2 and may direct recycling endosomes to the cell surface (Seebohm et al. 2012b).

Generally speaking, an increased number of channels in the surface membrane could be due to: i) a decreased endocytosis rate and less retrograde transport of channel molecules; ii) an increased number of newly synthesized channels or iii) an increased recycling rate of channels. The mechanism of action described for SGK3 in the previous paragraph can be assigned to these three groups. i) SGK3 could reduce the number of Kir2.2 channels that are internalized via a Nedd4-2 dependent mechanism; ii) SGK3 could increase the number of newly synthesized proteins by affecting FOXO3a and iii) SGK3 could elevate the amount of recycled channels via PIKfyve.

To investigate the mechanisms underlying the SGK3-mediated increase in Kir2.2 surface expression, I therefore systematically addressed these three general possibilities and, in addition, conducted experiments to specifically test the three mechanisms that have already be described to be responsible for the SGK3 induced upregulation of other membrane proteins.

(i) I confirmed the results of Boehmer *et al.,* 2008, showing that Kv1.5 current amplitude is decreased by coexpression with Nedd4-2 and that additional coexpression of SGK3 can prevent this downregulation. This is consistent with the idea that Nedd4-2 stimulates clathrin-mediated endocytosis of ubiquitinated Kv1.5 channels. However, coexpression of the inward rectifier channel Kir2.2 with Nedd4-2 did *not* lead to a reduction of current amplitude, indicating that Kir2.2 is not ubiquitinated by Nedd4-2 (Figure 4.10). This is consistent with the fact that Kir2.2 does not possess a PY- or a LPSY-motif. My further experiments

involving coexpression of Kir2.2, alone or together with SGK3, with the C-terminus of the clathrin adaptor AP180 established that SGK3 does not impede clathrin-mediated endocytosis of Kir2.2 in any way (Figure 4.11). These results were supported by an endocytosis assay, where the internalization of Kir2.2 in COS-7 cells was monitored in the presence of either a dominant negative or a constitutively active mutant of SGK3. No difference regarding the amount of endocytosed protein was observed (Figure 4.12).

(ii) To investigate whether SGK3 affects protein biosynthesis of Kir2.2, I used the translation elongation inhibitor cycloheximide to inhibit the synthesis of new proteins. I found that the Kir2.2 mediated current increase was not changed by incubation of *Xenopus* oocytes with cycloheximide; this rules out an upregulation of the Kir2.2 transcription rate by SGK3 (Figure 4.8). The lactone antibiotic Brefeldin A was further used to block anterograde transport of newly synthesized channel proteins to the surface membrane. In this case, too, I did not observe an effect on the SGK3 mediated Kir2.2-current increase in *Xenopus* oocytes, indicating that SGK3 does not affect the anterograde transport of newly synthesized Kir2.2 channels (Figure 4.9).

(iii) To investigate whether the PI5-kinase PIKfyve links SGK3 activity to an increased Kir2.2 surface expression, COS-7 cells and *Xenopus* oocytes were treated with the PIKfyve inhibitor YM201636. Incubation with the inhibitor did not significantly reduce the effect of SGK3 on the surface expression of Kir2.2 in either COS-7 cells or *Xenopus* oocytes (Figure 4.14). These results indicate that PIKfyve does not function downstream of SGK3 to mediate its effect on Kir2.2 surface expression, as had been proposed previously (Seebohm ***et al.,*** 2012b).

Taken together, these results suggest that SGK3 does not upregulate Kir2.2 surface expression through any of the mechanisms that have been described so far. Furthermore, I have shown that SGK3 does not affect the rate of endocytosis of Kir2.2 and does not increase the number of newly synthesized proteins or their anterograde transport to the plasma membrane.

5.3 SGK3 may elevate Kir2.2 surface expression by increasing the number of channels that are recycled back to the plasma membrane

The only obvious possibility that remained was that SGK3 promotes the recycling of Kir2.2 channels from an endosomal compartment back to the plasma membrane by a mechanism independent of PIKfyve. This would be consistent with the localization of SGK3 to PI(3)P-containing membranes described previously (Virbasius *et al.,* 2001; Tessier and Woodgett 2006a). To investigate whether SGK3 is in fact able to promote the recycling of Kir2.2 channels from an intracellular compartment back to the plasma membrane, an antibody based recycling assay was performed. This assay allowed me to monitor the amount of Kir2.2 channels that was internalized during a first 30 min incubation period at 37 °C and recycled back to the plasma membrane during a second 30 min incubation period at 37 °C in COS-7 cells. The recycling of channels was monitored in the presence of either SGK3-DN or SGK3-CA (Figure 4.13). Although it was not possible to quantify the amount of recycled protein in relation to the endocytosed protein, close analysis of the images indicated that co-transfection of SGK3-CA did lead to a higher number of recycled Kir2.2 channels in the stated time periods, leading to the conclusion that SGK3 does in fact promote the recycling of Kir2.2 channels.

5.4 The itinerary of endocytosed Kir2.2 channels through endosomal compartments

To further investigate how SGK3 could promote the recycling of Kir2.2 channels, the intracellular localization of SGK3 and Kir2.2 was analyzed in more detail. While the localization of SGK3 to PI(3)P containing membranes has been studied extensively (Virbasius *et al.,* 2001; Tessier and Woodgett 2006a; He *et al.,* 2011), little is known about the intracellular localization of Kir2.2. Since I could show an extensive colocalization of Kir2.2 and SGK3 in vesicular structures, an attempt was made to characterize the compartment in which the colocalization of both proteins took place. The monomeric GTPases (i) Rab5, (ii) Rab7, (iii) Rab4 and (iv) Rab11 were used as markers for the early (i) and

late (ii) endosomal compartments and a fast (iii) and a slow (iv) recycling pathway, respectively. The probe 2xFYVE was used as a general marker of PI(3)P containing membranes.
Rab proteins constitute the largest family of small GTPases and are reversibly associated with distinct intracellular membranes. Together with a group of highly specific phosphoinositide kinases and phosphatases, they serve as organizers of membrane trafficking processes and endosomal maturation.

The small G protein Rab5 is an essential factor for the biogenesis of early endosomes. Rab5 recruits the class III PI3K complex to the membranes of early endosomes. The PI3K complex phosphorylates phosphatidylinositol (PI) to produce phosphatidylinositol-3-phosphate [PI(3)P] (Christoforidis *et al.,* 1999). PI(3)P interacts with proteins that contain FYVE or PX domains, including the PI5-kinase PIKfyve and the serine/threonine kinase SGK3 (Jovic *et al.,* 2010; Mettlen *et al.,* 2010; McMahon and Boucrot 2011). Rab5 and PI(3)P cooperate in the recruitment of peripheral membrane proteins that stabilize Rab5. This represents a positive feedback loop that is essential for the formation of early endosomes. During the next stage, endosome maturation is initiated by Rab5/Rab7 conversion, i.e. the loss of Rab5 and the accompanying recruitment of Rab7 (Rink *et al.,* 2005; Del Conte-Zerial *et al.,* 2008; Spang 2009). This process is driven by the switch protein SAND-1/Mon1 (Poteryaev *et al.,* 2010) and the conversion PI(3)P to PI(3,5)P_2 by the PI5-kinase PIKfyve (Gary *et al.,* 1998).

From the results of the live cell imaging experiments with two different colours, some of the trafficking steps of the cargo molecule Kir2.2 were identified. (i) After endocytosis, Kir2.2 channels transit the small vesicles of the Rab5 positive early endosomal compartment relatively fast. (ii) The Rab5 and Kir2.2 positive vesicles synthesize PI(3)P, recruit PI(3)P associated proteins such as SGK3 and fuse with larger endosomal vesicles. (iii) When the endosomal vesicles containing Kir2.2, Rab5 and SGK3 have reached a certain size, Rab5/Rab7 conversion occurs (Rink *et al.,* 2005; Poteryaev *et al.,* 2010). (iv) The channel resides for a relatively long time in the SGK3- and Rab7-positive compartment,

from where it can be recycled to the surface membrane, probably via the Rab11-dependent recycling pathway.

This hypothesis is based on the following experimental observations. Step (i): Although I observed a weak colocalization of Kir2.2 and Rab5 (Figures 4.16B and 4.18) there was a much stronger colocalization of Kir2.2 with Rab7 (Figure 4.16C), indicating that Kir2.2 spends more time in Rab7-positive than in Rab5-positive vesicles. Step (ii): SGK3 was only localized to Rab5 positive vesicles at a certain distance from the cell membrane; the much smaller Rab5 positive vesicles in close proximity to the cell surface (diameter, <0.5 µm) were negative for SGK3 (Figure 4.17B). During the fusion events that could be observed between Kir2.2- or Rab5 positive vesicles and SGK3 positive vesicles, the SGK3 positive vesicles were slightly larger than the Kir2.2- or Rab5 positive vesicles (Figures 419A and 4.20A). Step (iii): SGK3-positive vesicles recruiting Rab7 to their membrane (Figure 4.20B) were even larger than the SGK3-positive vesicles fusing with Kir2.2- or Rab5-positive vesicles (diameter, 0.8-1.6 µm). The SGK3 and Rab7 positive vesicles exhibited a ring-like structure, similar to the Rab7 positive vesicles interacting with Kir2.2 containing vesicles (Figures 4.20B and 4.19B). Step (iv): I found strong colocalization of Kir2.2 and SGK3 (Figure 4.3C), Kir2.2 and Rab7 (Figure 4.16C) and SGK3 and Rab7 (Figure 4.17C) and observed frequent interactions of Kir2.2 positive, SGK3-positive and Rab7-positive vesicles with the Rab11 positive recycling endosomes (Figure 4.23). These interactions may promote the exchange of cargo molecules (including Kir2.2) destined for recycling.

5.5 Conclusions

On the basis of the sequential model of endosome maturation outlined above I derive the following hypothesis for the mechanism of action of SGK3 from my results: (i) The smaller, Rab5 positive and SGK3 negative vesicles in close proximity to the cell surface represent early endosomes in the very first stage in which PI(3)P has not been synthesized yet. (ii) The endosomes that are positive for both Rab5 and SGK3 are early endosomes in the second stage that contain PI(3)P in their membrane. (iii) Kir2.2 channels and SGK3 are most extensively colocalized in a PI(3)P and Rab7-positive endosomal compartment. I suspect this to be a transitional compartment between early and late endosomes: the

Rab5-to-Rab7 switch has already taken place but the predominant phosphoinositide is still PI(3)P and not PI(3,5)P_2. (iv) As the endosomal localization of SGK3 is crucial for its effect on Kir2.2, the kinase might affect the intracellular traffic of the channel in this transitional compartment. (v) SGK3, attached to this compartment, may bias the sorting decision in the direction of channel recycling via Rab11 positive vesicles; in this way SGK3 may increase surface expression of Kir2.2. This hypothesis is supported by the antibody-based based recycling assay, which showed that Kir2.2 is quickly endocytosed and recycled back to the plasma membrane (Figure 4.13), and also by the live-cell imaging sequences showing 'kiss-and-run' interactions between SGK3-positive and Kir2.2-positive vesicles and Rab11-positive recycling endosomes (Figure4.23). (vi) As pointed out above, it is unlikely that Kir2.2 is a direct target of SGK3. This suggests that the effect is mediated by a protein that is phosphorylated by SGK3 and endogenously expressed in a sufficient amount in both *Xenopus* oocytes and COS-7 cells. This might very well be a protein belonging to the endocytic machinery that controls membrane trafficking processes.

Taking into account all evidence presented in this study, I propose a model in which SGK3 promotes the recycling of a pool of Kir2.2 channels residing in an intermediate compartment between the early and the late endosome. This increase in the rate of recycling and the resulting increase in surface expression of the channels may be mediated by phosphorylation of a so far unknown target protein that is resident in this endosomal compartment and might belong to the trafficking machinery.

5.6 Pathological relevance

The further clarification of the mechanism by which SGK3 promotes the surface expression of membrane proteins might be of pathophysiological relevance and may help to elucidate its function in malignant signaling. SGK3 has been proposed to be involved in PI3-K dependent tumorigenesis and to drive the transformation of malignant cells by promoting cell survival and proliferation. The kinase is thought to modulate the function of some effector proteins by phosphorylation and the function of others by altering their transcription rate (Wang *et al.,* 2011; Liu *et al.,* 2012; Bruhn *et al.,* 2013) (compare 1.2.2). The

mechanism described in this study might also be of relevance for the role of SGK3 in tumorigenesis. The kinase might affect the trafficking and increase the membrane abundance of receptor proteins that play a role in the malignant transformation of cells, such as the vascular endothelial growth factor receptor or the human epidermal growth factor receptor 2.

5.7 Outlook

It would be worthwhile to perform further experiments to support the model in which SGK3 increases the recycling rate of the potassium channel Kir2.2.
SGK3 has a stimulatory effect on the surface expression on several channel and transporter proteins, but the underlying mechanisms remain unclear. I propose that the mechanism by which SGK3 affects Kir2.2 is mediated by a member of the protein machinery regulating membrane trafficking processes; this may to be a general mechanism that applies to the regulation of other membrane proteins by SGK3 as well. It would therefore be interesting to verify if other channel proteins are also upregulated by SGK3 through an increase in recycling rate.
In the context of the emerging role of SGK3 in malignant signalling it would be interesting to investigate whether SGK3 modulates the membrane expression of receptors that play a crucial role for survival, growth and migration of tumor cells.

6. References

Alexandrov K, Horiuchi H, Steele-Mortimer O, Seabra M and Zerial M (1994). Rab escort protein-1 is a multifunctional protein that accompanies newly prenylated rab proteins to their target membranes. EMBO J 13, 5262–5273.

Alonso L, Okada H and Pasolli H (2005). Sgk3 links growth factor signaling to maintenance of progenitor cells in the hair follicle. J Cell Biol 170, 559-570.

Alvarez de la Rosa D, Paunesc T, Els WJ, Helman SI and Canessa CM (2004). Mechanisms of regulation of epithelial sodium channel by SGK1 in A6 cells. J Gen Physiol 124, 395-407.

Bell, LM, Leong M, Kim B, Wang E, Park J, Hemmings B and Firestone G (2000). Hyperosmotic stress stimulates promoter activity and regulates cellular utilization of the serum- and glucocorticoid-inducible protein kinase (Sgk) by a p38 MAPK-dependent pathway. J Biol Chem 275, 25262-25272.

Benarroch E (2009). Potassium channels: brief overview and implications in epilepsy. Neurology 17, 664-669.

Bhalla V, Daidie D, Li H, Pao AC, LaGrange LP, Wang J, Vandewalle A, Stockand JD, Staub O and Pearce D (2005). Serum- and glucocorticoid-regulated kinase 1 regulates ubiquitin ligase neural precursor cell-expressed, developmentally down-regulated protein 4-2 by inducing interaction with 14-3-3. Mol Endocrinol 19, 3073-3084.

Biondi R, Kieloch A, Currie R, Deak M and Alessi D (2001). The PIF-binding pocket in PDK1 is essential for activation of S6K and SGK, but not PKB. EMBOJ 20, 4380-4390.

Boehmer C, Henke G, Schniepp R, Palmada M, Rothstein JD, Bröer S and Lang F (2003). Regulation of the glutamate transporter EAAT1 by the ubiquitin ligase Nedd4-2 and the serum and glucocorticoid-inducible kinase isoforms SGK1/3 and protein kinase B. J Neurochem 86, 1181-1188.

Boehmer C, Laufer J, Jeyaraj S, Klaus F, Lindner R, Lang F and Palmada R (2008). Modulation of the voltage-gated potassium channel Kv1.5 by the SGK1 protein kinase involves inhibition of channel ubiquitination. Cell Physiol Biochem 22, 591-600.

Bogusz AM, Brickley DR, Pew T and Conzen SD (2006). A novel N-terminal hydrophobic motif mediates constitutive degradation of serum- and glucocorticoid-induced kinase-1 by the ubiquitin-proteasome pathway. FEBS J 273, 2913-2928.

Böhmer C, Sopjani M, Klaus F, Lindner R, Laufer J, Jeyaraj S, Lang F and Palmada M (2010). The serum and glucocorticoid inducible kinases SGK1-3 stimulate the neutral amino acid transporter SLC6A19. Cell Physiol Biochem 25, 723-732.

Botelho R (2009). Changing phosphoinositides "on the fly": how trafficking vesicles avoid an identity crisis. Bioassays 10, 1127-1136.

Bruhn M, Pearson R, Hannan R and Sheppard K (2013). AKT-independent PI3-K signaling in cancer - emerging role for SGK3. Cancer Manag Res 5, 281-292.

Brunet A, Park J, Tran H, Hu LS, Hemmings BA and Greenberg ME (2001). Protein kinase SGK mediates survival signals by phosphorylating the forkhead transcription factor FKHRL1 (FOXO3a). Mol Cell Biol 21, 952-965.

Bucci C, Parton R, Mather I, Stunnenberg H, Simons K, Hoflack B and Zerial M (1992). The small GTPase rab5 functions as a regulatory factor in the early endocytic pathway. Cell 70, 715–728.

Buse P, Tran S, Luther E, Phu P, Aponte G and Firestone G (1999). Cell cycle and hormonal control of nuclear-cytoplasmic localization of the serum- and glucocorticoid-inducible protein kinase, SGK, in mammary tumor cells. A novel convergence point of anti-proliferative and proliferative cell signaling pathways. J Biol Chem 274, 7253-7263.

Cantley L (2002). The phosphoinositide 3-kinase pathway. Science 296, 1655-1657.

Carlton J and Cullen P (2005). Coincidence detection in phosphoinositide signaling. Trends Cell Biol 10, 540-547.

Chandran S, Li H, Dong W, Krasinska K, Adams C, Alexandrova L, Chien A, Hallows KR and Bhalla V (2011). Neural precursor cell-expressed developmentally down-regulated protein 4-2 (Nedd4-2) regulation by 14-3-3 protein binding at canonical serum and glucocorticoid kinase 1 (SGK1) phosphorylation sites. J Biol Chem 286, 37830-37840.

Chavrier P, Parton, R. G., Hauri, H. P., Simons, K. & and Zerial M (1990). Localization of low molecular weight GTP binding proteins to exocytic and endocytic compartments. Cell 62, 317-329.

Choe H, Sackin H and Palmer L (2000). Permeation properties of inwardrectifier potassium channels and their molecular determinants. J Gen Physiol 115, 391-404.

Christoforidis S, Miaczynska M, Ashman K, Wilm M, Zhao L, Yip S-C, Waterfield MD, Backer JM and Zerial M (1999). Phosphatidylinositol-3-OH kinases are Rab5 effectors. Nat Cell Biol 1, 249-252.

Chun J, Kwon T, Lee E, Suh P, Choi E and Sun Kang S (2002). The Na(+)/H(+) exchanger regulatory factor 2 mediates phosphorylation of serum- and glucocorticoid-induced protein kinase 1 by 3-phosphoinositide-dependent protein kinase 1. Biochem Biophys Res Commun 25, 207-215.

Czech M (2003). Dynamics of phosphoinositides in membrane retrieval and insertion. Annu Rev Physiol 65, 791-815.

Dai F, Yu L and He H (2002). Human serum and glucocorticoid-inducible kinase-like kinase (SGKL) phosphorylates glycogen syntheses kinase 3 beta (GSK-3beta) at serine-9 through direct interaction. . Biochem Biophys Res Commun 293, 1191-1196.

de Renzis S, Sönnichsen B and Zerial M (2002). Divalent Rab effectors regulate the sub-compartmental organization and sorting of early endosomes. Nat Cell Biol 2, 124-133.

Debonneville C, Flores S, Kamynina E, Plant P, Tauxe C, Thomas M, Münster C, Chraïbi A, Pratt J, Horisberger J, et al. (2001). Phosphorylation of Nedd4-2 by SGK1 regulates epithelial Na(+) channel cell surface expression. EMBO J 20, 7052-7059.

Del Conte-Zerial P, Brusch L, Rink JC, Collinet C, Kalaidzidis Y, Zerial M and Deutsch A (2008). Membrane identity and GTPase cascades regulated by toggle and cut-out switches. Mol Syst Biol 4, 206.

Doherty GJ and McMahon HT (2009). Mechanisms of endocytosis. Annu Rev Biochem 78, 857-902.

Doyle D, Morais Cabral J, Pfuetzner R, Kuo A, Gulbis J, Cohen S, Chait B and MacKinnon R (1998). The structure of the potassium channel: molecular basis of K+ conduction and selectivity. Science 280, 69-77.

Drobak B and Heras B (2002). Nuclear phosphoinositides could bring FYVE alive. Trends Plant Sci 3, 132-138.

Embark HM, Bohmer C, Vallon V, Luft F and Lang F (2003). Regulation of KCNE1-dependent K(+) current by the serum and glucocorticoid-inducible kinase (SGK) isoforms. Pflugers Arch 445, 601-606.

Failor K, Desyatnikov Y, Finger L and Firestone G (2007). Glucocorticoid-induced degradation of glycogen synthase kinase-3 protein is triggered by serum- and glucocorticoid-induced protein kinase and Akt signaling and controls beta-catenin dynamics and tight junction formation in mammary epithelial tumor cells. . Mol Endocrinol 21, 2403-3415.

Feng Y, Press B and Wandinger-Ness A (1995). Rab 7: An important regulator of late endocytic membrane traffic. J Cell Biol 131, 1435–1452.

Ficker E, Taglialatela M, Wible B, Henley C and Brown A (1994). Spermine and Spermidine as Gating Molecules for Inward Rectifier K+ Channels. Science 266, 1068-1072.

Gamper N, Fillon S, Feng Y, Friedrich B, Lang PA, Henke G, Huber SM, Kobayashi T, Cohen P and Lang F (2002). K+ channel activation by all three isoforms of serum- and glucocorticoid-dependent protein kinase SGK. Pflugers Arch 445, 60-66.

Garcia-Martinez JM and Alessi DR (2008). mTOR complex 2 (mTORC2) controls hydrophobic motif phosphorylation and activation of serum- and glucocorticoid-induced protein kinase 1 (SGK1). Biochem J 416, 375-385.

Gary J, Wurmser A, Bonangelino C, Weisman L and Emr S (1998). Fab1p is essential for PtdIns(3)P 5-kinase activity and the maintenance of vacuolar size and membrane homeostasis. J Cell Biol 143, 65-79.

Gillooly D, Morrow I, Lindsay M, Gould R, Bryant N, Gaullier J, Parton R and Stenmark H (2000). Localization of phosphatidylinositol 3-phosphate in yeast and mammalian cells. EMBO J 19, 4577-4588.

Gorvel J, Chavrier P, Zerial M and Gruenberg J (1991). Rab5 controls early endosome fusion in vitro. Cell 64, 915-925.

Guichard A, Nizet V and Bier E (2014). Rab11-mediated trafficking in host-pathogen interactions. Nat Rev Microbiol 9, 624-634.

Guo L and Kubo Y (1998). Comparison of the open-close kinetics of the cloned inward rectifier K+ channel IRK1 and its point mutant (Q140E) in the pore region. Receptor Channels 5, 273-389.

Guo Z, Hou X, Goody R and Itzen A (2013). Intermediates in the guanine nucleotide exchange reaction of Rab8 protein catalyzed by guanine nucleotide exchange factors Rabin8 and GRAB. J Biol Chem 288, 32466–32474.

Hagiwara S, Miyazaki S, Moody W and Patlak J (1978). Blocking effects of barium and hydrogen ions on the potassium current during anomalous rectification in the starfish egg. J Physiol 279, 167-185.

Hagiwara S, Miyazaki S and Rosenthal N (1976). Potassium current and the effect of cesium on this current during anomalous rectification of the egg cell membrane of a starfish. J Gen Physiol 67, 621-638.

Hansen S, Tao X and MacKinnon R (2012). Structural basis of PIP2 activation of the classical inward rectifier K+ channel Kir2.2. Nature 477, 495-498.

He P, Lee SJ, Lin S, Seidler U, Lang F, Fejes-Toth G, Naray-Fejes-Toth A and Yun CC (2011). Serum- and glucocorticoid-induced kinase 3 in recycling endosomes mediates acute activation of Na+/H+ exchanger NHE3 by glucocorticoids. Mol Biol Cell 22, 3812-3825.

Henke G, Setiawan I, Boehmer C and Lang F (2002). Activation of Na+/K+-ATPase by the serum and glucocorticoid-dependent kinase isoforms. Kidney Blood Press Res 25, 370-374.

Hibino H, Inanobe A, Furutani K, Murakami S, Findlay I and Kurachi Y (2010). Inwardly rectifying potassium channels: their structure, function, and physiological roles. Physiol Rev 90, 291-366.

Hilgemann D and Ball R (1996). Regulation of cardiac Na+,Ca2+ exchange and KATP potassium channels by PIP2. Science 273, 956-959.

Huang C, Feng S and Hilgemann D (1998). Direct activation of inward rectifier potassium channels by PIP2 and its stabilization by Gβɣ. Nature 391, 803-806.

Huotari J and Helenius A (2011). Endosome maturation. EMBO J 30, 3481-3500.

Hutagalung A and Novick P (2011). Role of Rab GTPases in membrane traffic and cell physiology. Physiol Rev 1, 119-149.

Hyvola N, Diao A, McKenzie E, Skippen A, Cockcroft S and Lowe M (2005). Membrane targeting and activation of the Lowe syndrome protein OCRL1 by rab GTPases. EMBO J 25, 3750-3761.

Ikonomov O, Sbrissa D, Fenner H and Shisheva A (2009). PIKfyve-ArPIKfyve-Sac3 core complex: contact sites and their consequence for Sac3 phosphatase activity and endocytic membrane homeostasis. J Biol Chem 284, 35794-35806.

Ishihara K and Ehara T (1998). A repolarization-induced transient increase in the outward current of the inward rectifier K+ channel in guinea-pig cardiac myocytes. J Physiol 510, 755-771.

Jefferies HB, Cooke FT, Jat P, Boucheron C, Koizumi T, Hayakawa M, Kaizawa H, Ohishi T, Workman P, Waterfield MD, et al. (2008). A selective PIKfyve inhibitor blocks PtdIns(3,5)P(2) production and disrupts endomembrane transport and retroviral budding. EMBO Rep 9, 164-170.

Jongsma H and Wilders R (2001). Channelopathies- Kir2.1 mutations jeopardize many cell functions. Curr Biol 11, 747–750.

Jovic M, Sharma M, Rahajeng J and Caplan S (2010). The early endosome: a busy sorting station for proteins at the crossroads. Histol Histopathol 25, 99-112.

Kamynina E, Debonneville C, Bens M, Vandewalle A and Staub O (2001). A novel mouse Nedd4 protein suppresses the activity of the epithelial Na+ channel. FASEB J 1, 204-214.

Katzmann D, Stefan C, Babst M and Emr S (2003). Vps27 recruits ESCRT machinery to endosomes during MVB sorting. J Cell Biol 162, 413-423.

Kilisch M, Lytovchenko O, Schwappach B, Renigunta V and Daut J (2015). The role of protein-protein interactions in the intracellular traffic of the potassium channels TASK-1 and TASK-3. Pflugers Arch.

Klausner R, Donaldson J and Lippincott-Schwartz J (1992). Brefeldin A: insights into the control of membrane traffic and organelle structure. J Cell Biol 116, 1071-1080.

Kobayashi T and Cohen P (1999). Activation of serum- and glucocorticoid-regulated protein kinase by agonists that activate phosphatidylinositide 3-kinase is mediated by 3-phosphoinositide-dependent protein kinase-1 (PDK1) and PDK2. Biochem J 319-328.

Kobayashi T, Deak M, Morrice N and Cohen P (1999). Characterization of the structure and regulation of two novel isoforms of Serum- and glucocorticoid-induced protein kinase. Biochem J 344, 189-197.

Krauss M and Haucke V (2011). Shaping membranes for endocytosis. Rev Physiol Biochem Pharmacol 161, 45-66.

Kubo Y and Murata Y (2001). Control of rectification and permeation by two distinct sites after the second transmembrane region in Kir2.1 K+ channel. J Physiol 531, 645-660.

Kurachi Y (1985). Voltage-Dependent activation of the inward-rectifier Potassium Channel in the ventricular cell membrane of guinea-pig heart. J Physiol 366, 365-385.

Kutateladze T (2010). Translation of the phosphoinositide code by PI effectors. Nat Chem Biol 7, 507-513.

Lai H and Jan L (2006). The distribution and targeting of neuronal voltage-gated ion channels. Nat Rev Neurosci 7, 548-562.

Lamothe SM and Zhang S (2013). The serum- and glucocorticoid-inducible kinases SGK1 and SGK3 regulate hERG channel expression via ubiquitin ligase Nedd4-2 and GTPase Rab11. J Biol Chem 288, 15075-15084.

Lang F, Boehmer C, Palmada M, Seebohm G, Strutz-Seebohm N and Vallon V (2006). (Patho)physiological significance of the Serum- and Glucocorticoid-inducible Kinase isoforms. Physiol Rev 86, 1151-1178.

Lawe D, Patki V, Heller-Harrison R, Lambright D and Corvera S (2000). The FYVE domain of early endosome antigen 1 is required for both phosphatidylinositol 3-phosphate and Rab5 binding. Critical role of this dual interaction for endosomal localization. J Biol Chem 275, 3699-3705.

Lee J, John S and Weiss J (1999). Novel gating mechanism of polyamine block in the strong inward rectifier K channel Kir2.1. J Gen Physiol 113, 555-564.

Lemmon MA (2008). Membrane recognition by phospholipid-binding domains. Nat Rev Mol Cell Biol 9, 99-111.

Liang S, Wang Q, Zhang W, Zhang H, Tan S, Ahmed A and Y G (2014). Carbon monoxide inhibits inward rectifier potassium channels in cardiomyocytes. Nat Commun. 5, 4676.

Liu M, Chen L and Chan T (2012). Serum and glucocorticoid kinase 3 at 8q13.1 promotes cell proliferation and survival in hepatocellular carcinoma. Hepatology 55, 1754-1765.

Lombardi D, Soldati T, Riederer M, Goda Y, Zerial M and Pfeffer S (1993). Rab9 functions in transport between late endosomes and the trans Golgi network. EMBO J 2, 677-682.

Lopatin A, Makhina E and Nichols C (1994). Potassium channel block by cytoplasmic polyamines as the mechanism of intrinsic rectification. Nature 372, 366-369.

Lopatin A, Makhina E and Nichols C (1995). The mechanism of inward rectification of potassium channels: "long-pore plugging" by cytoplasmic polyamines. J Gen Physiol 106, 923-925.

Lu Z and MacKinnon R (1994). Electrostatic tuning of Mg2+ affinity in an inward-rectifier K+ channel. Nature 371, 243-246.

Ma D, Zerangue N, Lin YF, Collins A, Yu M, Jan YN and Jan LY (2001). Role of ER export signals in controlling surface potassium channel numbers. Science 291, 316-319.

Maiyar A, Leong M and Firestone G (2003). Importin-alpha mediates the regulated nuclear targeting of serum- and glucocorticoid-inducible protein

kinase (Sgk) by recognition of a nuclear localization signal in the kinase central domain. Mol Biol Cell 1221-1239.

Manning B and Cantley L (2007). KT/PKB signaling: navigating downstream. Cell 129, 1261-1274.

Margeta-Mitrovic M (2002). Assembly-dependent trafficking assays in the detection of receptor-receptor interactions. Methods 27, 311–317.

Martin T (2001). PI(4,5)P(2) regulation of surface membrane traffic. Curr Opin Cell Biol 4, 493-499.

Matsui Y, Kikuchi A, Araki S, Hata Y, Kondo J, Teranishi Y and Takai Y (1990). Molecular cloning and characterization of a novel type of regulatory protein (GDI) for smg p25A, a ras p21-like GTP-binding protein. Mol Cell Biol 10, 4116–4122.

Mayor S, Presley J and Maxfield F (1993). Sorting of membrane components from endosomes and subsequent recycling to the cell surface occurs by a bulk flow process. J Cell Biol 121, 1257-1269.

McCormick J, Feng Y, Dawson K, Behne M, Yu B, Wang J, Wyatt A, Henke G, Grahammer F, Mauro T, et al. (2004). Targeted disruption of the protein kinase SGK3/CISK impairs postnatal hair follicle development. Mol Biol Cell 9, 4278-4288.

McLauchlan H, Newell J, Morrice N, Osborne A, West M and Smythe E (1998). A novel role for Rab5–GDI in ligand sequestration into clathrin-coated pits. Curr Biol 8, 34-45.

McMahon HT and Boucrot E (2011). Molecular mechanism and physiological functions of clathrin-mediated endocytosis. Nat Rev Mol Cell Biol 12, 517-533.

Méresse S, Gorvel J and Chavrier P (1995). The Rab7 GTPase resides on a vesicular compartment connected to lysosomes. J Cell Sci 108, 3349-3358.

Mettlen M, Loerke D, Yarar D, Danuser G and Schmid S (2010). Cargo- and adaptor-specific mechanisms regulate clathrin-mediated endocytosis. J Cell Biol 188, 919-933.

Morais-Cabral J, Zhou Y and MacKinnon R (2001). Energetic optimization of ion conduction rate by the K+ selectivity filter. Nature 414, 37-42.

Naray-Fejes-Toth A, Canessa C, Cleaveland ES, Aldrich G and Fejes-Toth G (1999). SGK is an aldosterone-induced kinase in the renal collecting duct. Effects on epithelial na+ channels. J Biol Chem 274, 16973-16978.

Nichols C, Makhina E, Pearson W, Sha Q and Lopatin A (1996). Inward rectification and implications for cardiac excitability. Circulation 78, 1-7.

Nielsen E, Christoforidis S, Uttenweiler-Joseph S, Miaczynska M, Dewitte F, Wilm M, Hoflack B and Zerial M (2000). Rabenosyn-5, a novel Rab5 effector, is complexed with hVPS45 and recruited to endosomes through a FYVE finger domain. J Cell Biol 151, 601-612.

Pakladok T, Almilaji A, Munoz C, Alesutan I and Lang F (2013). PIKfyve sensitivity of hERG channels. Cell Physiol Biochem 31, 785-794.

Park H (2013). Structural basis of membrane trafficking by Rab family small G protein. Int J Mol Sci 14, 8912–8923.

Park J, Leong M, Buse P, Maiyar A, Firestone G and Hemmings B (1999). Serum and glucocorticoid-inducible kinase (SGK) is a target of the PI 3-kinase-stimulated signaling pathway. EMBO J 18, 3024-3033.

Plaster N, Tawil R, Tristani-Firouzi M, Canun S, Bendahhou S, Tsunoda A, Donaldson M, Iannaccone S, Brunt E, Barohn R, et al. (2001). Mutations in Kir2.1 cause the developmental and episodic electrical phenotypes of Andersen's syndrome. Cell 105, 511–519.

Poteryaev D, Datta S, Ackema K, Zerial M and Spang A (2010). Identification of the switch in early-to-late endosome transition. Cell 141, 497-508.

Preisig-Muller R, Schlichthorl G, Goerge T, Heinen S, Bruggemann A, Rajan S, Derst C, Veh RW and Daut J (2002). Heteromerization of Kir2.x potassium channels contributes to the phenotype of Andersen's syndrome. Proc Natl Acad Sci USA 99, 7774-7779.

Proks P, Capener C, Jones P and Ashcroft F (2001). Mutations within the P-loop of Kir6.2 modulate the intraburst kinetics of the ATPsensitive potassium channel. J Gen Physiol 118, 341-353.

Rangone H, Poizat G, Troncoso J, Ross C, MacDonald M, Saudou F and Humbert S (2004). The serum- and glucocorticoid-induced kinase SGK inhibits

mutant huntingtin-induced toxicity by phosphorylating serine 421 of huntingtin. Eur J Neurosci 19, 273-279.

Rink J, Ghigo E, Kalaidzidis Y and Zerial M (2005). Rab conversion as a mechanism of progression from early to late endosomes. Cell 122, 735-749.

Sakmann B and Trube G (1984). Conductance properties of single inwardly rectifying potassium channels in ventricular cells from guinea-pig heart. J Physiol 347, 641-657.

Sasaki T, Kikuchi A, Araki S, Hata Y, Isomura M, Kuroda S and Takai Y (1990). Purification and characterization from bovine brain cytosol of a protein that inhibits the dissociation of GDP from and the subsequent binding of GTP to smg p25A, a ras p21-like GTP-binding protein. J Biol Chem 265, 2333-2337.

Sato T, Overduin M and Emr S (2001). Location, location, location: membrane targeting directed by PX domains. Science 294, 1881-1885

Sbrissa D, Ikonomov O, Fenner H and Shisheva A (2008). ArPIKfyve homomeric and heteromeric interactions scaffold PIKfyve and Sac3 in a complex to promote PIKfyve activity and functionality. J Mol Biol 384, 766-779.

Sbrissa D, Ikonomov OC, Filios C, Delvecchio K and Shisheva A (2012). Functional dissociation between PIKfyve-synthesized PtdIns5P and PtdIns(3,5)P2 by means of the PIKfyve inhibitor YM201636. Am J Physiol Cell Physiol 303, 436-446.

Schmid S, Fuchs R, Male P and Mellman I (1988). Two distinct subpopulations of endosomes involved in membrane recycling and transport to lysosomes. Cell 52, 73-83.

Schmid S and Mettlen M (2013). Lipid switches and traffic control. Nature 499, 161-162.

Schnatwinkel C, Christoforidis S, Lindsay M, Uttenweiler-Joseph S, Wilm M, Parton R and Zerial M (2004). The Rab5 effector Rabankyrin-5 regulates and coordinates different endocytic mechanisms. PLoS Biol. 9.

Schneider-Poetsch T, Ju J, Eyler D, Dang Y, Bhat S, Merrick W, Green R, Shen B and Liu J (2010). Inhibition of eukaryotic translation elongation by cycloheximide and lactimidomycin. Nat Chem Biol 3, 209-217.

Schram G, Melnyk P, Pourrier M, Wang Z and Nattel S (2002). Kir2.4 and Kir2.1 K+ channel subunits co-assemble: a potential new contributor to inward rectifier current heterogeneity. J Physiol 544, 337-349.

Seabra M (1991). Nucleotide dependence of Rab geranylgeranylation. Rab escort protein interacts preferentially with GDP-bound Rab. J Biol Chem 271, 14398–14404.

Seebohm G, Neumann, S, , Theiss C, Novkovic T, Hill E, Tavaré J, Lang F, Hollmann M, Manahan-Vaughan, D, and Strutz-Seebohm N (2012a). Identification of a Novel Signaling Pathway and Its Relvance for GluA1 Recycling. Plos One 7, 1-10.

Seebohm G, Strutz-Seebohm N, Ursu O, Preisig-Muller R, Zuzarte M, Hill E, Kienitz M, Bendahhou S, Fauler M, Tapken D, et al. (2012b). Altered stress stimulation of inward rectifier potassium channels in Andersen-Tawil syndrome. FASEB J 26, 513-522.

Shimoni Y, Clark R and Giles W (1992). Role of an inwardly rectifying potassium current in rabbit ventricular action potential. J Physiol 488, 709-727.

Shin H, Hayashi M, Christoforidis S, Lacas-Gervais S, Hoepfner S, Wenk M, Modregger J, Uttenweiler-Joseph S, Wilm M, Nystuen A, et al. (2005). An enzymatic cascade of Rab5 effectors regulates phosphoinositide turnover in the endocytic pathway. J Cell Biol 170, 607-618.

Simonsen A, Lippé R, Christoforidis S, Gaullier J, Brech A, Callaghan J, Toh B, Murphy C, Zerial M and Stenmark H (1998). EEA1 links PI(3)K function to Rab5 regulation of endosome fusion. Nature 394, 495-498.

Sivars U, Aivazian D and Pfeffer S (2003). Yip3 catalyses the dissociation of endosomal Rab–GDI complexes. Nature 425, 856–859.

Somsel Rodman J and Wandinger-Ness A (2000). Rab GTPases coordinate endocytosis. j cell sci 113, 183-192.

Sönnichsen B, De Renzis S, Nielsen E, Rietdorf J and Zerial M (2000). Distinct membrane domains on endosomes in the recycling pathway visualized by multicolor imaging of Rab4, Rab5, and Rab11. J Cell Biol 149, 901-914.

Sopjani M, Kunert A, Czarkowski K, Klaus F, Laufer J, Foller M and Lang F (2010). Regulation of the Ca(2+) channel TRPV6 by the kinases SGK1, PKB/Akt, and PIKfyve. J Membr Biol 233, 35-41.

Spang A (2009). On the fate of early endosomes. Biol Chem 390, 753-759.

Stanfield P, Davies N, Shelton P, Khan I, Brammar W, Standen N and Conley E (1994). The intrinsic gating of inward rectifier K+ channels expressed from the murine IRK1 gene depends on voltage, K+ and Mg2+. J Physiol 475, 1-7.

Stenmark H (2009). Rab GTPases as coordinators of vesicle traffic. Nat Rev Mol Cell Biol 10, 513-525.

Teo H, Gil lD, Sun J, Perisic O, Veprintsev D, Vallis Y, Emr S and Williams R (2006). ESCRT-I core and ESCRT-II GLUE domain structures reveal role for GLUE in linking to ESCRT-I and membranes. Cell 125, 99-111.

Tessier M and Woodgett JR (2006a). Role of the Phox homology domain and phosphorylation in activation of serum and glucocorticoid-regulated kinase-3. J Biol Chem 281, 23978-23989.

Tessier M and Woodgett JR (2006b). Serum and glucocorticoid-regulated protein kinases: variations on a theme. J Cell Biochem 98, 1391-1407.

Thomas AM, Harmer SC, Khambra T and Tinker A (2011). Characterization of a binding site for anionic phospholipids on KCNQ1. J Biol Chem 286, 2088-2100.

Tong Y, Brandt G, Li M, Shapovalov G, Slimko E, Karschin A, Dougherty D and Lester H (2001). Tyrosine decaging leads to substantial membrane trafficking during modulation of an inward rectifier potassium channel. J Gen Physiol 117, 103-118.

Trapp S, Proks P, Tucker S and Ashcroft F (1998). Molecular analysis of ATP-sensitive K channel gating and implications for channel inhibition by ATP. J Gen Physiol 112, 333-349.

Ullrich O, Reinsch S, Urbé S, Zerial M and Parton R (1996). Rab11 regulates recycling through the pericentriolar recycling endosome. J Cell Biol 4, 913-924.

Ullrich O, Stenmark H, Alexandrov K, Huber L, Kaibuchi K, Sasaki T, Takai Y and Zerial M (1993). Rab GDP dissociation inhibitor as a general regulator for the membrane association of rab proteins. J Biol Chem 268, 18143–18150.

Ullrich S, Berchtold S, Ranta F, Seebohm G, Henke G, Lupescu A, Mack A, Chao C, Su J, Nitschke R, et al. (2005). Serum- and glucocorticoid-inducible kinase 1 (SGK1) mediates glucocorticoid-induced inhibition of insulin secretion. Diabetes 54, 1090-1099.

Valiyaveetil F, Sekedat M, MacKinnon R and Muir T (2006). Structural and functional consequences of an amide-to-ester substitution in the selectivity filter of a potassium channel. J Am Chem Soc 128, 11591.

van der Sluijs P, Hull M, Huber L, Mâle P, Goud B and Mellman I (1992). Reversible phosphorylation–dephosphorylation determines the localization of rab4 during the cell cycle. EMBO J 11, 4379–4389.

Virbasius JV, Song X, Pomerleau DP, Zhan Y, Zhou GW and Czech MP (2001). Activation of the Akt-related cytokine-independent survival kinase requires interaction of its phox domain with endosomal phosphatidylinositol 3-phosphate. Proc Natl Acad Sci USA 98, 12908-12913.

Vivanco I and Sawyers C (2002). The phosphatidylinositol 3-Kinase AKT pathway in human cancer. Nat Rev Cancer 7, 489–501.

Vuagniaux G, Vallet V, Jaeger N, Hummler E and Rossier B (2002). Synergistic Activation of ENaC by Three Membrane-bound Channel-activating Serine Proteases (mCAP1, mCAP2, and mCAP3) and Serum- and Glucocorticoid-regulated Kinase (Sgk1) in Xenopus Oocytes. J Gen Physiol 120, 191-201.

Wandinger-Ness A and Zerial M (2014). Rab Proteins and the Compartmentalization of the Endosomal System. Cold Spring Harborg Perspect Biol 6.

Wang Y, Zhou D and Chen S (2014). SGK3 is an androgen-inducible kinase promoting prostate cancer cell proliferation through activation of p70 S6 kinase and up-regulation of cyclin D1. Mol Endocrinol 6, 935-948.

Wang Y, Zhou D, Phung S, Masri S, Smith D and Chen S (2011). SGK3 is an estrogen-inducible kinase promoting estrogen-mediated survival of breast cancer cells. Mol Endocrinol 1, 72-82.

Webster M, Goya L, Ge Y, Maiyar A and Firestone G (1993). Characterization of sgk, a novel member of the serine/threonine protein kinase gene family which

is transcriptionally induced by glucocorticoids and serum. Mol Cell Biol 4, 2031-2040.

Welling P (2013). Regulation of potassium channel trafficking in the distal nephron. Curr Opin Nephrol Hypertens. 22, 559-565.

Wesch D, Miranda P, Afonso-Oramas D, Althaus, M, , Castro-Hernández J, Dominguez, J, Morty, RE, , Clauss W, González-Hernández T, Alvarez de la Rosa D and Giraldez T (2010). The neuronal-specific SGK1.1 kinase regulates gama-epithelial Na+ channel independently of PY motifs and couples it to phospholipase C signaling. Am J Physiol Cell Physiol 299, 779-790.

Whitley P, Reaves B, Hashimoto M, Riley A, Potter B and Holman G (2003). Identification of mammalian Vps24p as an effector of phosphatidylinositol 3,5-bisphosphate-dependent endosome compartmentalization. J Biol Chem 278, 38786-38795.

Wiemuth D, Lott JS, Ly K, Ke Y, Teesdale-Spittle P, Snyder PM and McDonald FJ (2010). Interaction of serum- and glucocorticoid regulated kinase 1 (SGK1) with the WW-domains of Nedd4-2 is required for epithelial sodium channel regulation. PLoS One 5, e12163.

Wulff P, Vallon V, Huang D, Volkl H, Yu F, Richter K, Jansen M, Schlunz M, Klingel K, Loffing J, et al. (2002). Impaired renal Na(+) retention in the sgk1-knockout mouse. J Clin Invest 110, 1263-1268.

Xing Y, Liu D, Zhang R, Joachimiak A, Songyang Z and Xu W (2004). Structural basis of membrane targeting by the Phox homology domain of cytokine-independent survival kinase (CISK-PX). J Biol Chem 279, 30662-30669.

Xu B, Stippec S, Chu P, Lazrak A, Li X, Lee B, English J, Ortega B, Huang C and Cobb M (2005). WNK1 activates SGK1 to regulate the epithelial sodium channel. Proc Natl Acad Sci USA 102, 10315-10320.

Xu J, Liao L, Qin J, Xu J, Liu D and Songyang Z (2009). Identification of Flightless-I as a substrate of the cytokine-independent survival kinase CISK. J Biol Chem 284, 14377-14385.

Yang J, Jan Y and Jan L (1995). Control of rectification and permeation by residues in two distinct domains in an inward rectifier K+ channel. Neuron 4, 1047-1054.

Yao L, McCormick J, Wang J, Yang K, Kidwai A, Colussi G, Boini K, Birnbaum M, Lang F, German M, et al. (2011). Novel role for SGK3 in glucose homeostasis revealed in SGK3/Akt2 double-null mice. Mol Endocrinol.

Yi B, Minor D, Lin Y, Jan Y and Jan L (2001). Controlling potassium channel activities: interplay between the membrane and intracellular factors. Proc Natl Acad Sci USA 98, 11016–11023.

Yoshimura S, Gerondopoulos A, Linford A, Rigden D and FA B (2010). Family-wide characterization of the DENN domain Rab GDP–GTP exchange factors. J Cell Biol 191, 367–381.

Yun CC (2002). The Serum and Glucocorticoid-Inducible Kinase SGK1 and the Na+/H+ Exchange Regulating Factor NHERF2 Synergize to Stimulate the Renal Outer Medullary K+ Channel ROMK1. J Am Soc Nephrol 13, 2823-2830.

Zadeh AD, Xu H, Loewen ME, Noble GP, Steele DF and Fedida D (2008). Internalized Kv1.5 traffics via Rab-dependent pathways. J Physiol 586, 4793-4813.

Zerial M and McBride H (2001). Rab Proteins as Membrane Organizers.pdf. Nature Reviews 2, 107-119.

Zhou Y, Morais-Cabral J, Kaufman A and MacKinnon R (2001). Chemistry of ion coordination and hydration revealed by a K+ channel-Fab complex at 2.0 A resolution. Nature 414, 43-48.

Zobel C, Cho HC, Nguyen TT, Pekhletski R, Diaz RJ, Wilson GJ and Backx PH (2003). Molecular dissection of the inward rectifier potassium current (IK1) in rabbit cardiomyocytes: evidence for heteromeric co-assembly of Kir2.1 and Kir2.2. J Physiol 550, 365-372.

6. Appendix

6.1 Abbreviations

A	alanine
Ba^{2+}	barium ion
Ca^{+}	calcium ion
$CaCl_2$	calcium chloride
CCV	clathrin coated vesicles
Cl^{-}	chloride ion
CO	carbon monoxide
cRNA	complementary ribonucleic acid
Cs^{+}	caesium ion
ctrl.	control
D	aspartic acid
ddH_2O	double distilled water
DMEM	dulbecco's modified eagle's medium
DMSO	dimethylsulfoxide
DNA	deoxyribonucleic acid
DNAse	desoxyribonuclease
dNTP	desoxynucleosidtriphosphate
E. coli	Escherichia coli
EDTA	ethylenediaminetetraacetic acid
EE	early endosome
EEA1	early endosome antigen 1
EGFP	enhanced green fluorescent protein
ENAC	epithelial sodium channel
E_K	equilibrium potential for potassium
E_R	resting membrane potential
ER	endoplasmic reticulum
ER	estrogen receptor
FBS	fetal bovine serum
FCS	fetal calf serum
Fig.	figure
FOXO3a	forkhead-box-protein O3a

g	gram
GAP	GTPase activating proteins
GDF	GDI displacement factor
GDI	GDP-dissociation inhibitor
GDP	guanosine diphosphate
GEF	guanine nucleotide exchange factors
GGT	geranylgeranyl transferase
gp	guinea pig
GSK3β	glycogen synthase kinase 3β
GTP	guanosine triphosphate
h	hour
h	human
HA	hemagglutinin
HCl	hydrogen chloride
HEPES	4-(2-hydroxyethyl)-1-piperazineethanesulfonic acid
hERG	human ether-à-go-go-related gene
HM	hydrophobic motif
K	lysine
K^+	potassium ion
K2P	two-pore-domain potassium channel
KCl	potassium chloride
Kir	inwardly rectifying potassium channel
I	current
IgG	Immunglobulin G
l	liter
LB	lysogeny broth
LE	late endosome
m	mili
M	molar
µ	micro
min	minutes
Mg^{2+}	magnesium ion
$MgCl_2$	magnesium chloride
MOPS	3-(N-morpholino)propanesulfonic acid

mRNA	messenger RNA
N	asparagines
Na^+	sodium ion
NaCl	sodium chloride
NaOH	sodium hydroxide
NHERF2	Na+/H+ exchanger regulating factor 2
NLS	nuclear localization signal
n.s.	not significant
NTP	nucleotide triphosphate
P	pore loop
PBS	phosphate buffered saline
PCR	polymerase chain reaction
PDK1	3-phosphoinositide dependent kinase
PFA	polyformaldehyde
PH	phox homology
PI	phosphoinositide
PI3K	phosphatidylinositol-3-kinase
PIF	PDK interacting fragment
R	arginine
REP	Rab escort protein
RNA	ribonucleic acid
RNAse	ribonuclease
rpm	rounds per minute
RT	room temperature
S	serine
Ser	serine
SGK	serum- and glucocorticoid-inducible kinase
T	threonine
Thr	threonine
tab.	table
TAE	tris-acetate-EDTA buffer
TEVC	two electrode voltage clamp
TGN	trans-Golgi network
TM	transmembrane domain

TRIS	tris(hydroxymethyl)aminomethane
tRNA	transfer RNA
U	units
UK	United Kingdom
USA	United States of America
UV	ultra violet
V	volt
v	volume
v/v	volume / volume
w/v	weight / volume
WT	wild type

6.3 Academic teachers

My academic teachers in Braunschweig were:

Arnold, Bittner, Buchberger-Seidel, Dersch, Dübel, Frenzel, Hänsch, Hempel, Hohm, Hust, Jahn, Jördening, Korte, Krull, Kwade, Lang, Lange, Mendel, du Mont, Schirrmann, Schmidt, Schnabel, Schomburg, Schulz, Vauti, Walla, Winter.

6.4 Ehrenwörtliche Erklärung

Ich erkläre ehrenwörtlich, dass ich die dem Fachbereich Medizin Marburg zur Promotionsprüfung eingereichte Arbeit mit dem Titel ‚The serine/threonine-protein kinase SGK3 stimulates endosomal recycling of the potassium channel Kir2.2.' im Institut für Physiologie und Pathophysiologie unter Leitung von Prof. Dr. Dr. Daut ohne sonstige Hilfe selbst durchgeführt und bei der Abfassung der Arbeit keine anderen als die in der Dissertation aufgeführten Hilfsmittel benutzt habe. Ich habe bisher an keinem in- oder ausländischen Medizinischen Fachbereich ein Gesuch um Zulassung zur Promotion eingereicht, noch die vorliegende oder eine andere Arbeit als Dissertation vorgelegt.
Vorliegende Arbeit wird in folgendem Publikationsorgan veröffentlicht:

Molecular Biology of the Cell

6.5 Danksagung

Zunächst möchte ich mich an dieser Stelle bei meinem Doktorvater Prof. Dr. Dr. Jürgen Daut für die Möglichkeit bedanken, meine Doktorarbeit in diesem spannenden Feld durchzuführen, sowie die Unterstützung und Motivation während der gesamten Zeit.

Weiterhin möchte ich mich bei Dr. Günter Schlichthörl für seine Unterstützung bei den TEVC-Messungen und seine Hilfe bei allen anderen größeren oder kleineren technischen Problemen bedanken. Dr. Thomas Fischer gilt mein Dank für seine Hilfestellung bei den Fluoreszenzmikroskopie-Aufnahmen.

Bei der gesamten Arbeitsgruppe möchte ich mich außerdem für die gute Atmosphäre und unseren tollen ‚Betriebsausflug' nach Südfrankreich bedanken! Ein ganz besonderer Dank geht an Günter, Mandy, Kristin, Xinle, Tu Wei, Philip und Julia für die gemeinsamen Mittagspausen, Diskussionen und aufmunternden Worte während der gemeinsamen Zeit. Ihr habt dafür gesorgt, dass es auch im Laboralltag immer etwas zu lachen gab und insbesondere unsere Unternehmungen außerhalb des Labors haben diese Zeit unvergesslich gemacht! ☺

Last but not least möchte ich mich bei meiner Familie und meinem Freund für den Glauben an mich und die bedingungslose Unterstützung während meines Studiums und meiner Doktorarbeit bedanken. Danke, dass ihr immer für mich da wart!